Copy 427
RM L58D04

NACA RM L58D04

NACA

RESEARCH MEMORANDUM

INVESTIGATION OF THE STATIC STABILITY CHARACTERISTICS OF FIVE HYPERSONIC MISSILE CONFIGURATIONS AT MACH NUMBERS FROM 2.29 TO 4.65

By Kenneth L. Turner and W. H. Appich, Jr.

Langley Aeronautical Laboratory
Langley Field, Va.

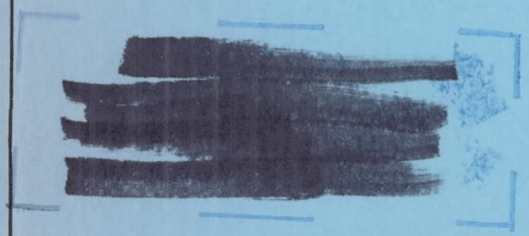

NATIONAL ADVISORY COMMITTEE
FOR AERONAUTICS

WASHINGTON

June 30, 1958

NACA RM L58D04

A

NATIONAL ADVISORY COMMITTEE FOR AERONAUTICS

RESEARCH MEMORANDUM

INVESTIGATION OF THE STATIC STABILITY CHARACTERISTICS OF FIVE HYPERSONIC MISSILE CONFIGURATIONS AT MACH NUMBERS FROM 2.29 TO 4.65

By Kenneth L. Turner and W. H. Appich, Jr.

SUMMARY

An investigation has been conducted in the Langley Unitary Plan wind tunnel to determine the static stability characteristics of five hypersonic missile configurations. The models tested were a basic body with length-diameter ratio of 10 and an ogival nose with a fineness ratio of 5, the body with a 10° flared afterbody (skirt), and the body with two sets of low-aspect-ratio cruciform fins. An additional model, known as the hypersonic test vehicle, was included to simulate a Langley Pilotless Aircraft Research Division free-flight test vehicle.

Tests were performed at Mach numbers of 2.29, 2.75, 3.22, 3.71, and 4.65 and at Reynolds numbers, based on the body length, from approximately 2.5×10^6 to 15×10^6.

The results show that there is little effect of Mach number, within the test Mach number range, on the slope of the normal-force curve at low angles of attack for the configurations tested. A skirt of the type tested is effective in producing lift and pitching moment in the test angle-of-attack range. The use of a skirt, however, leads to a drag penalty with a corresponding loss in lift-drag ratio. With the center of gravity at 50 percent of the body length, the skirted and finned models are directionally stable at the low angles of attack. At the higher test Mach numbers and at the higher angles of attack, the directional stability for the finned models becomes greater than that experienced at angles of attack near 0°. However, at the high angles of attack and low Mach numbers, the finned models tend toward instability.

INTRODUCTION

The design of hypersonic missiles is, to a large degree, dictated by considerations of aerodynamic heating. Configurations which have surfaces that present small angles to the airstream (e.g., highly swept lifting surfaces) have been shown to have comparatively low heating rates, and are therefore being considered for use as hypersonic air-to-air and ground-to-air missiles. In order to obtain more information on such configurations, the National Advisory Committee for Aeronautics has recently undertaken an investigation to determine the aerodynamic characteristics of a family of missile configurations. This investigation is to be performed at supersonic and hypersonic speeds, and is to cover a large Reynolds number range.

The models to be investigated include a basic body with length-diameter ratio of 10 and an ogival nose with a fineness ratio of 5, the body with a 10° flared afterbody, and the body with two different sets of low-aspect-ratio cruciform fins. An additional model, known as the hypersonic test vehicle, is included to simulate a Langley Pilotless Aircraft Research Division free-flight test vehicle. These models were previously tested in the Langley 4- by 4-foot supersonic pressure tunnel at a Mach number of 2.01 and the results are presented in reference 1.

The present paper contains the results of tests made in the Langley Unitary Plan wind tunnel to determine drag and static longitudinal and lateral stability characteristics obtained at Mach numbers of 2.29, 2.75, 3.22, 3.71, and 4.65 and at Reynolds numbers, based on the body length, from approximately 2.5×10^6 to 15×10^6. Also included in this paper are comparisons of the data of this report with data of reference 1.

SYMBOLS

The coefficients of forces and moments are referred to the body axes system. All aerodynamic moments are taken about the center of gravity which is located at the 50-percent length of the missile being tested. Symbols used in this paper are as follows:

C_A axial-force coefficient, $\frac{\text{Axial force}}{qS}$

$C_{A,B}$ base axial-force coefficient, $\frac{\text{Base axial force}}{qS}$

C_l	rolling-moment coefficient, $\frac{\text{Rolling moment}}{qSl}$
C_m	pitching-moment coefficient, $\frac{\text{Pitching moment}}{qSl}$
C_{m_α}	slope of pitching-moment curve, $\frac{\partial C_m}{\partial \alpha}$
C_{m_o}	pitching-moment coefficient at zero normal force
C_n	yawing-moment coefficient, $\frac{\text{Yawing moment}}{qSl}$
C_{n_β}	slope of yawing-moment curve, $\frac{\partial C_n}{\partial \beta}$
C_N	normal-force coefficient, $\frac{\text{Normal force}}{qS}$
C_{N_α}	slope of normal-force curve, $\frac{\partial C_N}{\partial \alpha}$
C_Y	side-force coefficient, $\frac{\text{Side force}}{qS}$
C_{Y_β}	slope of side-force curve, $\frac{\partial C_Y}{\partial \beta}$
l	missile length, in.
M	free-stream Mach number
q	free-stream dynamic pressure, lb/sq ft
R	Reynolds number
S	maximum cross-sectional area of the cylindrical body, sq ft
x,y	coordinates of nose of missile (measured from point unless otherwise noted), in.
α	angle of attack of missile center line, deg
$\Delta\alpha$	tunnel flow angle, deg
β	angle of sideslip of missile center line, deg

APPARATUS AND METHODS

Tunnel

The tests were performed in the high Mach number test section of the Langley Unitary Plan wind tunnel, which is a variable pressure, continuous-flow type. The test section is 4 feet square and approximately 7 feet long. The nozzle leading to the test section is of the asymmetric sliding-block type which permits a continuous variation of Mach number from approximately 2.29 to 4.65.

Models

A drawing showing the five models tested is presented in figure 1 and table I gives the geometric characteristics of these models.

The missile configurations were

Model I - body alone (length-diameter ratio of 10)
Model II - body with 10° flared skirt
Model III - body with cruciform 5° delta fins
Model IV - body with cruciform 15° delta fins
Model V - hypersonic test vehicle

The first four models incorporate a cylindrical body with an ogive nose, the point of which has a 0.3-inch radius of curvature. The fifth model (which is somewhat longer) has the same cylindrical portion of the body but it has a modified von Kármán nose, the point of which has a 0.054-inch radius of curvature. This model also incorporates a 10° skirt.

Henceforth, these models will be referred to as models I to V. The models are of steel construction except for the nose portion of model V and the flared skirts which were made of an aluminum alloy. A photograph of model III as installed in the test section is presented as figure 2.

Forces and moments were measured by means of an internally mounted, six-component, strain-gage balance.

Test Conditions and Procedure

The tests were performed at Mach numbers of 2.29, 2.75, 3.22, 3.71, and 4.65. The dewpoint temperature was maintained below -30° F for all Mach numbers except 4.65, at which Mach number it was allowed to rise to -20° F. The stagnation temperature was maintained at approximately

140° F at all test Mach numbers except 4.65, at which Mach number it was held at approximately 175° F.

The following table presents the test conditions of each model:

Model	Nominal angles of attack, deg	Nominal angles of sideslip, deg	Mach number	R
I	-2 to 25	0	2.29 2.75 3.22 3.71 4.65	12.5×10^6 12.5 12.5 12.5 12.5
II	-2 to 25	0	2.29 2.75 3.22 3.71 4.65	5.0 and 12.5×10^6 5.0 and 12.5 5.0 and 12.5 5.0 and 12.5 7.5 and 12.5
III	-2 to 25 0, 7, 14, and 20	0 -3 to 12	2.29 2.75 3.22 3.71 4.65	2.5, 5.0, and 12.5×10^6 2.5, 5.0, and 12.5 2.5, 5.0, and 12.5 2.5, 5.0, and 12.5 5.0, 7.5, and 12.5
IV	-2 to 25 0, 7, 14, and 20	0 -3 to 12	2.29 2.75 3.22 3.71 4.65	12.5×10^6 12.5 12.5 12.5 12.5
V	-2 to 25	0	2.29 2.75 3.22 3.71 4.65	15.0×10^6 15.0 15.0 15.0 15.0

CORRECTIONS AND ACCURACY

The angles of attack and sideslip have been corrected for deflection of the balance and sting under load.

In order to obtain reliable values of base axial force, a base block was fitted securely to the model sting with about 1/8-inch gap between the block and the base of the model. The base block for each model was cylindrical and of the same diameter as the base of the model being investigated. (See fig. 2.) Measurements were taken of the pressure existing between the base block and the model base and these pressure measurements were converted into base axial force. The axial-force data on the plots of aerodynamic coefficients are not adjusted for base axial force. In order to adjust these data, the base axial force for a given model at a given attitude and Mach number must be subtracted from the axial force for the same model at the same attitude and Mach number. During tests of model V, faulty equipment curtailed base pressure measurements, and base-axial-force data for this model are not presented.

The accuracy of the individual measured quantities, based on calibration and repeatability of data, is estimated to be within the following limits:

	Accuracy at -		
	$R = 2.5 \times 10^6$	$R = 5 \times 10^6$	$R = 12.5 \times 10^6$ or 15×10^6
C_N . . .	±0.134	±0.067	±0.029
C_A . . .	±0.007	±0.003	±0.002
C_m . . .	±0.055	±0.027	±0.011
C_l . . .	±0.004	±0.002	±0.001
C_n . . .	±0.055	±0.027	±0.011
C_Y . . .	±0.134	±0.067	±0.029
α, deg .	±0.100	±0.100	±0.100
β, deg ..	±0.100	±0.100	±0.100
M	±0.015	±0.015	±0.015

Calibration of the tunnel test section has not been completed. Measured pressure gradients are sufficiently small, however, to assure negligible corrections due to model buoyancy effects.

The data have not been corrected for flow angularity. These corrections at the corresponding Mach numbers are independent of model angle of attack and are as follows:

M	$\Delta\alpha$, deg
2.29	0.40
2.75	.30
3.22	.10
3.71	.30
4.65	.95

PRESENTATION OF RESULTS

The results of the investigation are presented in the following figures:

	Figure
Typical schlieren photographs of model II	3
Typical schlieren photographs of model III	4
Variation of base axial-force coefficient with angle of attack	5
Effect of base block on aerodynamic characteristics of model III	6
Aerodynamic characteristics of model I in pitch. $\beta = 0^\circ$	7
Aerodynamic characteristics of model II in pitch. $\beta = 0^\circ$	8
Aerodynamic characteristics of model III in pitch. $\beta = 0^\circ$	9
Aerodynamic characteristics of model IV in pitch. $\beta = 0^\circ$	10
Aerodynamic characteristics of model V in pitch. $\beta = 0^\circ$	11
Aerodynamic characteristics of model III in sideslip. $\alpha = 0^\circ$	12
Aerodynamic characteristics of model III in sideslip. $\alpha = 7.2^\circ$	13
Aerodynamic characteristics of model III in sideslip. $\alpha = 14.6^\circ$	14
Aerodynamic characteristics of model III in sideslip. $\alpha = 20.9^\circ$	15
Aerodynamic characteristics of model IV in sideslip	16

Figure

Summary of longitudinal stability characteristics of the five missile configurations 17
Summary of lateral stability characteristics of model III . . 18
Summary of lateral stability characteristics of model IV . . 19

DISCUSSION OF RESULTS

Effect of Base Block

In order to determine the effect of the base block on the stability characteristics presented, model III was tested with and without the base block. (See fig. 6.) The results show that the addition of the base block produces a positive C_{m_o} shift, but the degree of stability is not materially altered. The base blocks were in place for all other test results presented.

Longitudinal Stability

The longitudinal stability characteristics of the five missiles are presented in summary form plotted against Mach number in figure 17. It may be seen that the normal-force-curve slopes of all five models are invariant with Mach number at the low angles of attack. At the high angles of attack, however, the normal-force-curve slopes decrease with an increase in Mach number. It may be noted that the increment of normal-force-curve slope provided by the fins and skirts is essentially invariant with Mach number and that the decrease in normal-force-curve slope noted at high angles is due to loss of lift on the body and not on the fins or skirts.

Of the models tested at the low angles of attack, the finned models (models III and IV) have the greatest normal-force-curve slope, and the model without fins or skirt (model I) has the least normal-force-curve slope. Model III develops more lift than model IV, as would be expected, from consideration of the geometry of the two models.

A comparison of model II and model IV shows that the skirt for model II is approximately as long as the fins of model IV, but the leading-edge angle of the fins of model IV is much larger. The data indicate that model II develops slightly less lift and has more drag than model IV. Similar results in reference 2 point out that an increase in the leading-edge angle or length of a skirt will increase the lift developed by the skirt. The use of a skirt, however, leads to a drag penalty with a corresponding loss in lift-drag ratio.

Figure 17 also shows that some stabilizing device is necessary for model I at the low angles of attack in order to obtain a longitudinally stable missile in the test Mach number range with the center of gravity at 50 percent of the body length. These data indicate that at Mach numbers slightly below the test range, the skirt used on model V may not be large enough to produce positive longitudinal stability. The longitudinal stability of the skirted models increases somewhat with increase in Mach number at the low and high angles of attack, whereas the longitudinal stability of model IV decreases with increase in Mach number.

Model III has the largest static margin of the models tested. At the low angles of attack, the longitudinal stability characteristics for model III are relatively constant with variation in Mach number in the test Mach number range.

It may also be seen in figure 17 that the data obtained at the test Mach numbers agree very well with data shown in reference 1 at a Mach number of 2.01. (Ref. 1 data are indicated by symbols in fig. 17.)

Directional stability

Models III and IV, the finned models, were the only models tested in sideslip. Data presented in figures 12 to 16 for the finned missiles, show the missiles, in general, to be directionally stable. These figures also show a nonlinearity in the yawing-moment curve at low sideslip angles. This nonlinearity increases with angle of attack and, in some instances, the missiles are directionally unstable for a small sideslip range near 0°. This instability disappears, however, at the higher sideslip angles. These figures also show little change in longitudinal stability or normal-force coefficient throughout the angle-of-sideslip range. The yawing-moment and side-force derivatives presented in figures 18 and 19 for both finned missiles are for slopes between $\pm 2^\circ$ of sideslip, and because of the aforementioned nonlinearity in the yawing-moment curves do not present the complete stability picture.

It may be seen in figures 18 and 19 that at the lower angles of attack, 0° and 7.0° for model III and 0° for model IV, the directional stability of the finned missiles decreases with increase in Mach number; however, at the higher angles of attack (14.5° and 20.9°) the directional stability increases with increase in Mach number. It is also interesting to note that at the higher test Mach numbers and at an angle of attack of 20.9° the directional stability for model III (and to a limited extent, model IV) becomes greater than that experienced at angles of attack near 0°. It is believed that the reason for this

phenomenon is that at the high angles of attack there is an increase in dynamic pressure on the lower fin which increases the effectiveness of the lower fin at a greater rate than that at which the upper fin is losing effectiveness.

The pitching-moment-curve and normal-force-curve slopes (C_{m_α} and C_{N_α}) of these hypersonic missiles at a Mach number of 2.01 have been obtained from reference 1 and are plotted in figures 18 and 19. Since the models are all symmetrical, it is permissible to compare C_{m_α} and C_{N_α} at zero angle of sideslip with C_{n_β} and C_{Y_β} at zero angle of attack. These slopes, shown in symbol form in figures 18 and 19, show excellent agreement with the data reported on herein.

The data on the basic plots indicate that the dihedral effect is essentially zero for the finned models through the test Mach number and angle-of-attack range.

Figures 18 and 19 indicate negative values of C_{Y_β} at all angles of attack. A comparison of these two figures shows that model III has the larger negative values of C_{Y_β}. This would be expected on the basis of the difference in model geometry.

All models other than III and IV are symmetrical models and would therefore have identical longitudinal and lateral stability characteristics around 0° angle of attack and sideslip.

Reynolds Number Effect

The stability data for models II and III at Reynolds numbers of 2.5×10^6, 5.0×10^6, 7.5×10^6, and 12.5×10^6 are shown in figures 8, 9, 12, and 14. It is easily seen that the pitch and sideslip curves have the same relative shape, regardless of Reynolds number in the test Reynolds number range. There is a general intermixing of data points, however, for the three test Reynolds numbers, dependent on attitude and Mach number. It is believed, moreover, that the data taken at a Reynolds number of 12.5×10^6 accurately define the stability curves, since the balance loads at this higher Reynolds number are in the range to obtain accurate data. The inability of the data taken at the lower Reynolds numbers to check those taken at the higher Reynolds number is believed to be entirely due to balance accuracy. (See section entitled "Corrections and Accuracy.")

CONCLUSIONS

The results of an investigation of five hypersonic missile configurations at Mach numbers of 2.29, 2.75, 3.22, 3.71, and 4.65 and at Reynolds numbers, based on the body length, from approximately 2.5×10^6 to 15×10^6 indicate the following conclusions:

1. With the center of gravity at 50 percent of the body length, the skirted and finned models are directionally stable at the low angles of attack. At the higher test Mach numbers and at the higher angles of attack, the directional stability for the finned models becomes greater than that experienced at angles of attack near 0°. However, at the high angles of attack and low Mach numbers, the finned models tend toward instability.

2. A skirt of the type tested is effective in producing lift and pitching moment in the test angle-of-attack range. The use of a skirt, however, leads to a drag penalty with a corresponding loss in lift-drag ratio.

3. The model with the 5° fins has the largest static margin and normal-force-curve slope of the models tested.

4. There is little effect of Mach number on the slope of the normal-force curve at low angles of attack.

Langley Aeronautical Laboratory,
National Advisory Committee for Aeronautics,
Langley Field, Va., March 19, 1958.

REFERENCES

1. Robinson, Ross B.: Wind-Tunnel Investigation at a Mach Number of 2.01 of the Aerodynamic Characteristics in Combined Angles of Attack and Sideslip of Several Hypersonic Missile Configurations With Various Canard Controls. NACA RM L58A21, 1958.

2. Lavender, Robert E.: Normal Force, Pitching Moment, and Center of Pressure of Eighty Cone-Cylinder-Frustum Bodies of Revolution at Mach Number 1.50. Rep. 6R3N3, Ord. Missile Labs., Redstone Arsenal (Huntsville, Ala.), Apr. 5, 1956.

TABLE I.- MODEL GEOMETRIC CHARACTERISTICS

	Model I	Model II	Model III	Model IV	Model V
Body:					
Length, in.	30.00	30.00	30.00	30.00	35.11
Diameter, in.	3.00	3.00	3.00	3.00	3.00
Cross-sectional area, sq in.	7.07	7.07	7.07	7.07	7.07
Fineness ratio of nose	5.00	5.00	5.00	5.00	5.00
Length-diameter ratio	10.00	10.00	10.00	10.00	11.70
Moment-center location, percent length	50.00	50.00	50.00	50.00	50.00
Skirt:					
Length, in.		6.01			4.67
Base diameter, in.		5.13			4.64
Base area, sq in.		20.66			16.91
Leading-edge angle, deg		10.00			10.00
Fins:					
Area exposed, 2 fins, sq in.			34.36	9.55	
Root chord, in.			19.12	5.97	
Tip chord, in.			0	0	
Span exposed, in.			3.20	3.20	
Span total, in.			6.20	6.20	
Taper ratio			0	0	
Aspect ratio, exposed			0.268	1.07	
Span diameter ratio			2.07	2.07	
Leading-edge angle, deg			5	15	

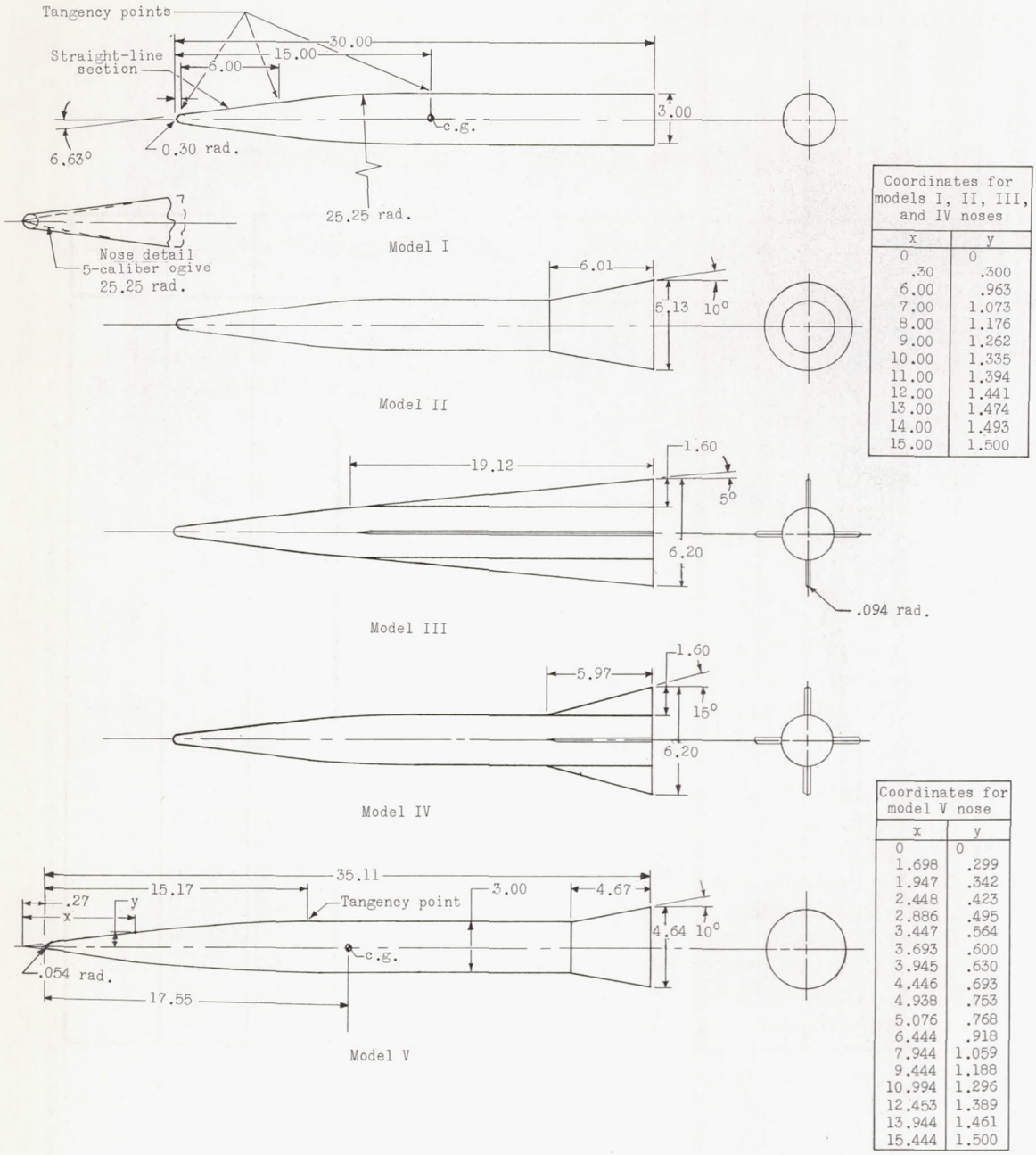

Coordinates for models I, II, III, and IV noses

x	y
0	0
.30	.300
6.00	.963
7.00	1.073
8.00	1.176
9.00	1.262
10.00	1.335
11.00	1.394
12.00	1.441
13.00	1.474
14.00	1.493
15.00	1.500

Coordinates for model V nose

x	y
0	0
1.698	.299
1.947	.342
2.448	.423
2.886	.495
3.447	.564
3.693	.600
3.945	.630
4.446	.693
4.938	.753
5.076	.768
6.444	.918
7.944	1.059
9.444	1.188
10.994	1.296
12.453	1.389
13.944	1.461
15.444	1.500

Figure 1.- Missile configurations tested. (All dimensions in inches unless otherwise stated.)

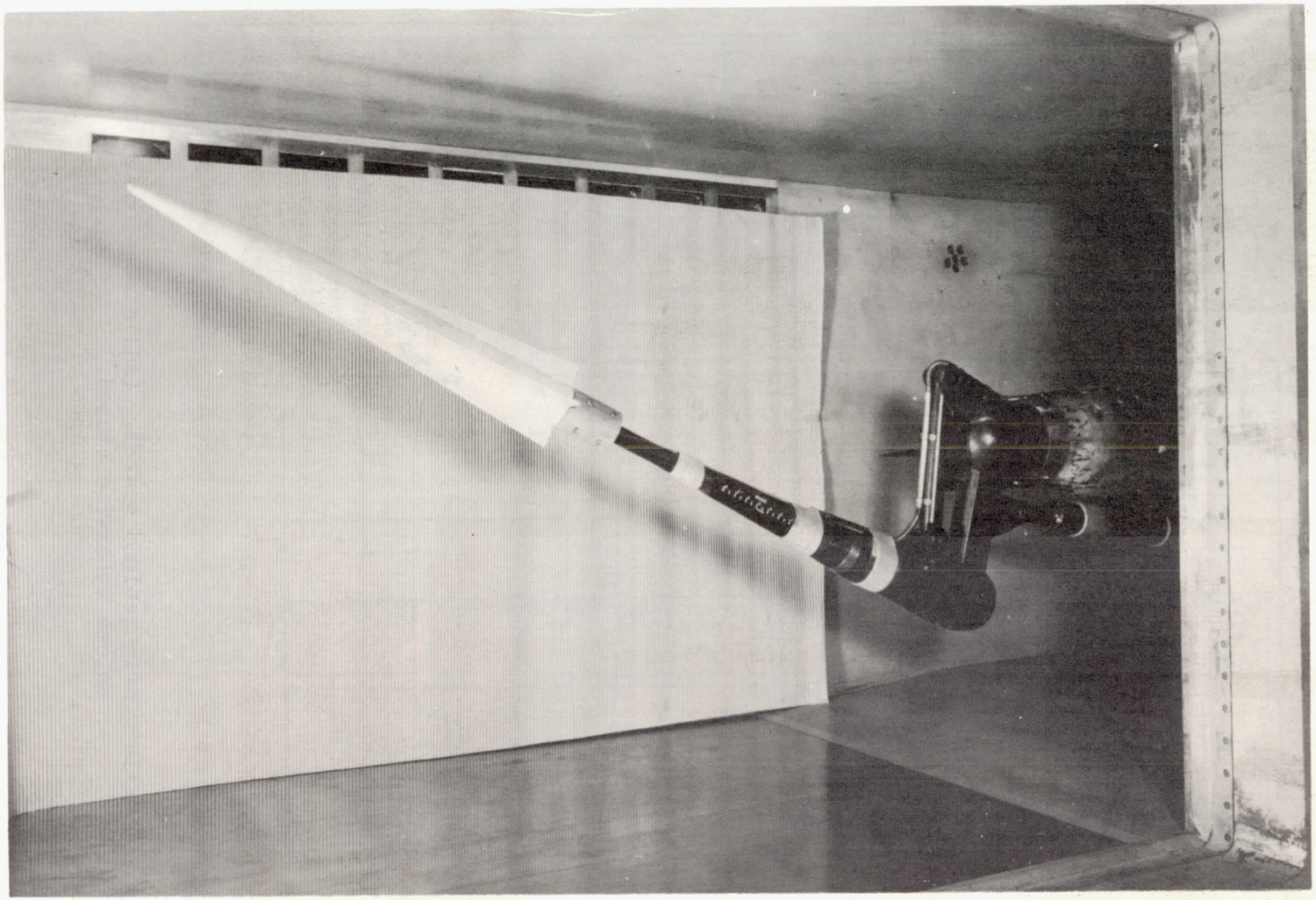

Figure 2.- Photograph of model III with base block as installed in the tunnel. L-57-538

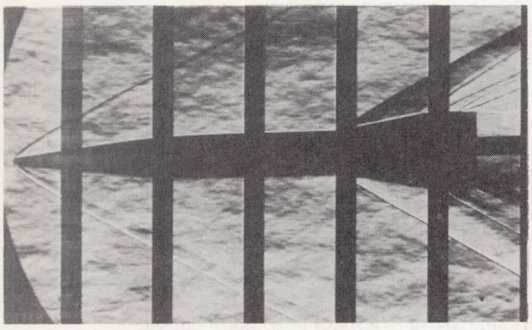

α = -2.4°

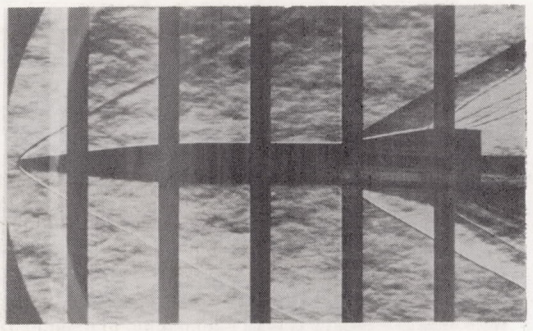

α = 0°

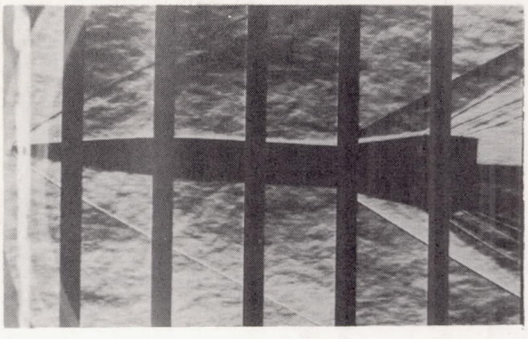

α = 2.0°

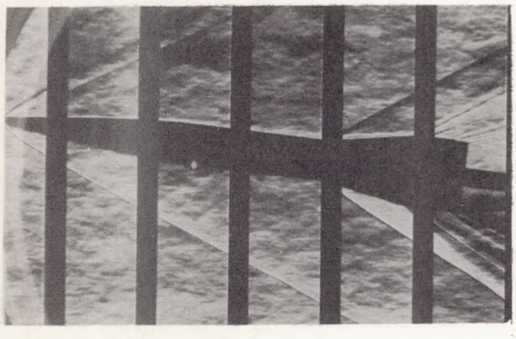

α = 6.2°

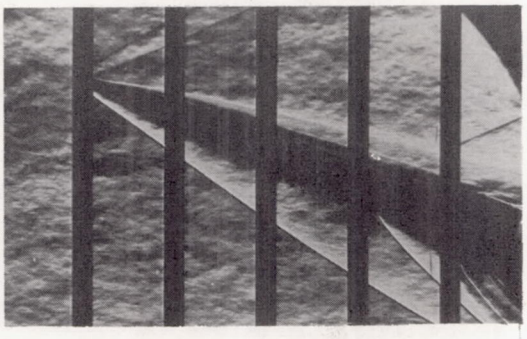

α = 20.9°

(a) M = 2.29. L-58-180

Figure 3.- Typical schlieren photographs of model II. β = 0°.

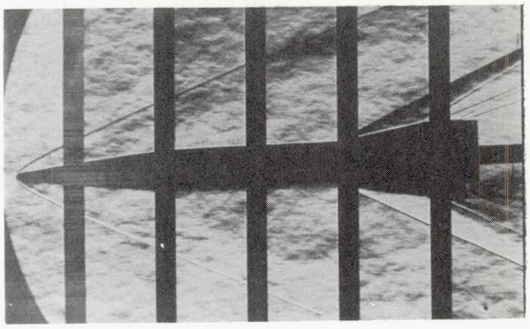

α = -2.4°

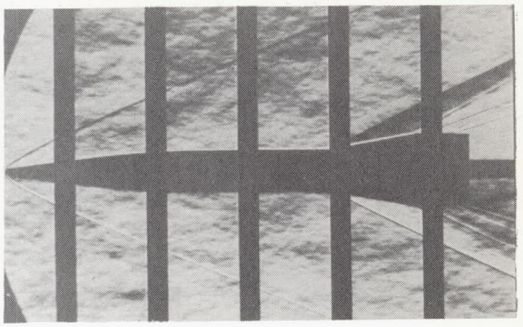

α = 0°

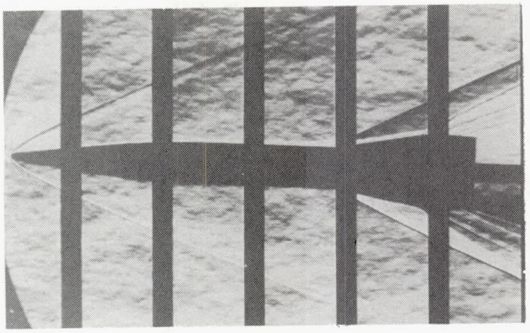

α = 2.0°

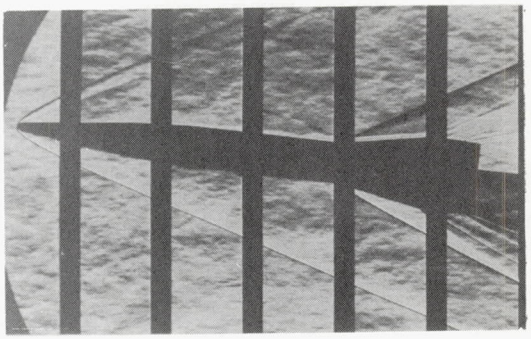

α = 6.2°

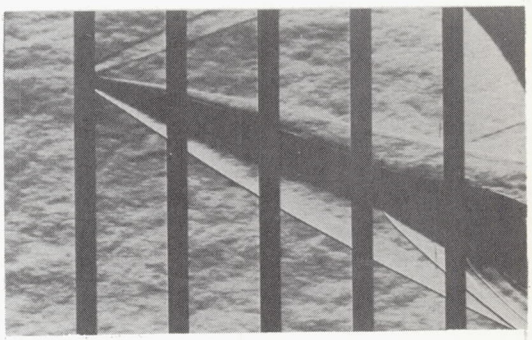

α = 20.9°

(b) M = 2.75. L-58-181

Figure 3.- Continued.

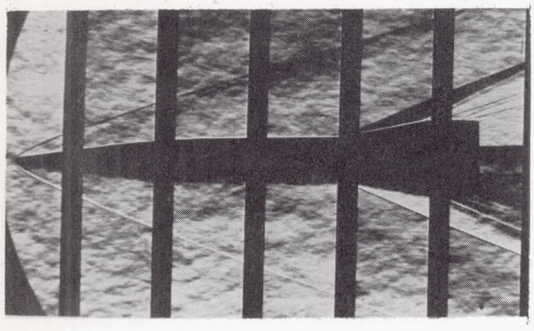

α = -2.5°

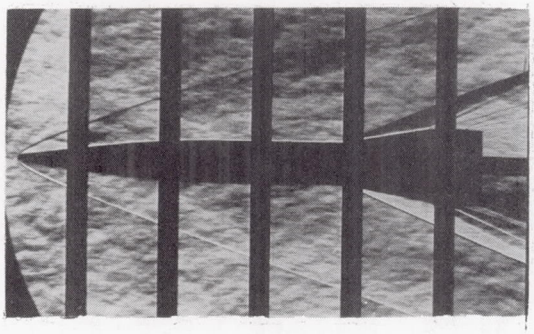

α = 0°

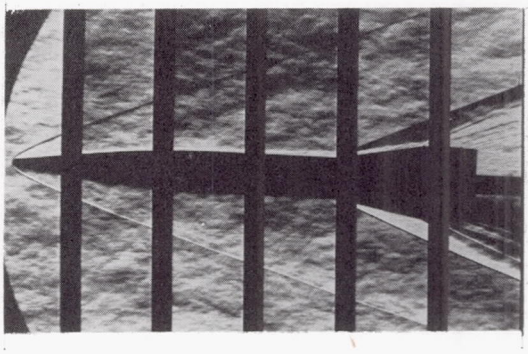

α = 2.0°

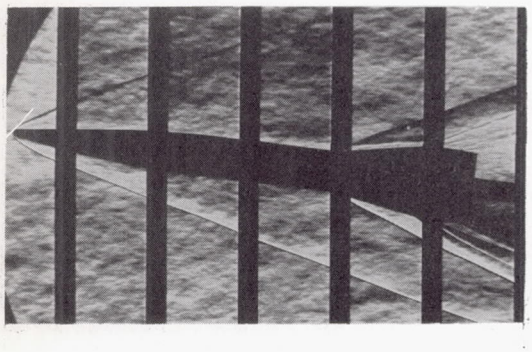

α = 6.1°

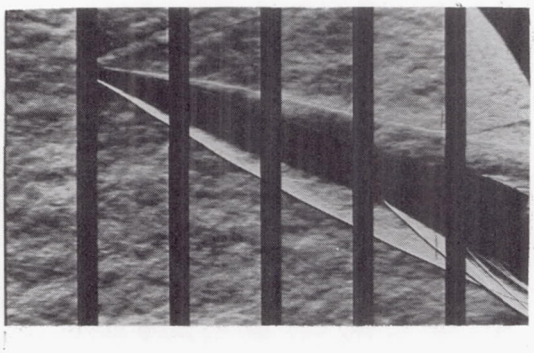

α = 20.7°

(c) M = 3.22. L-58-182

Figure 3.- Continued.

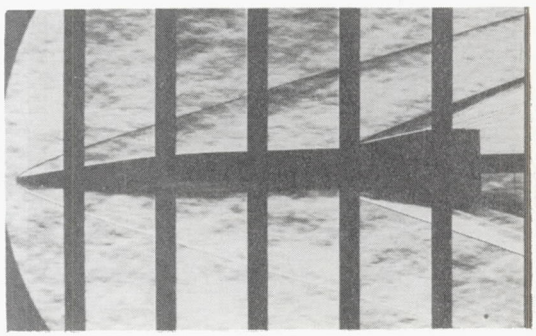

α = -2.4°

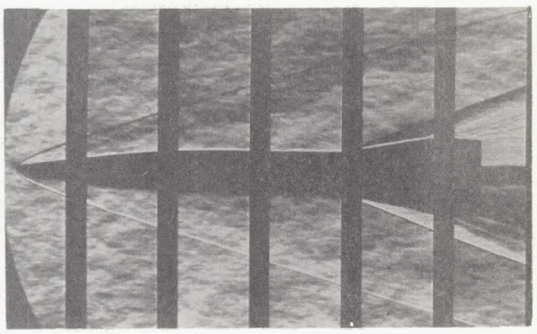

α = 0°

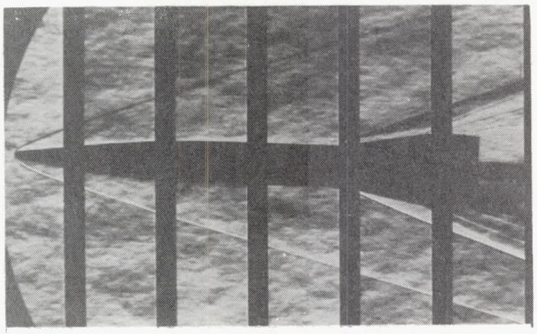

α = 2.1°

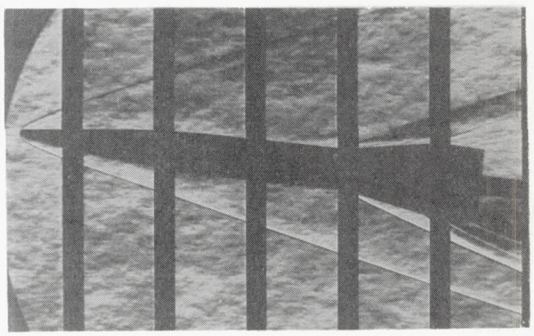

α = 6.1°

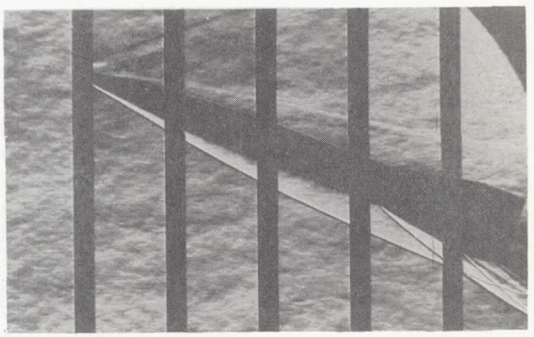

α = 20.7°

(d) M = 3.71. L-58-183

Figure 3.- Continued.

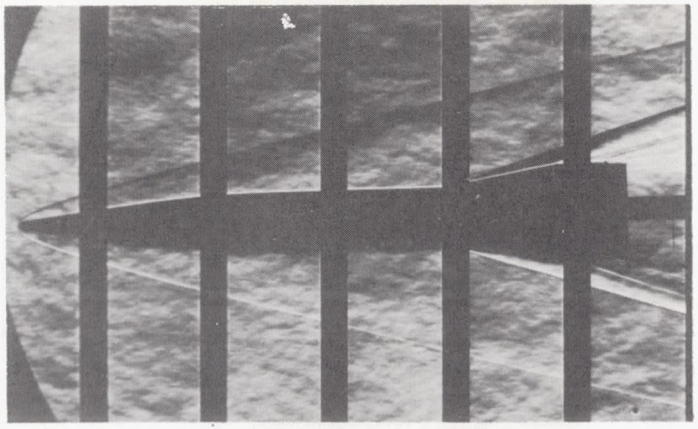

α = -2.4°

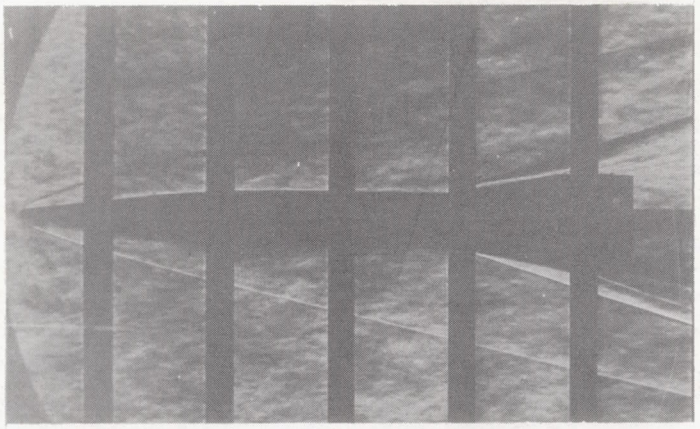

α = 0°

(e) M = 4.65. L-58-184

Figure 3.- Concluded.

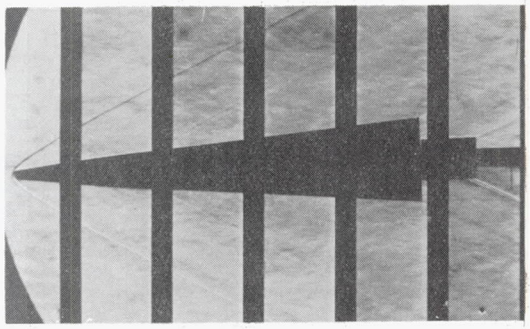

α=-2.4°

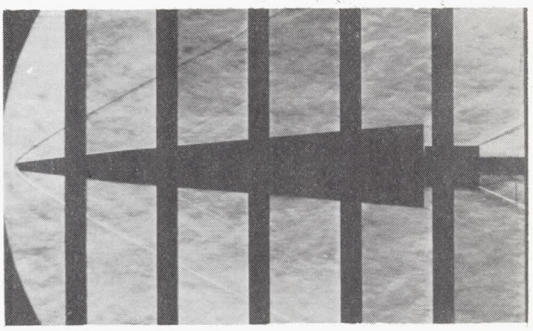

α = 0°

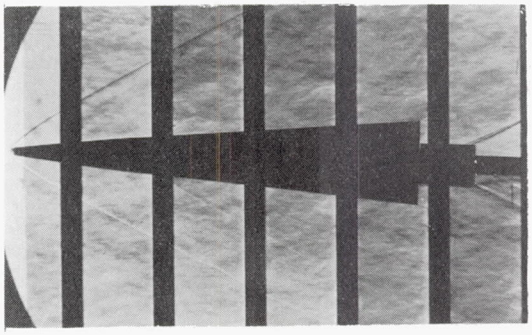

α = 2.0°

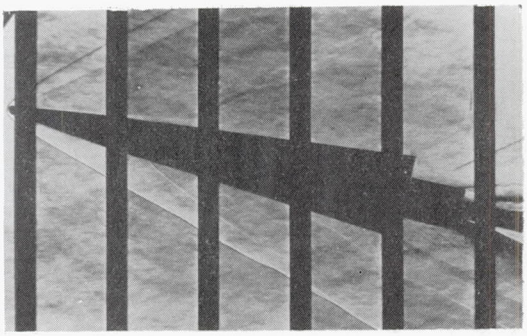

α = 12.4°

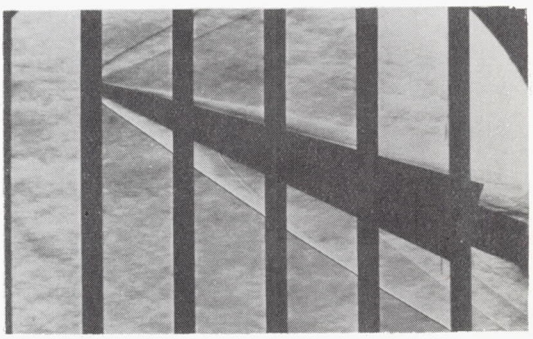

α = 20.6°

(a) M = 2.29. L-58-185

Figure 4.- Typical schlieren photographs of model III. β = 0°.

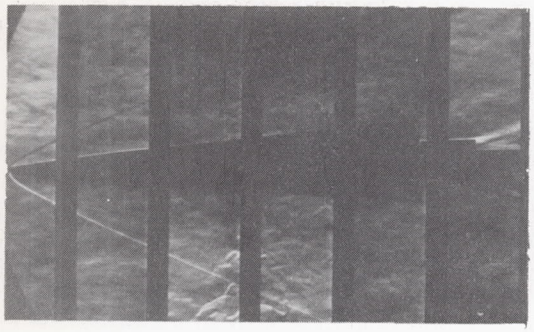

α = -2.4°

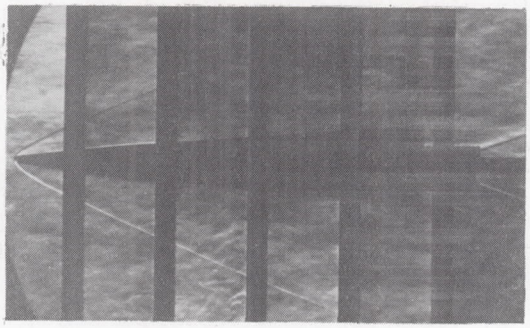

α = 0°

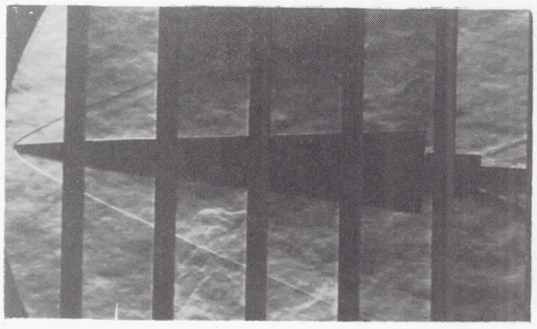

α = 2.0°

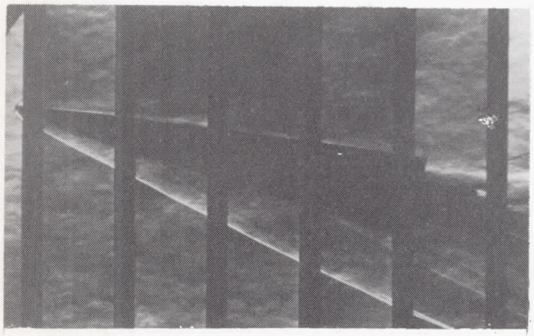

α = 12.3°

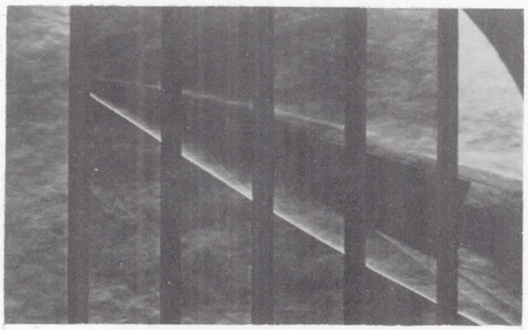

α = 20.5°

(b) M = 2.75. L-58-186

Figure 4.- Continued.

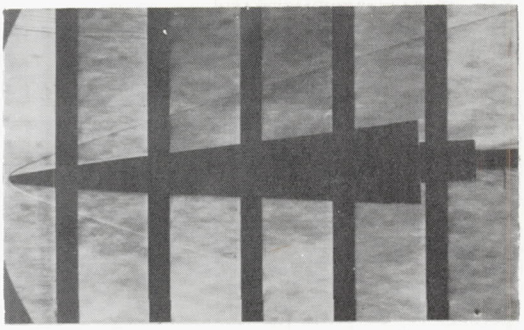

α = -2.4°

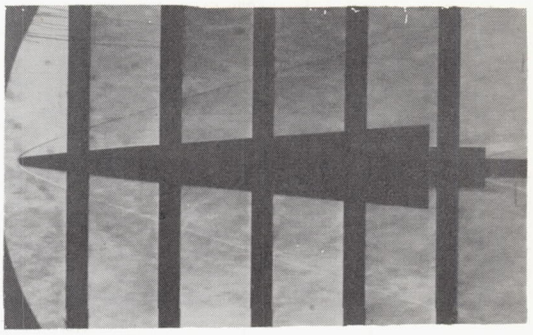

α = 0°

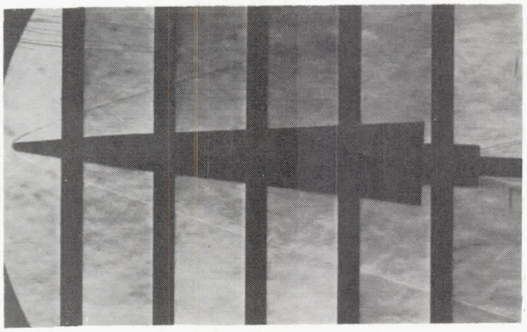

α = 2.0°

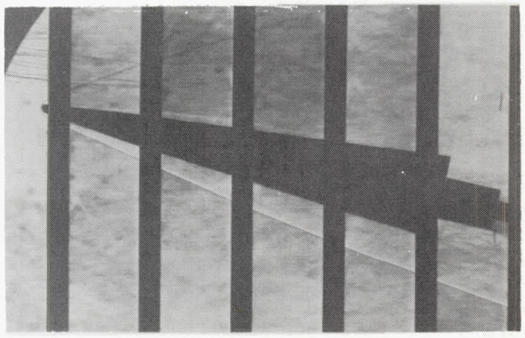

α = 12.2°

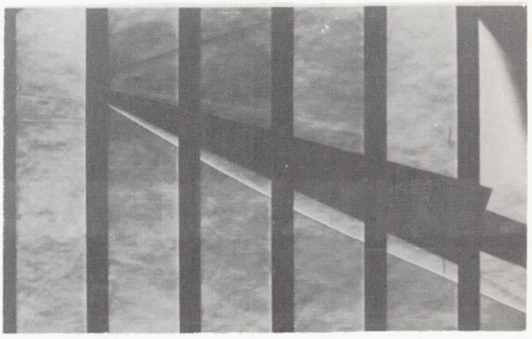

α = 20.2°

(c) M = 3.71. L-58-187

Figure 4.- Concluded.

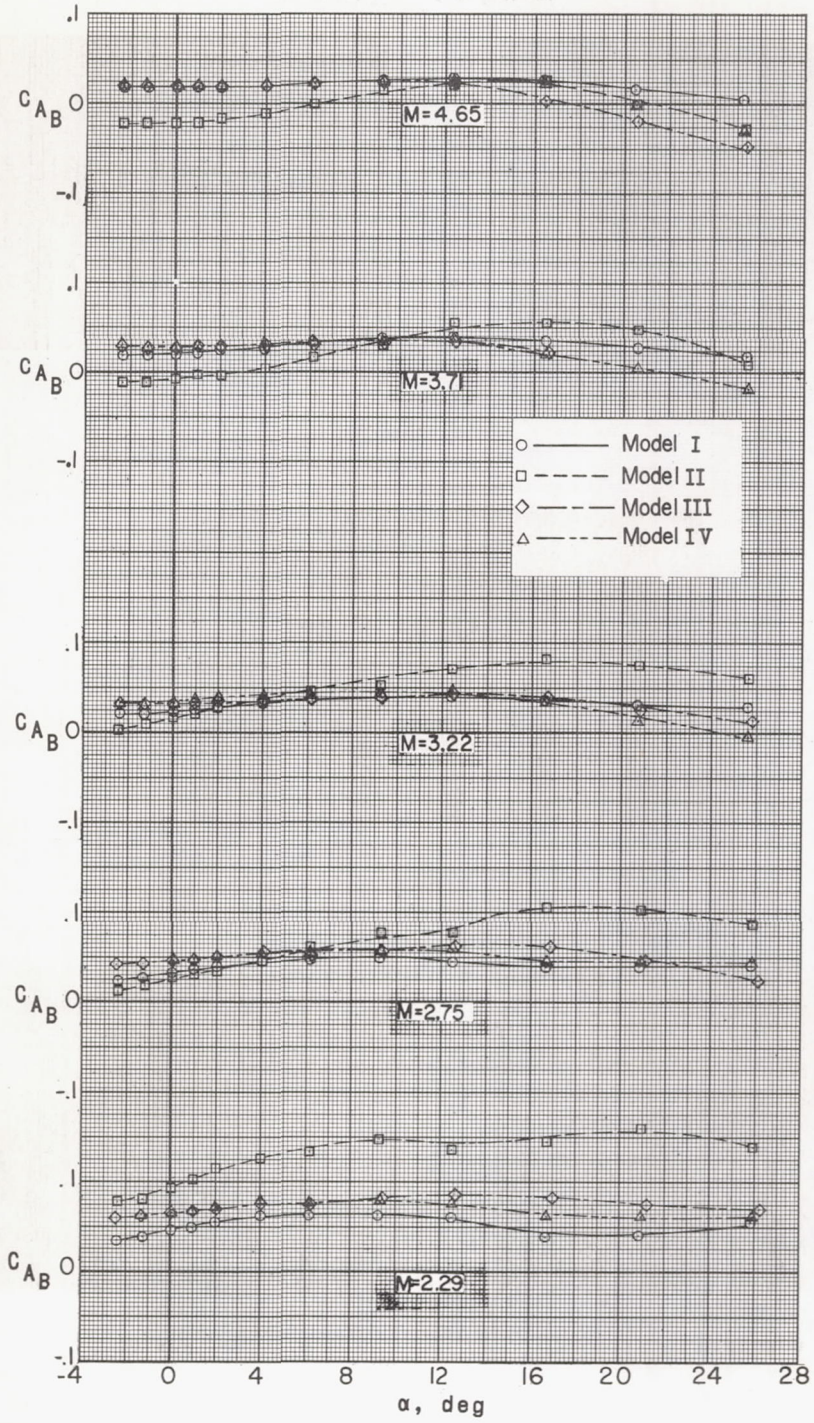

Figure 5.- Variation of base axial-force coefficient with angle of attack. $\beta = 0^{o}$.

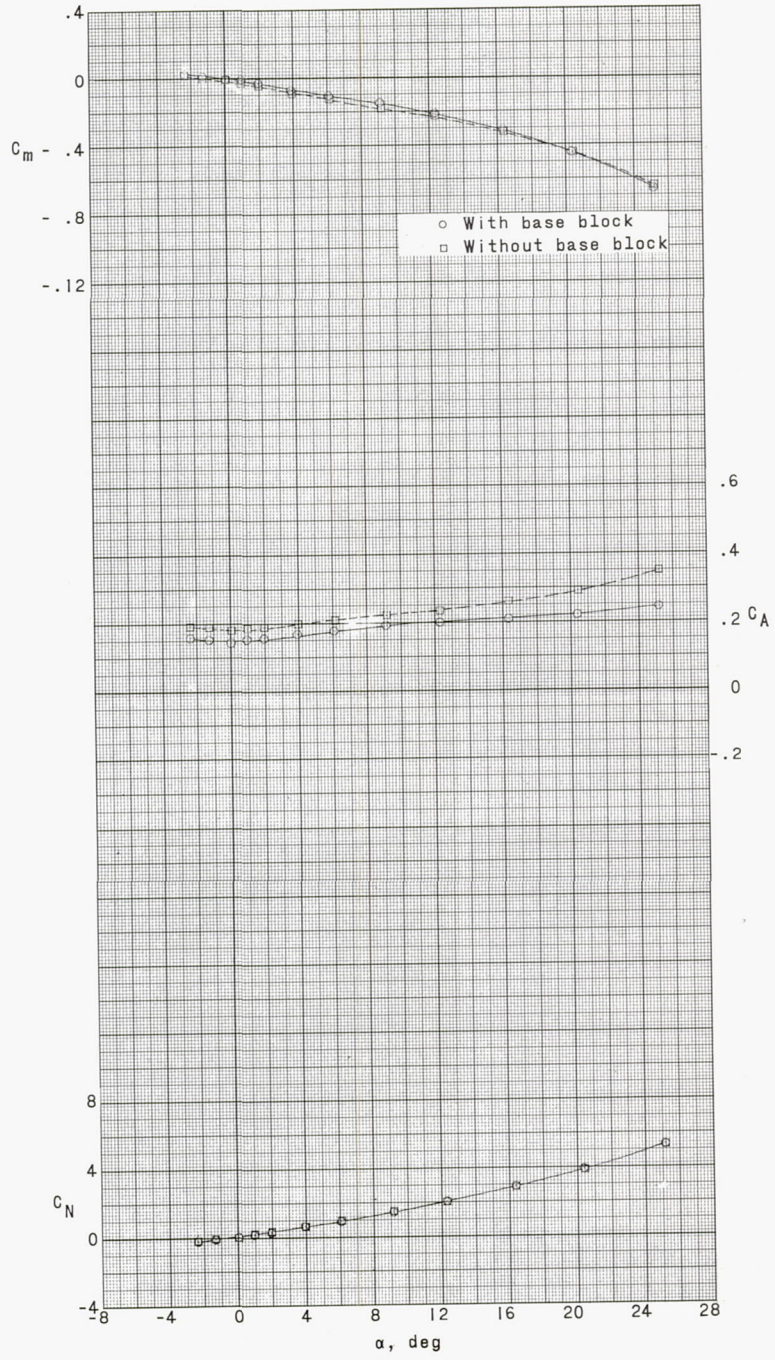

(a) M = 4.65; β = 0°.

Figure 6.- Effect of base block on aerodynamic characteristics of model III. R = 7.5 × 10^6.

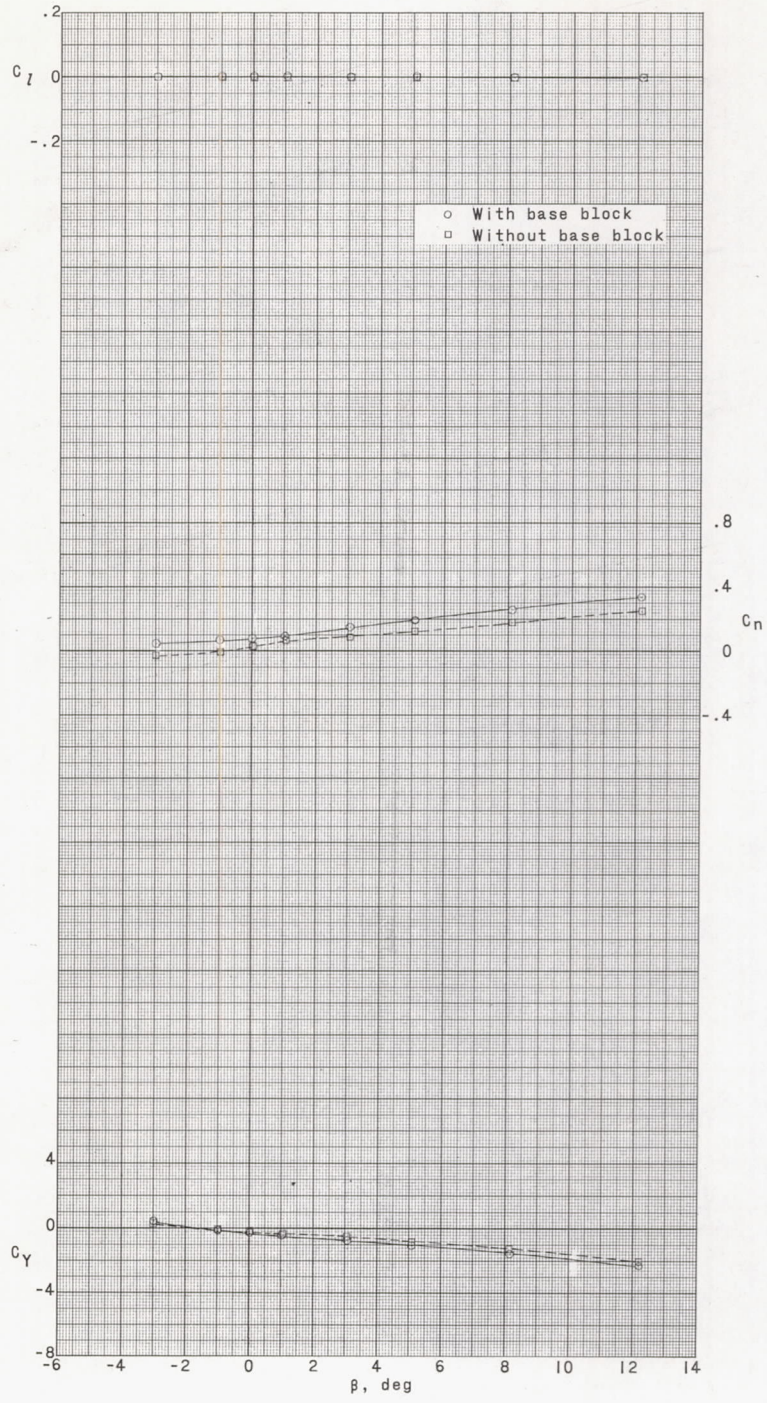

(b) M = 4.65; $\alpha = 0^\circ$.

Figure 6.- Concluded.

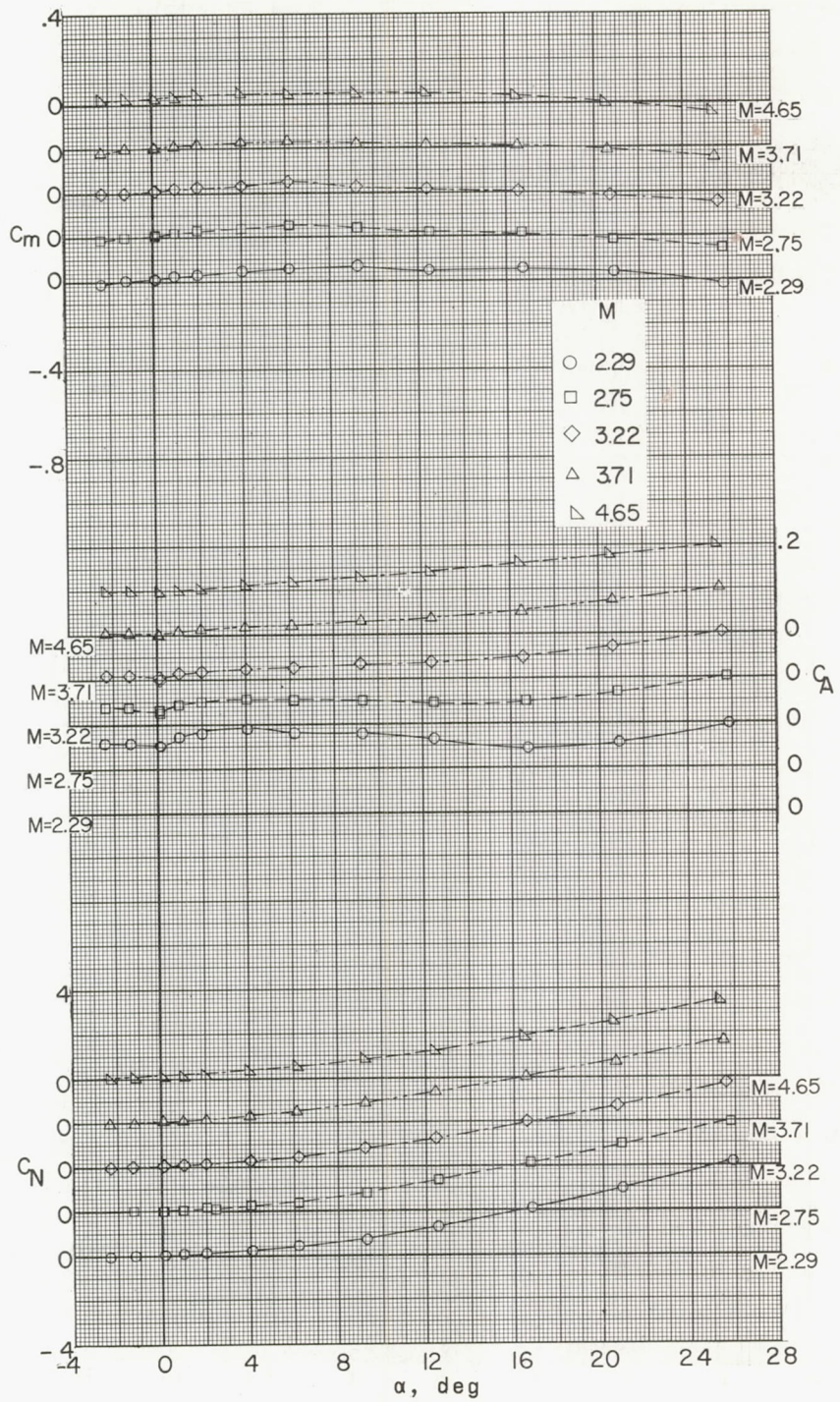

Figure 7.- Aerodynamic characteristics of model I in pitch. $\beta = 0^{o}$; $R = 12.5 \times 10^{6}$.

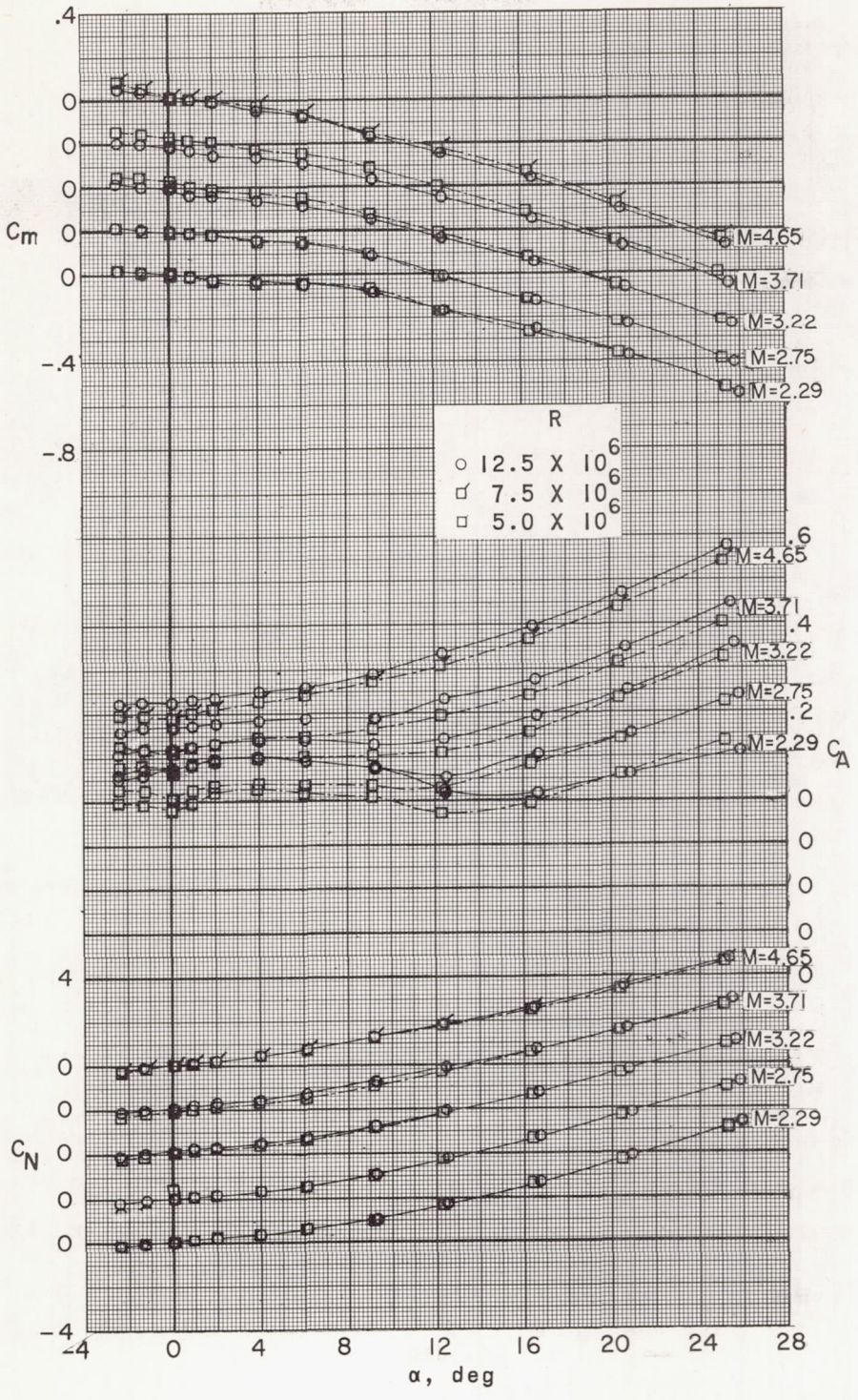

Figure 8.- Aerodynamic characteristics of model II in pitch. $\beta = 0^\circ$.

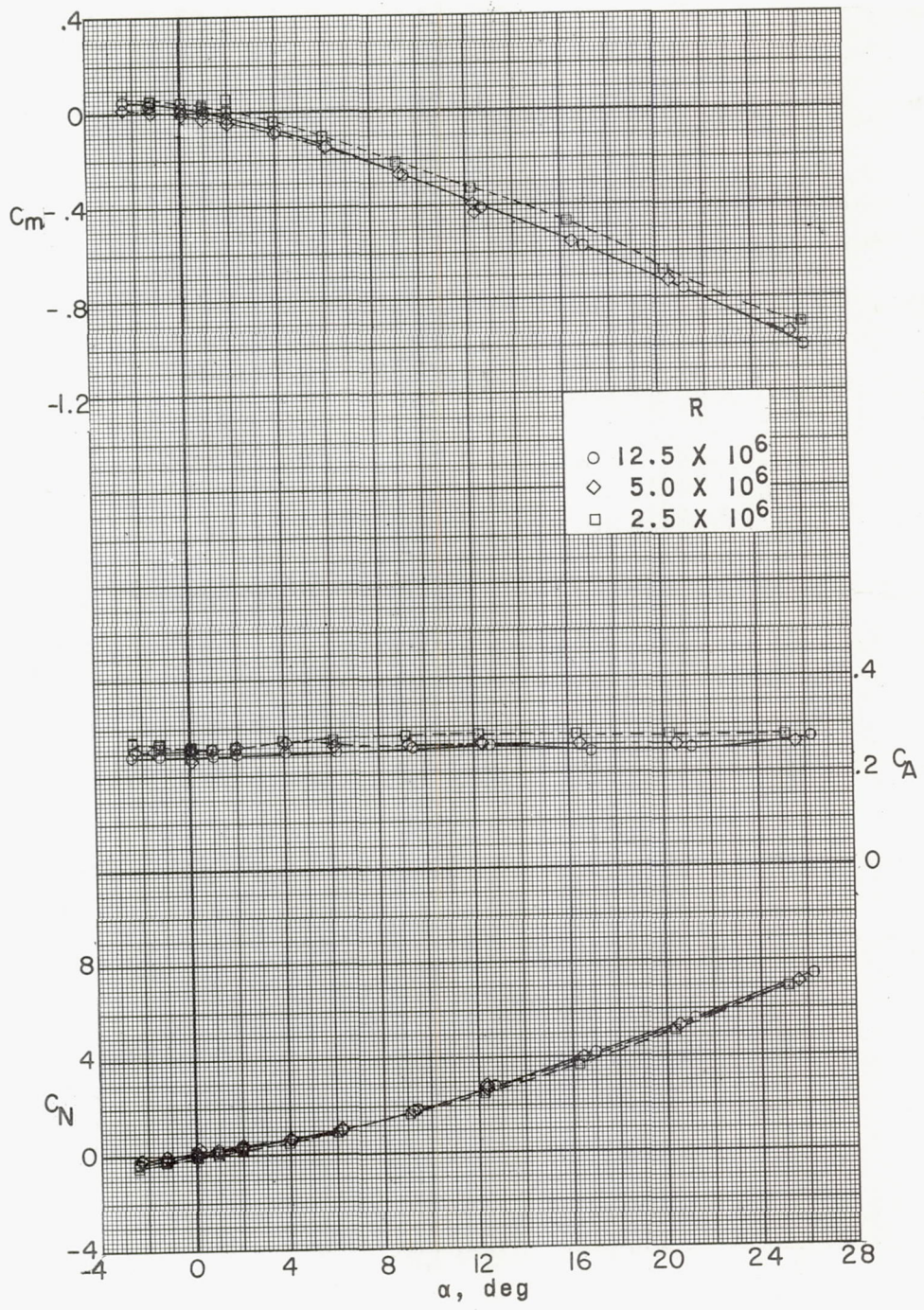

(a) M = 2.29.

Figure 9.- Aerodynamic characteristics of model III in pitch. $\beta = 0^\circ$.

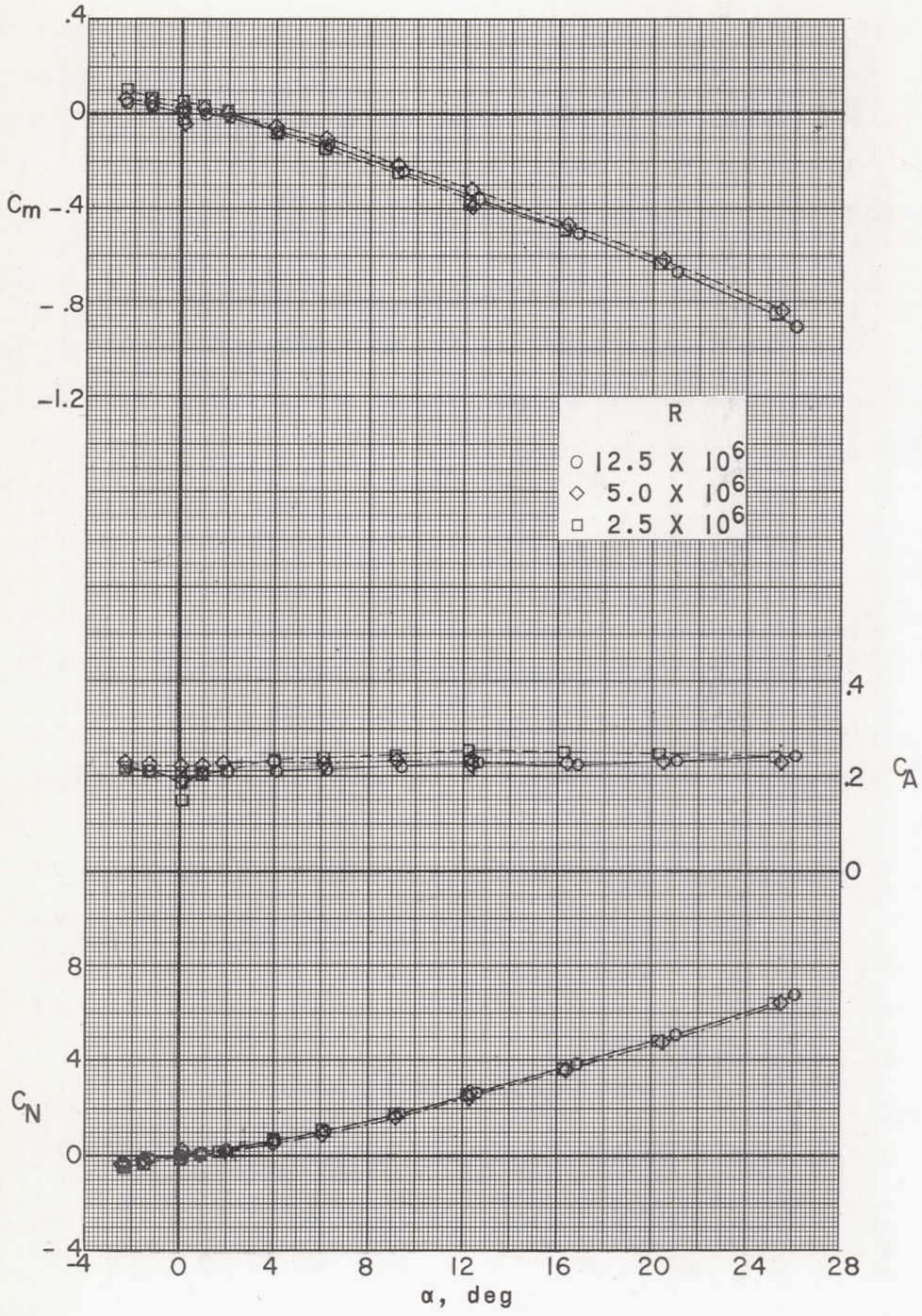

(b) M = 2.75.

Figure 9.- Continued.

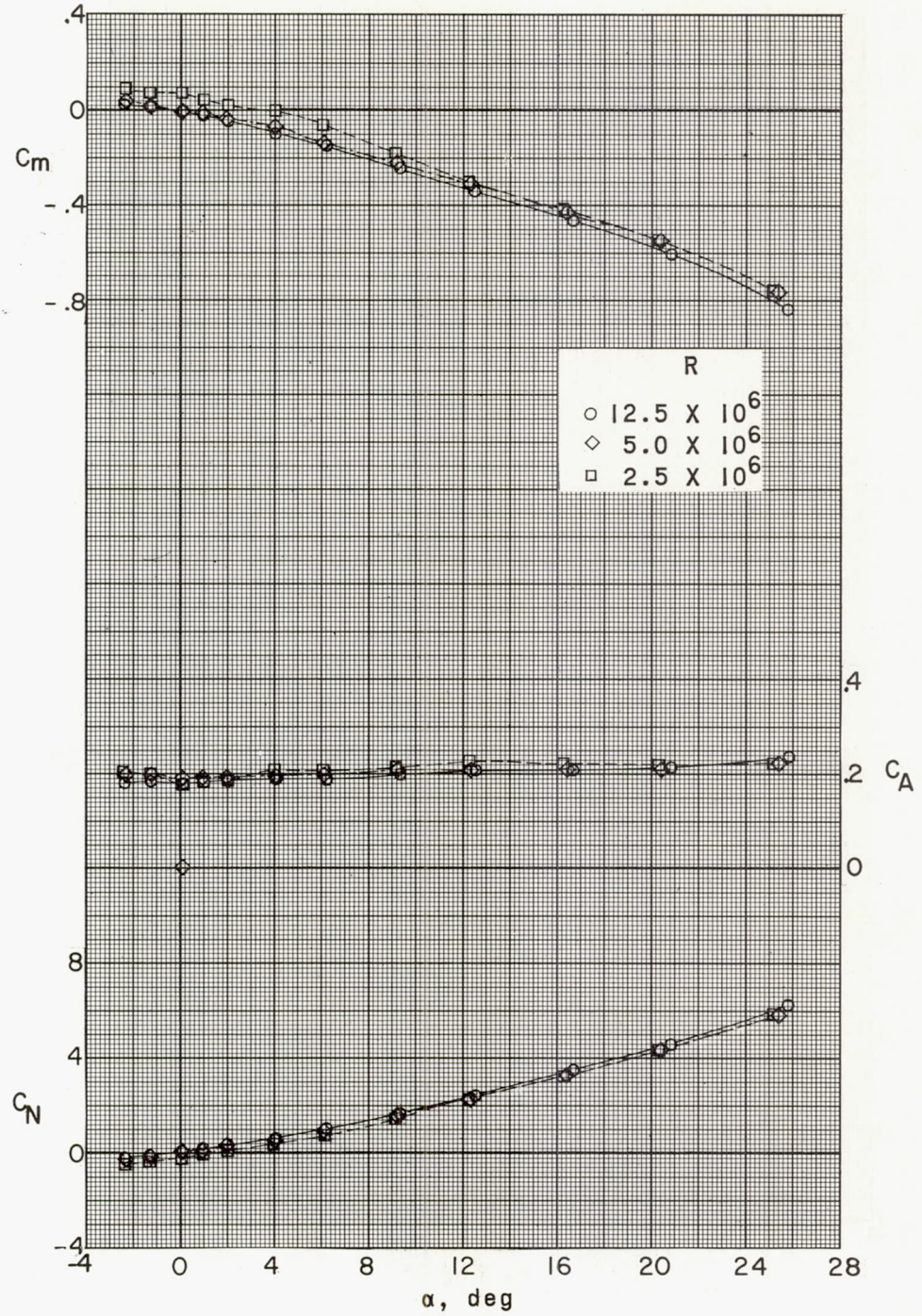

(c) M = 3.22.

Figure 9.- Continued.

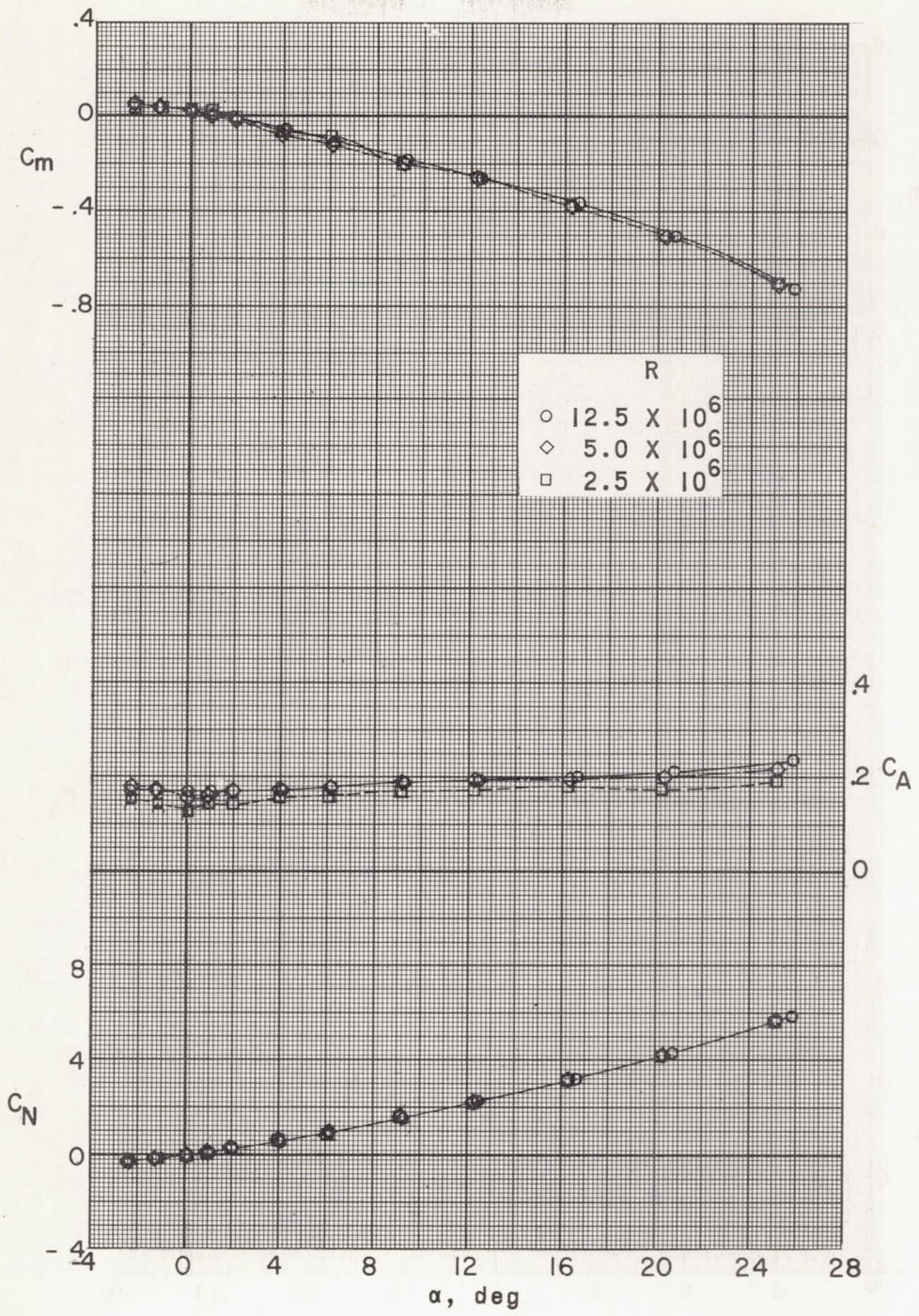

(d) M = 3.71.

Figure 9.- Continued.

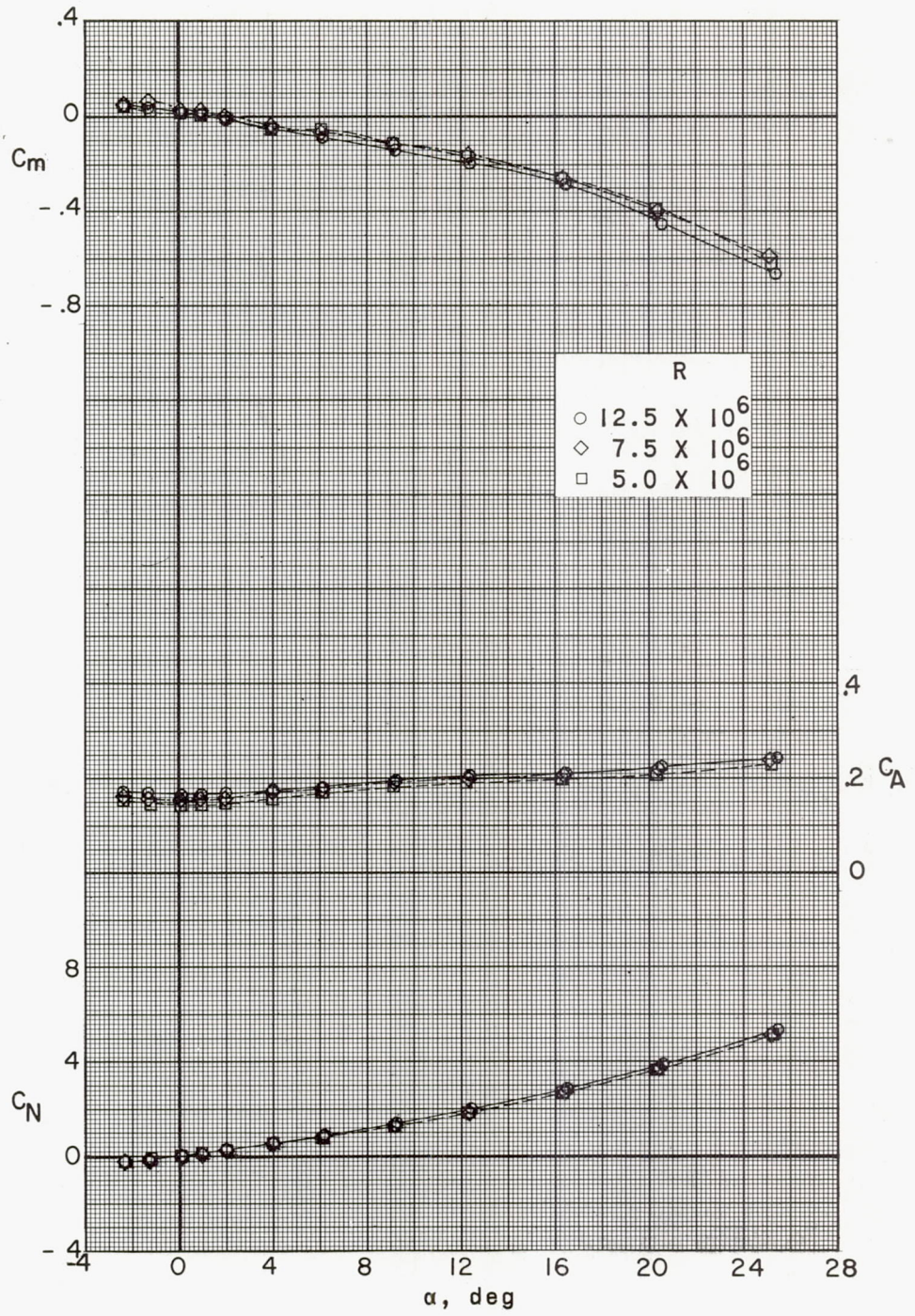

(e) M = 4.65.

Figure 9.- Concluded.

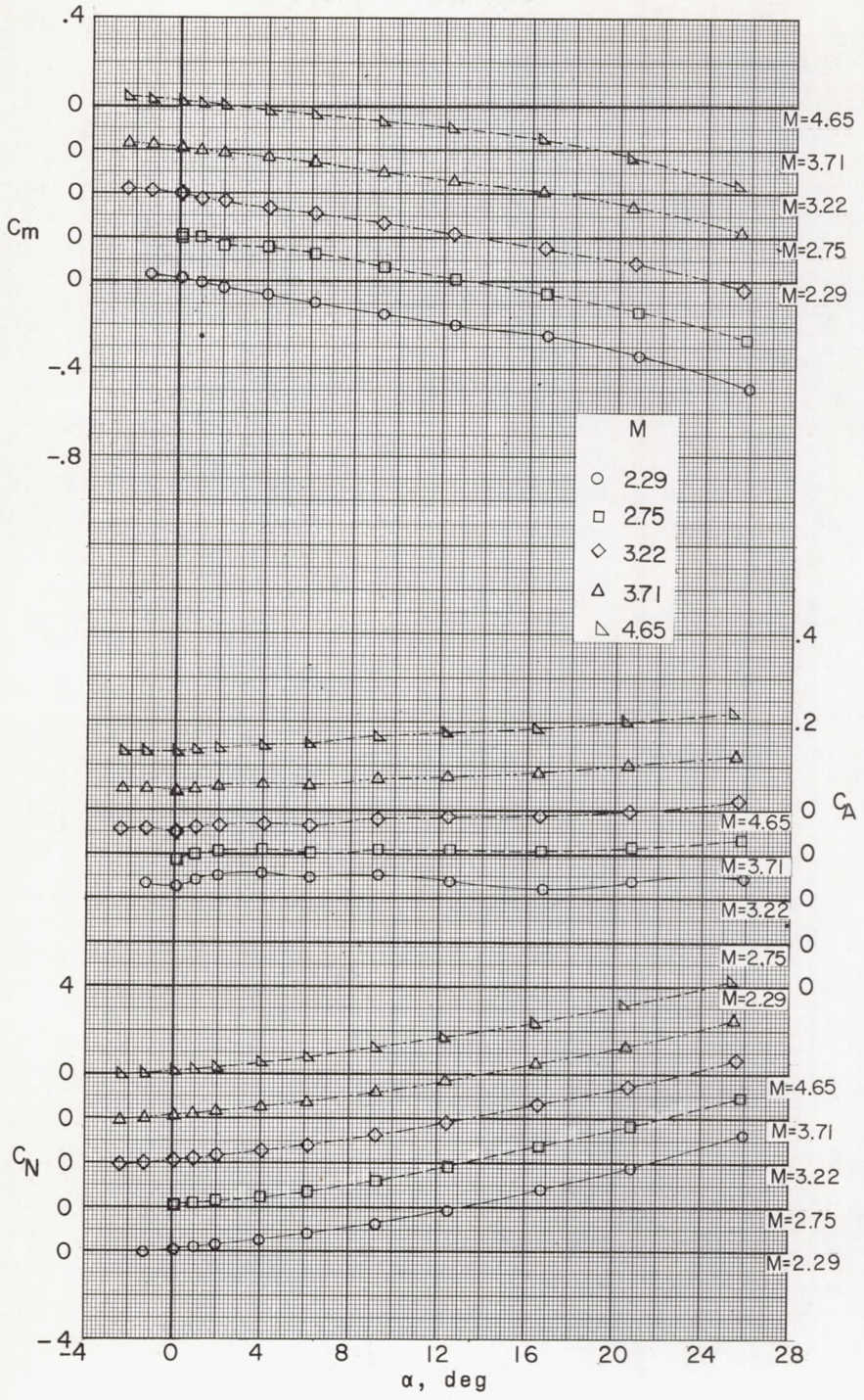

Figure 10.- Aerodynamic characteristics of model IV in pitch. $\beta = 0^{\circ}$; $R = 12.5 \times 10^{6}$.

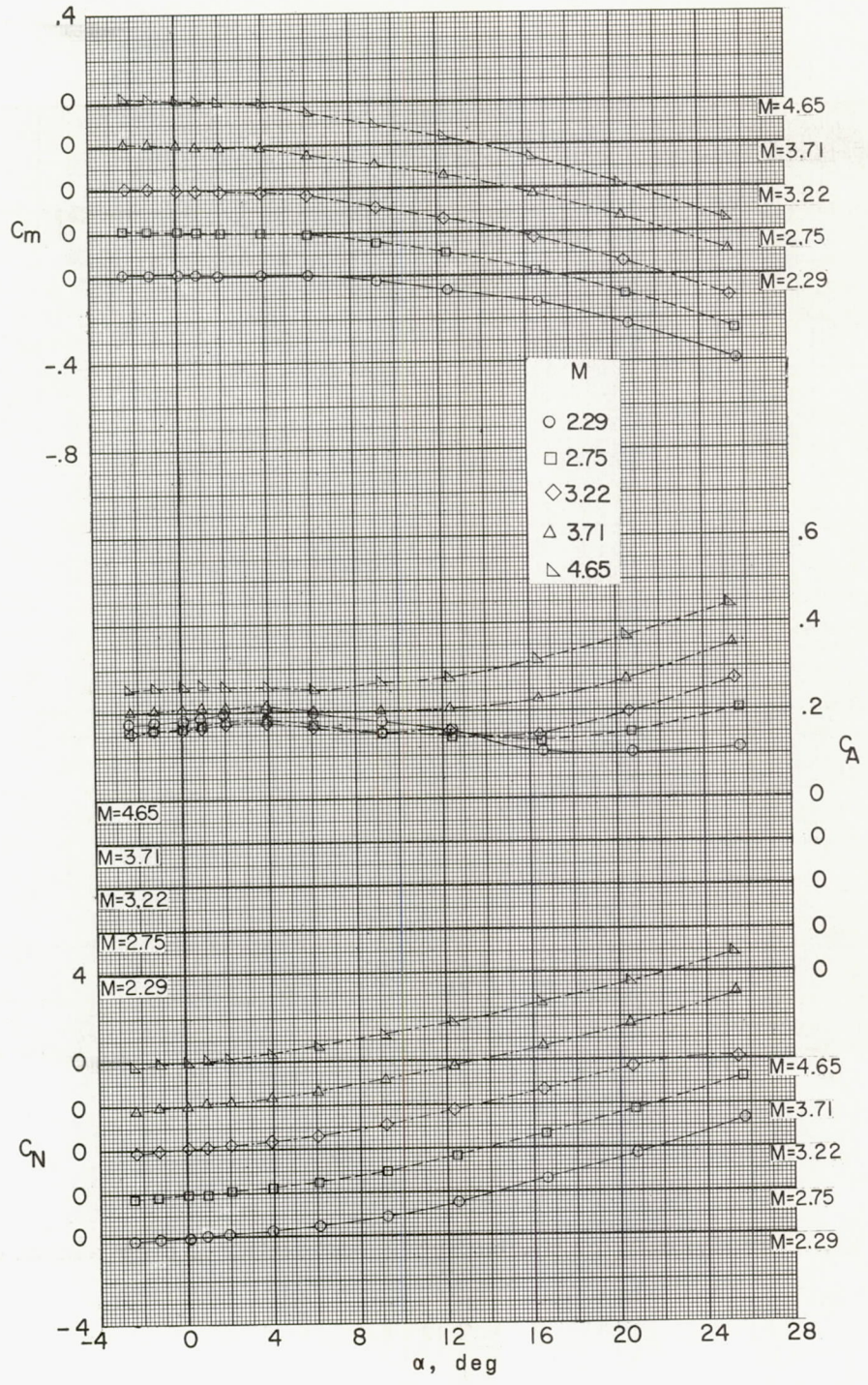

Figure 11.- Aerodynamic characteristics of model V in pitch. $\beta = 0^{\circ}$; $R = 15 \times 10^{6}$.

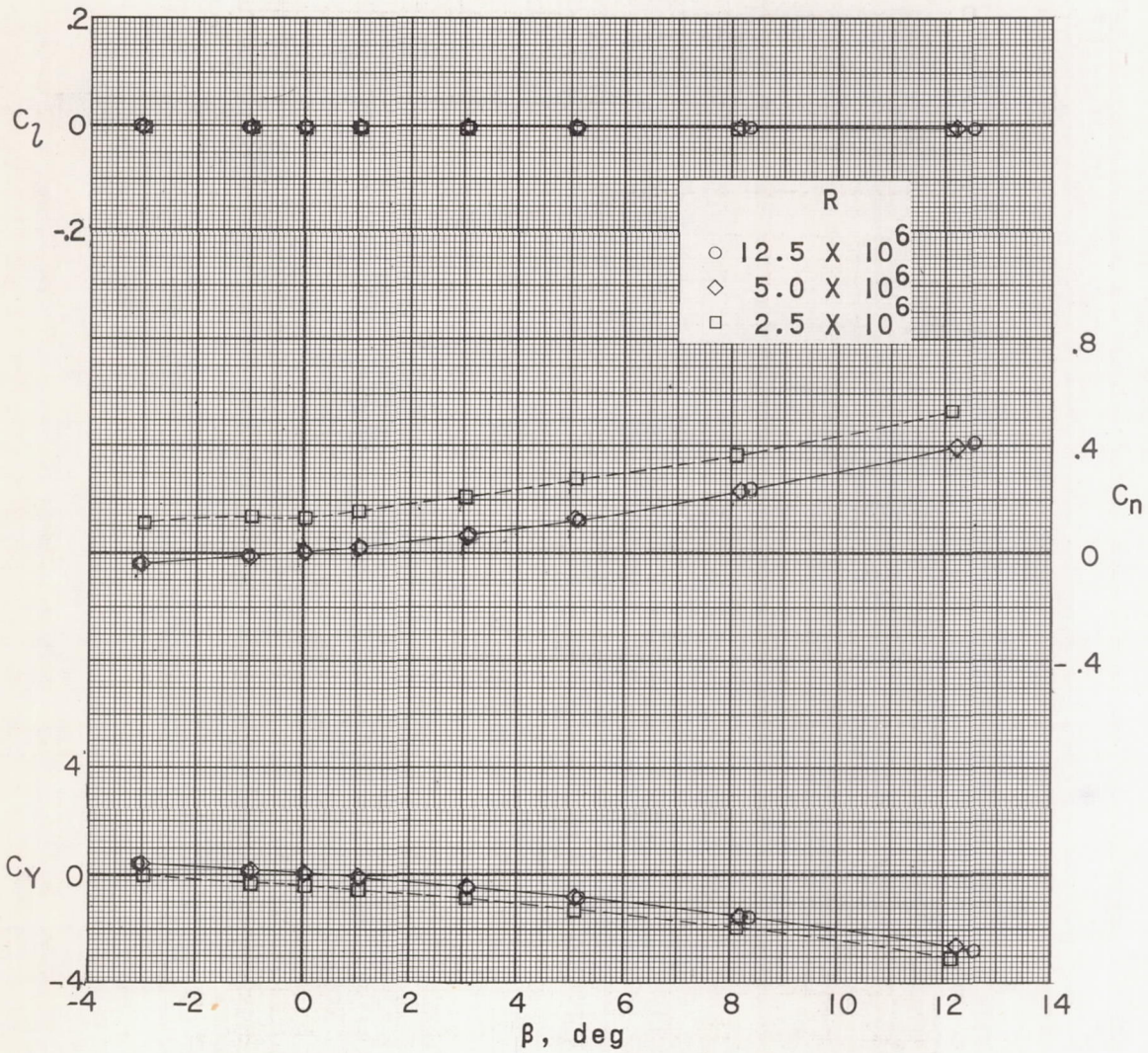

(a) M = 2.29.

Figure 12.- Aerodynamic characteristics of model III in sideslip. $\alpha = 0^\circ$.

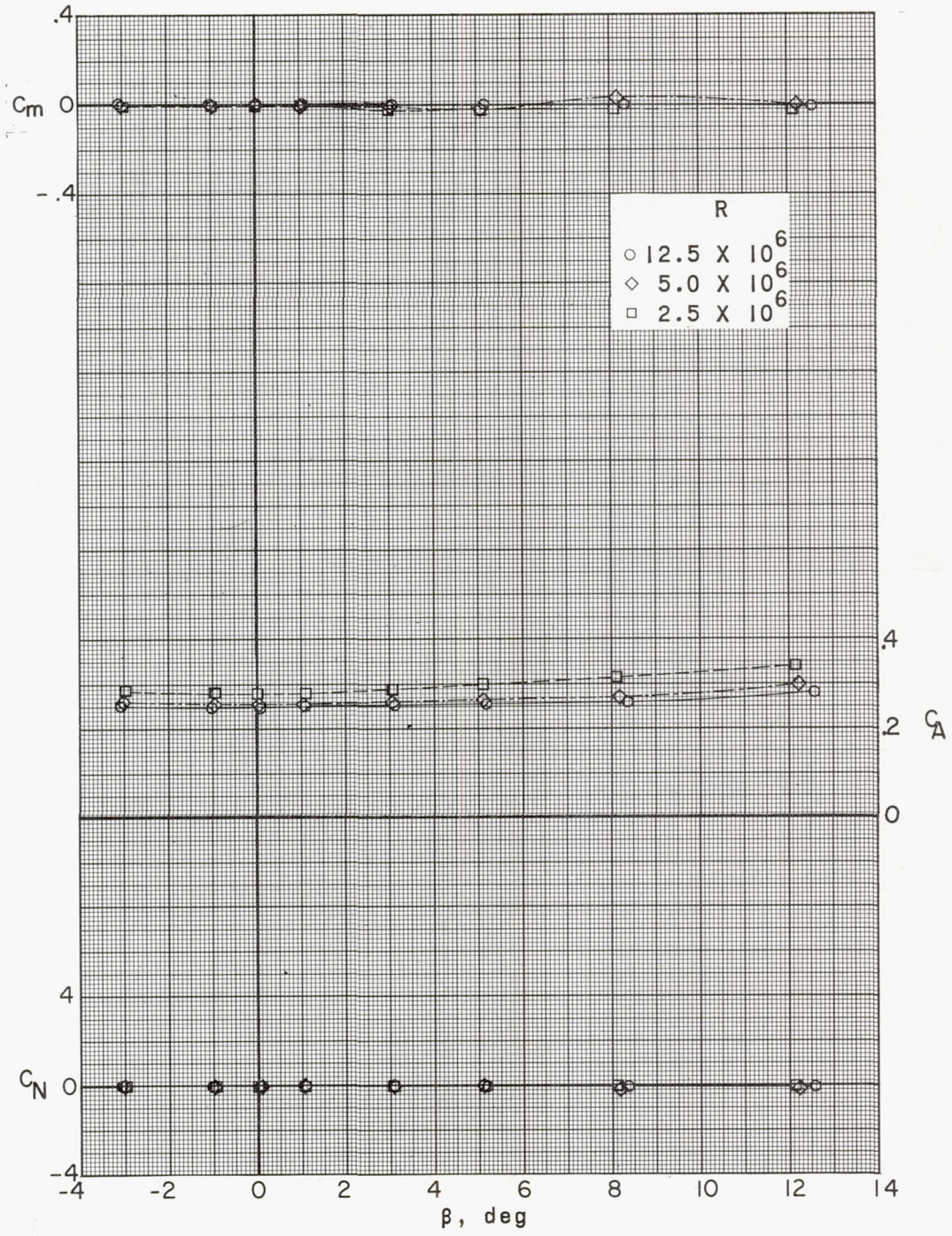

(a) Concluded.

Figure 12.- Continued.

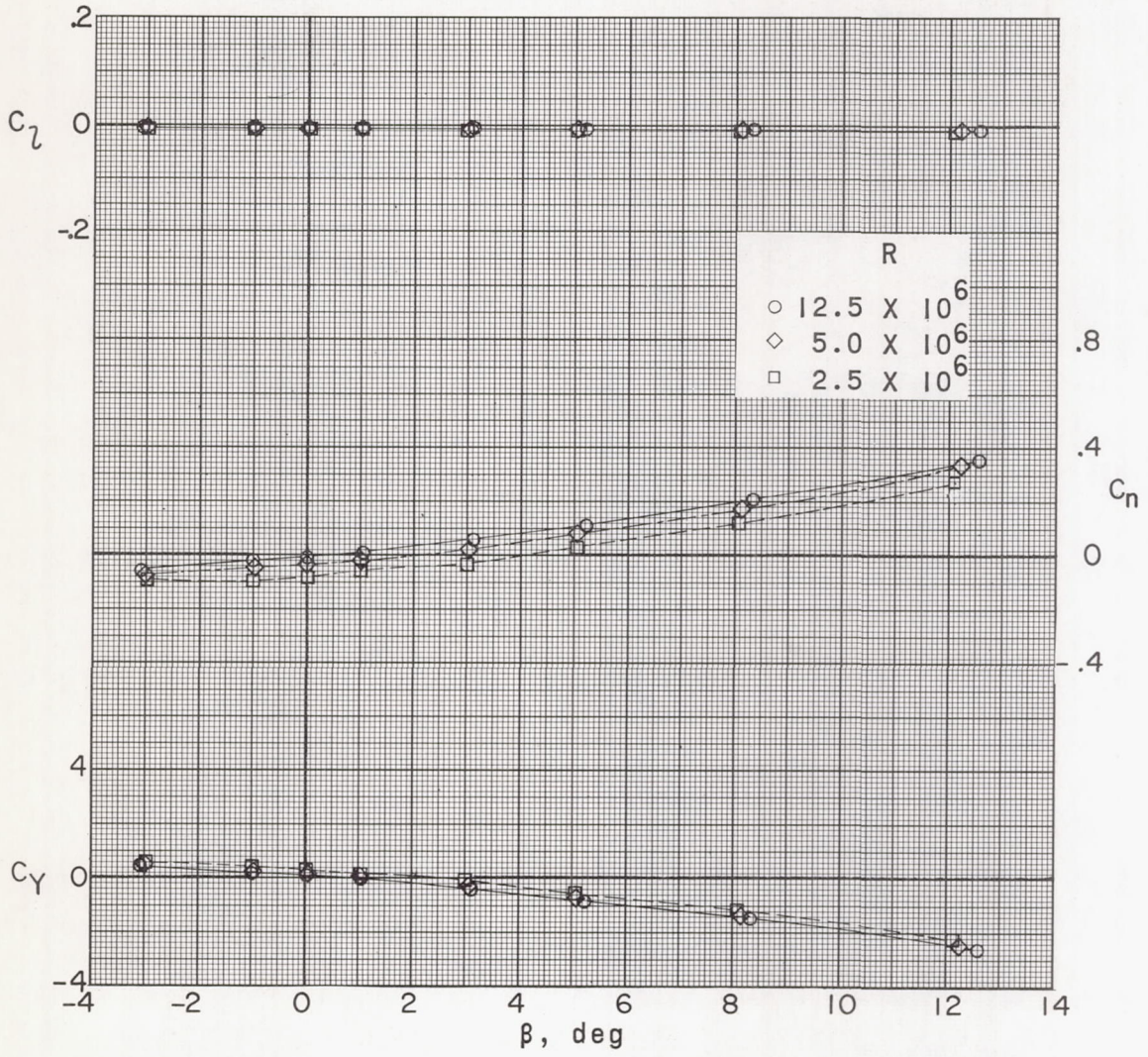

(b) M = 2.75.

Figure 12.- Continued.

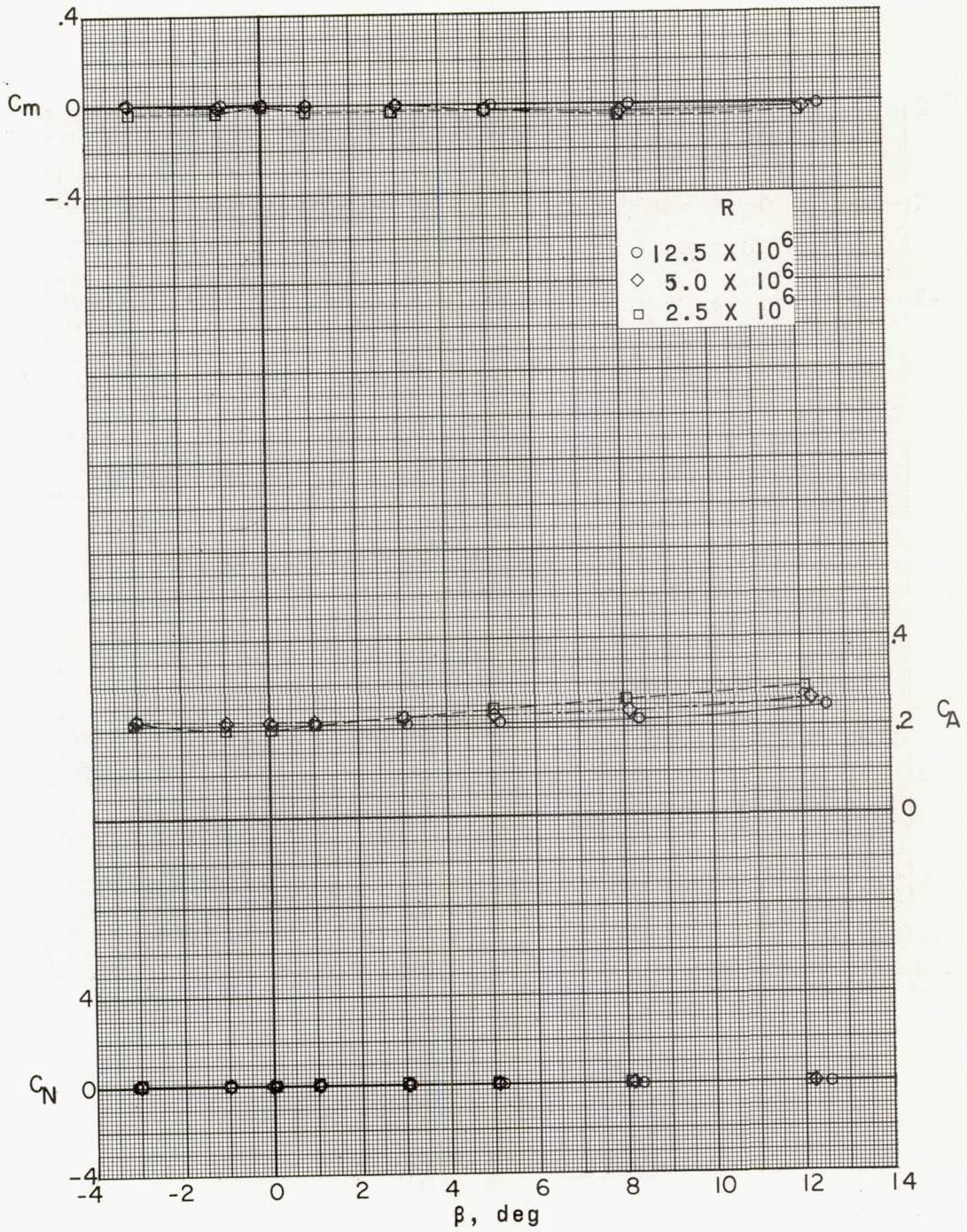

(b) Concluded.

Figure 12.- Continued.

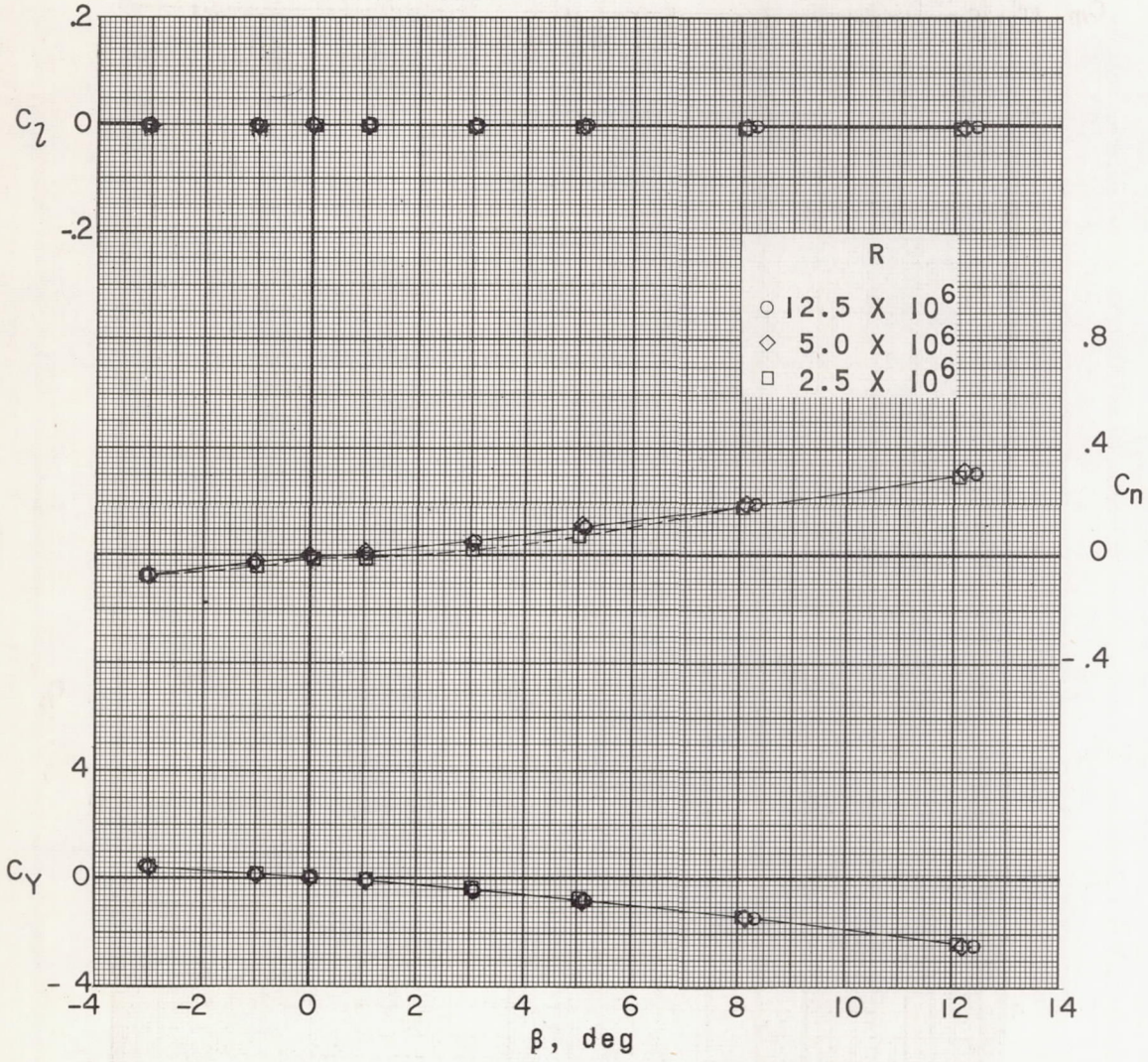

(c) M = 3.22.

Figure 12.- Continued.

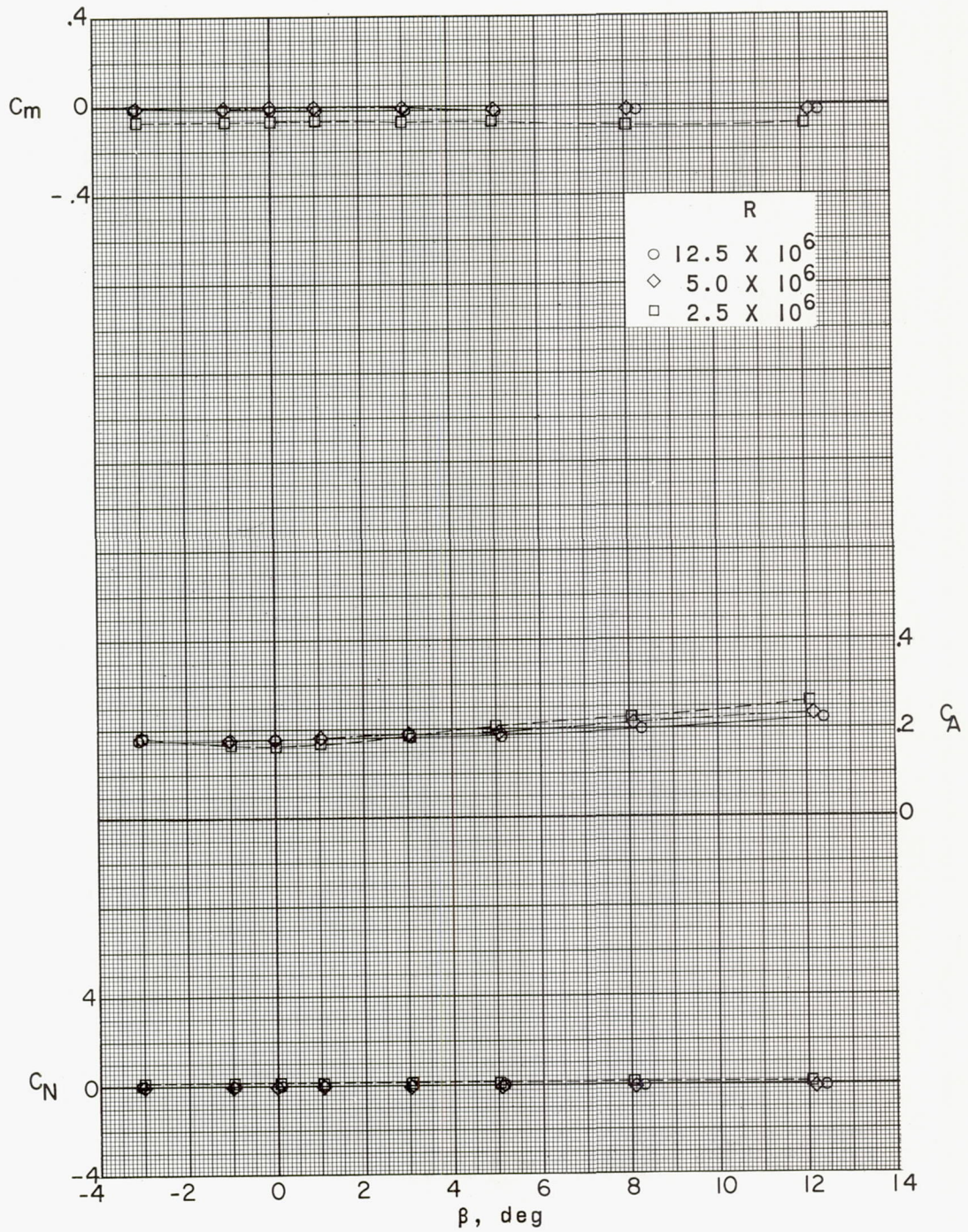

(c) Concluded.

Figure 12.- Continued.

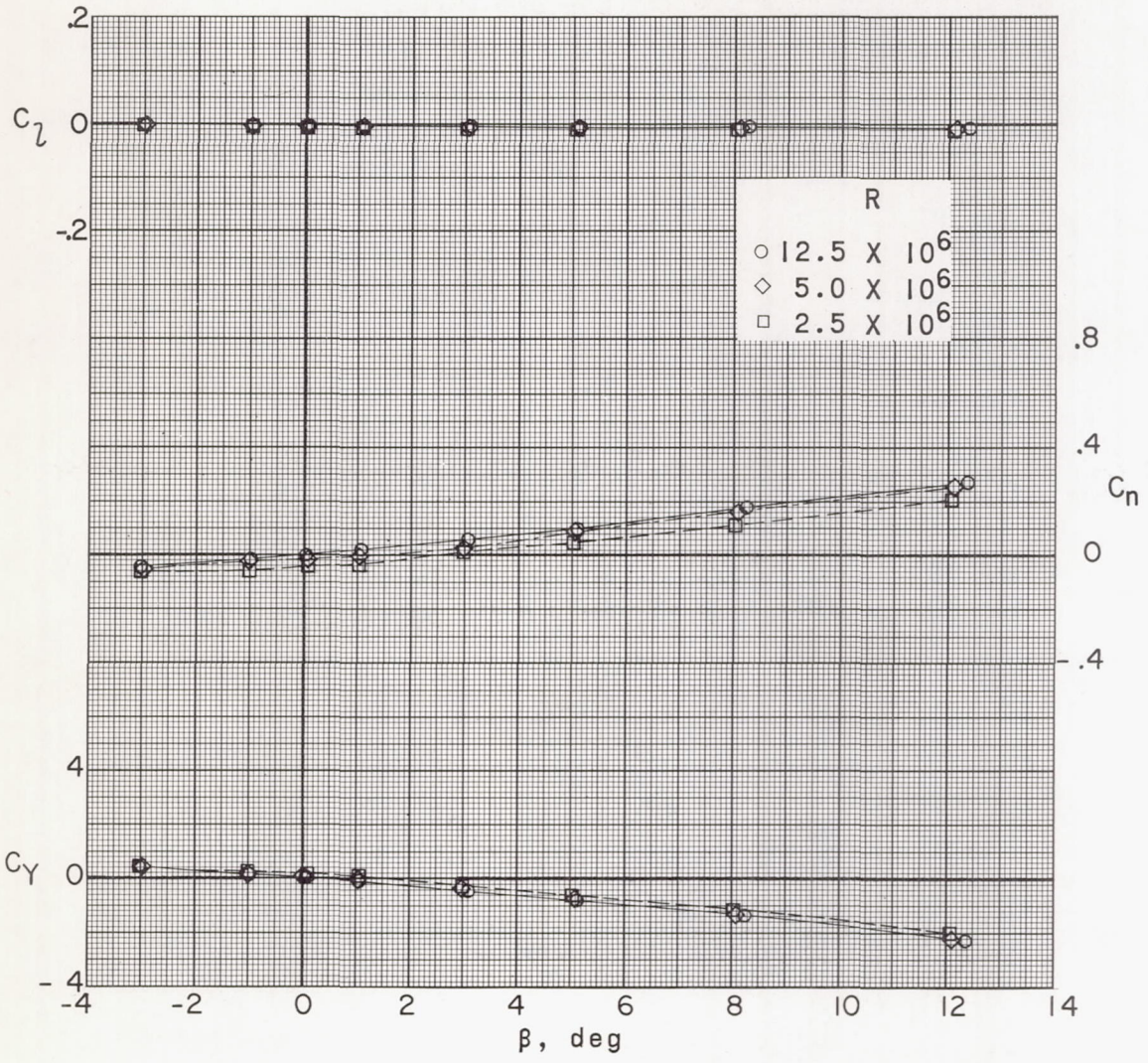

(d) M = 3.71.

Figure 12.- Continued.

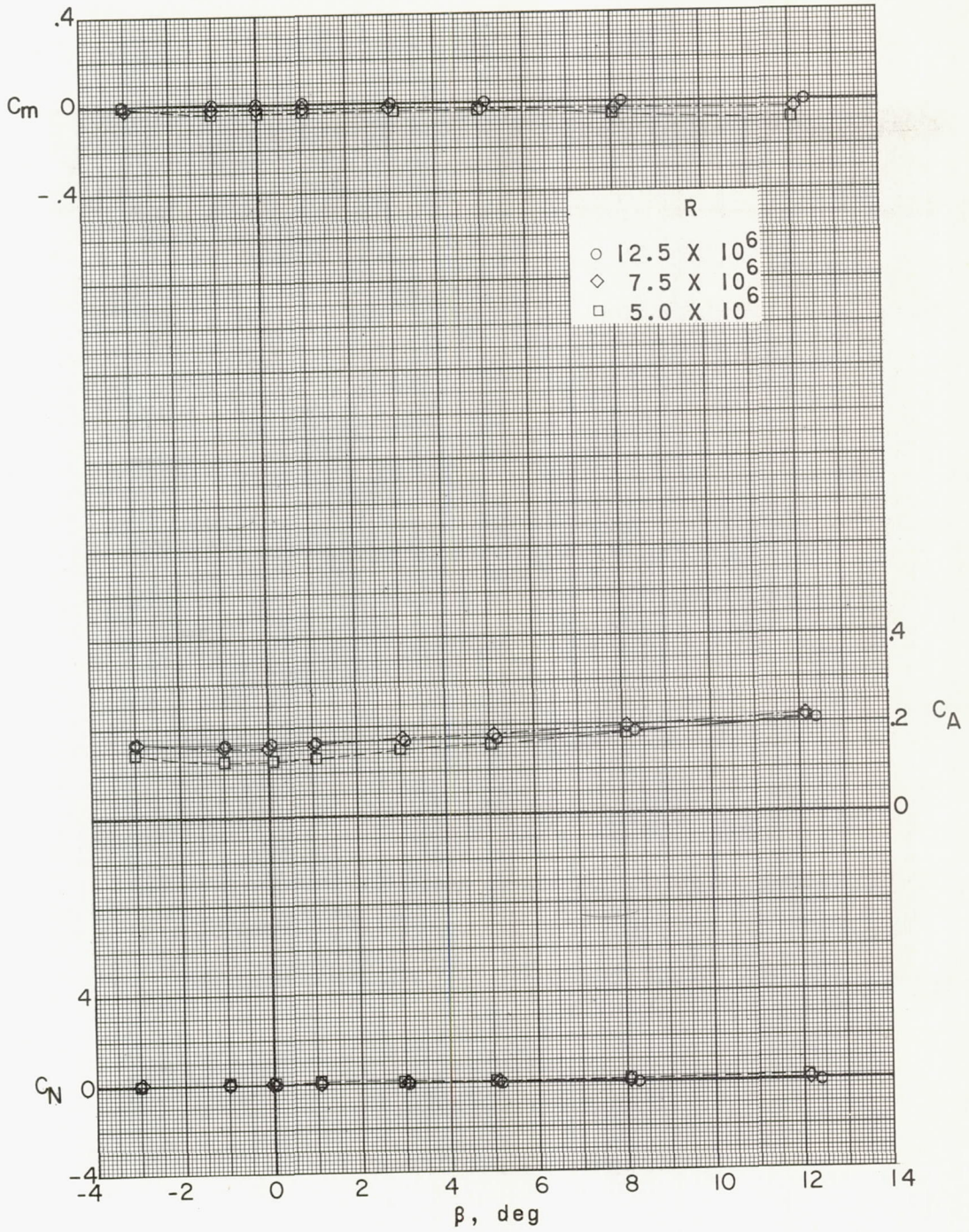

(d) Concluded.

Figure 12.- Continued.

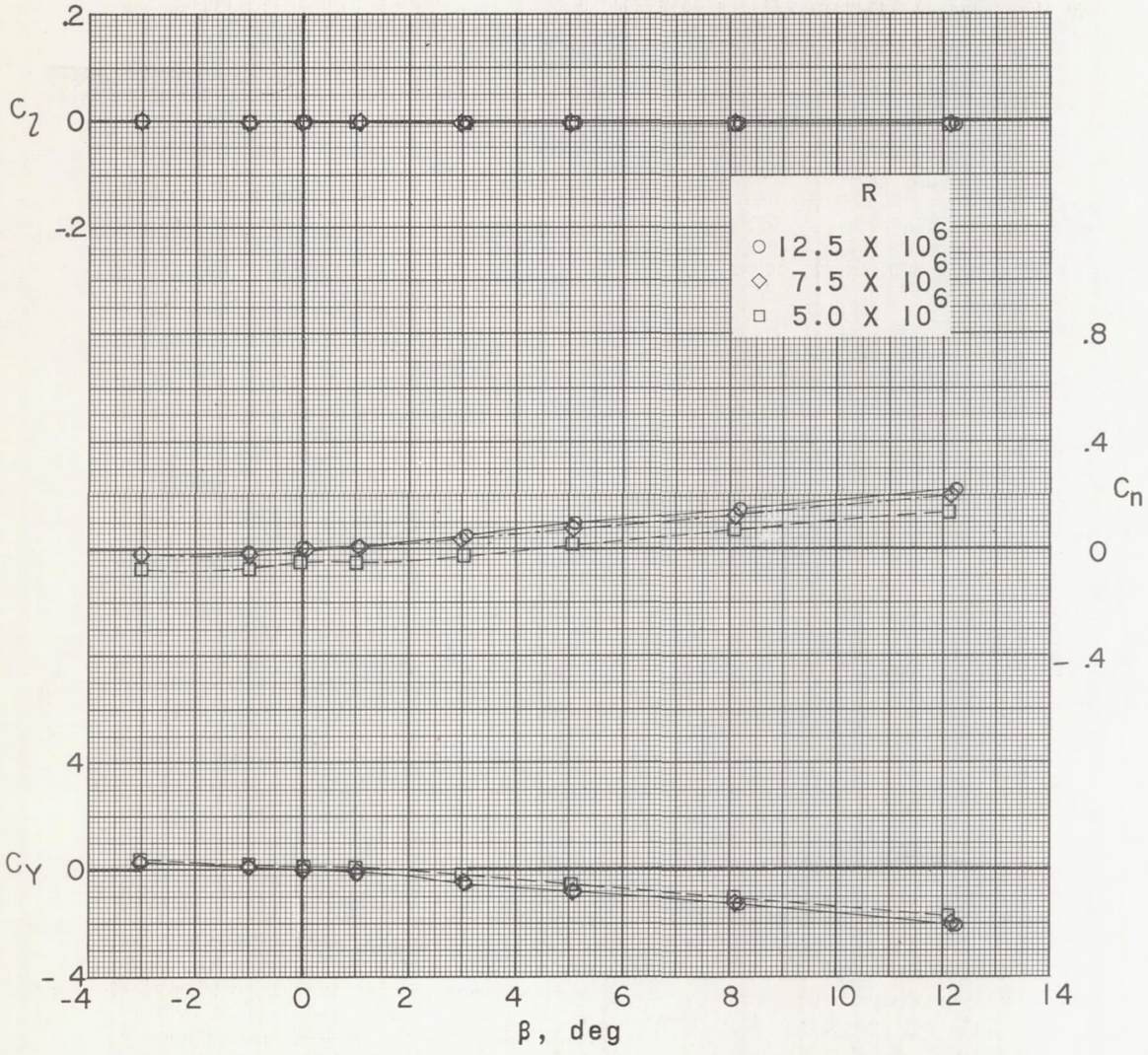

(e) M = 4.65.

Figure 12.- Continued.

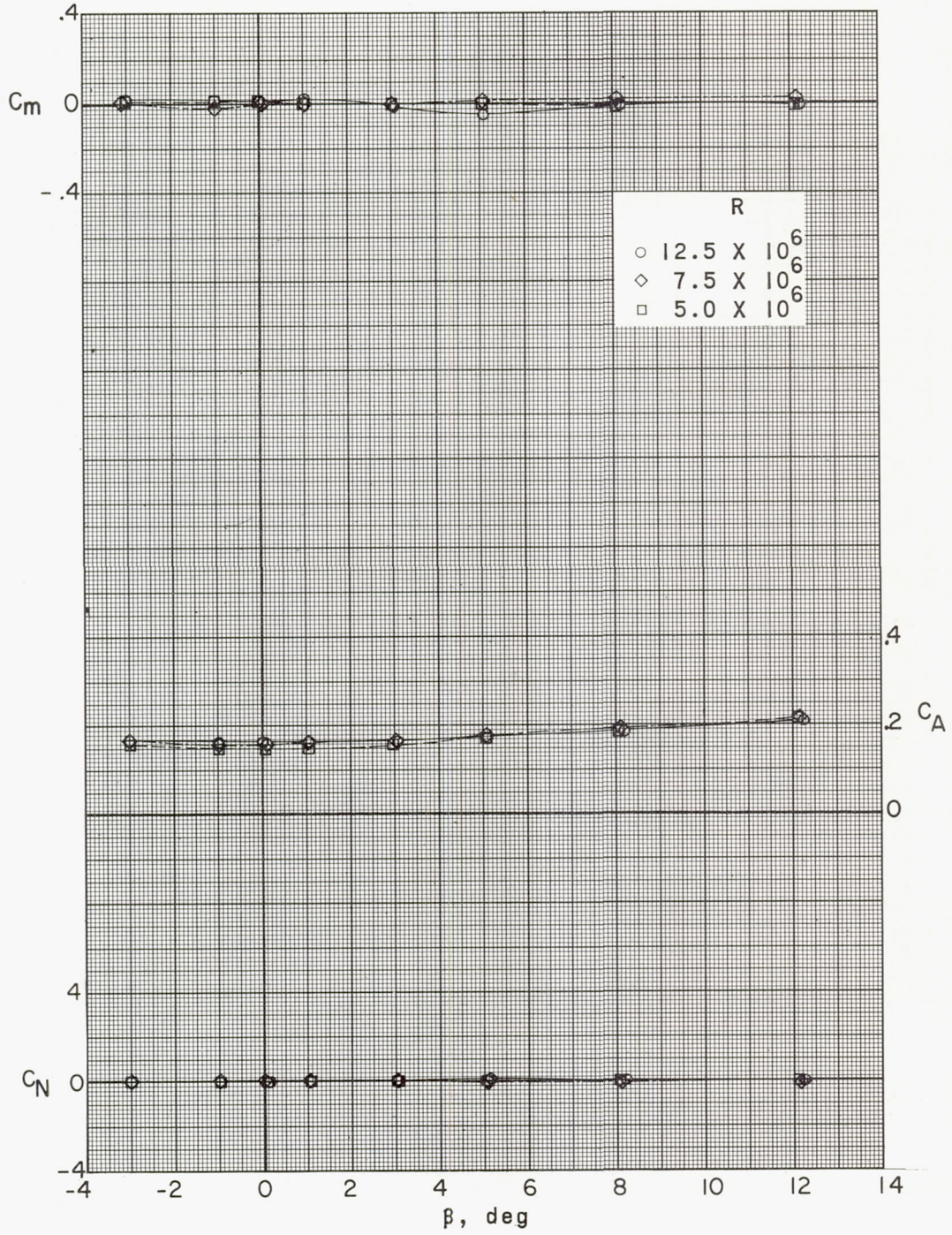

(e) Concluded.

Figure 12.- Concluded.

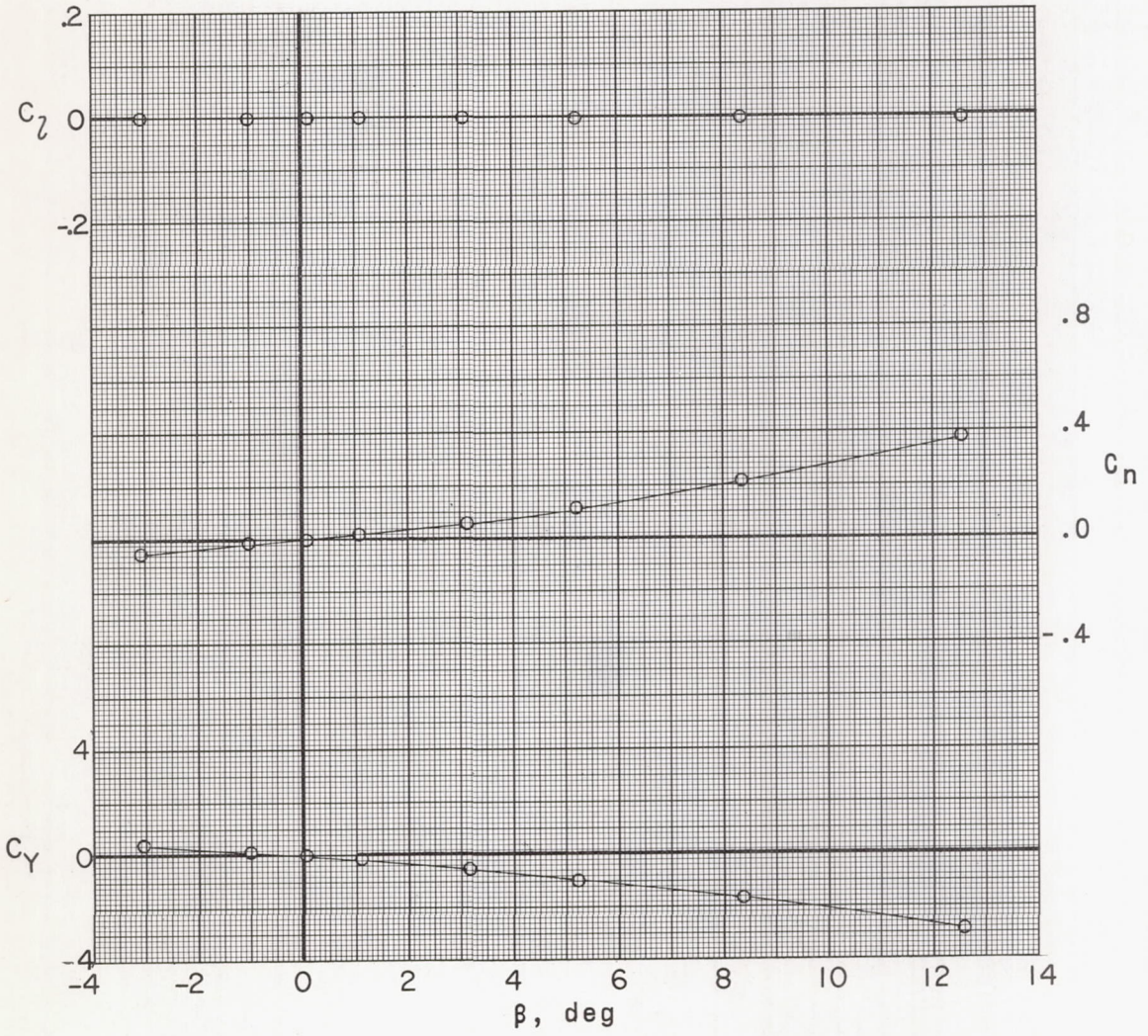

(a) M = 2.29.

Figure 13.- Aerodynamic characteristics of model III in sideslip. $\alpha = 7.2^{\circ}$; $R = 12.5 \times 10^6$.

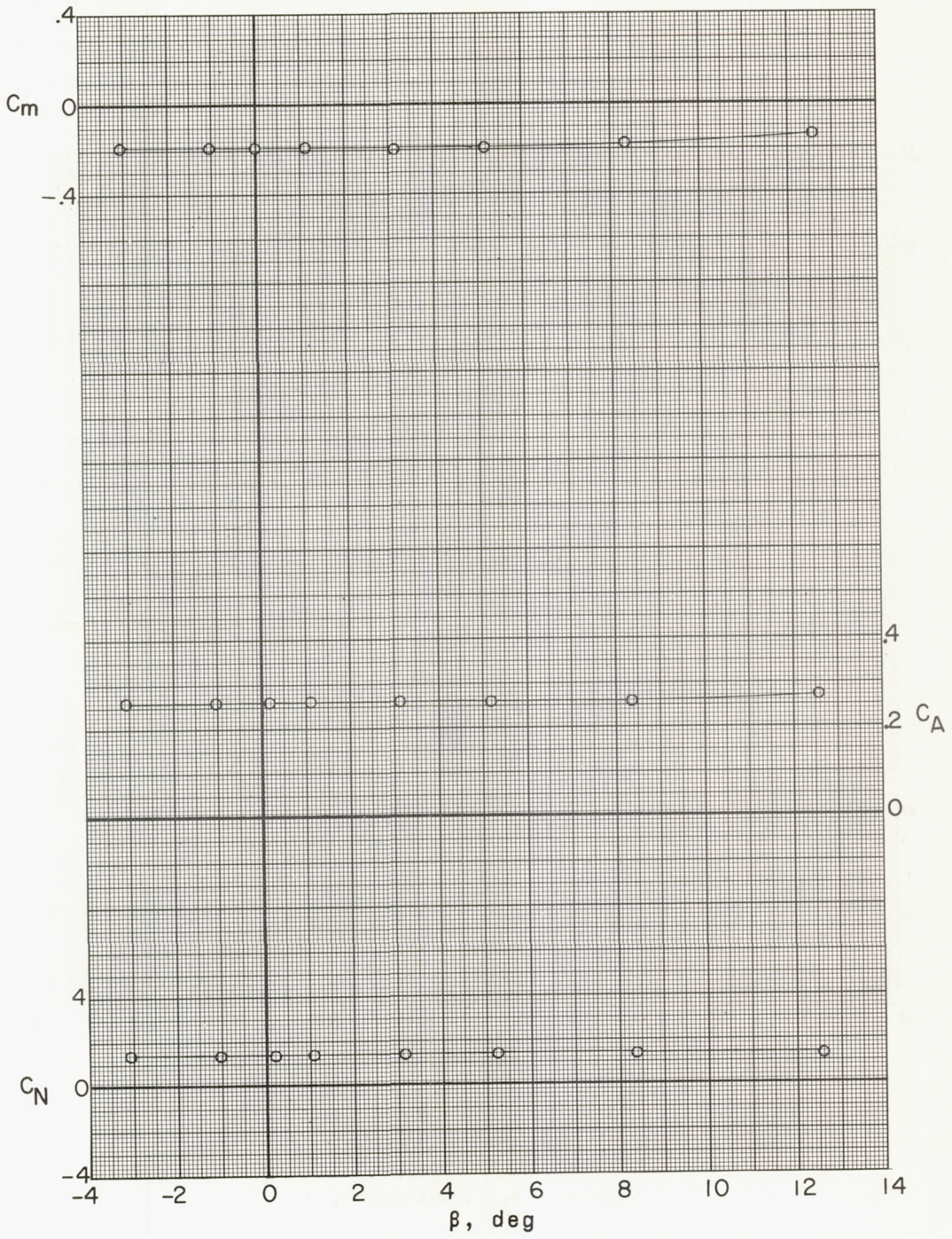

(a) Concluded.

Figure 13.- Continued.

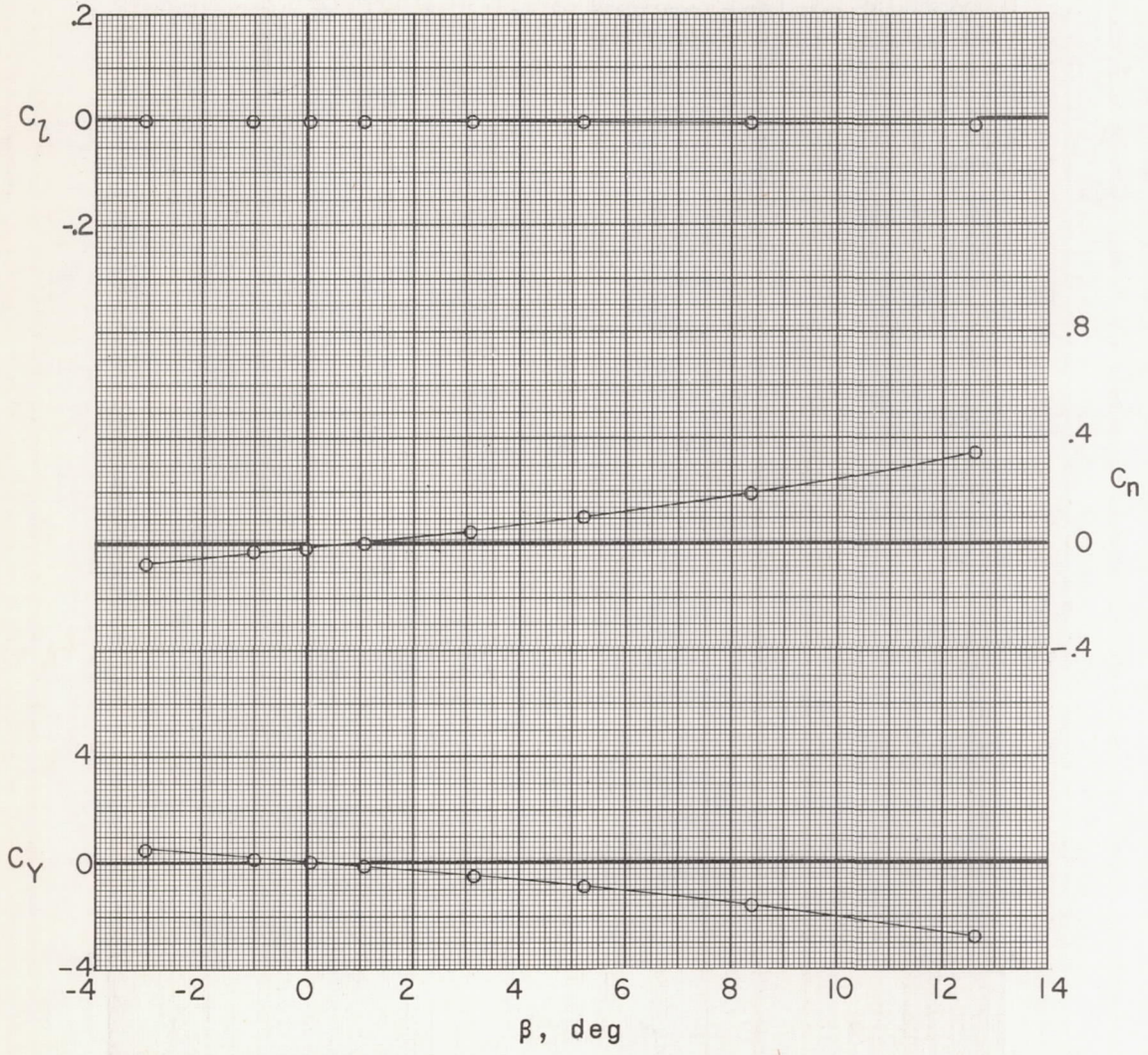

(b) M = 2.75.

Figure 13.- Continued.

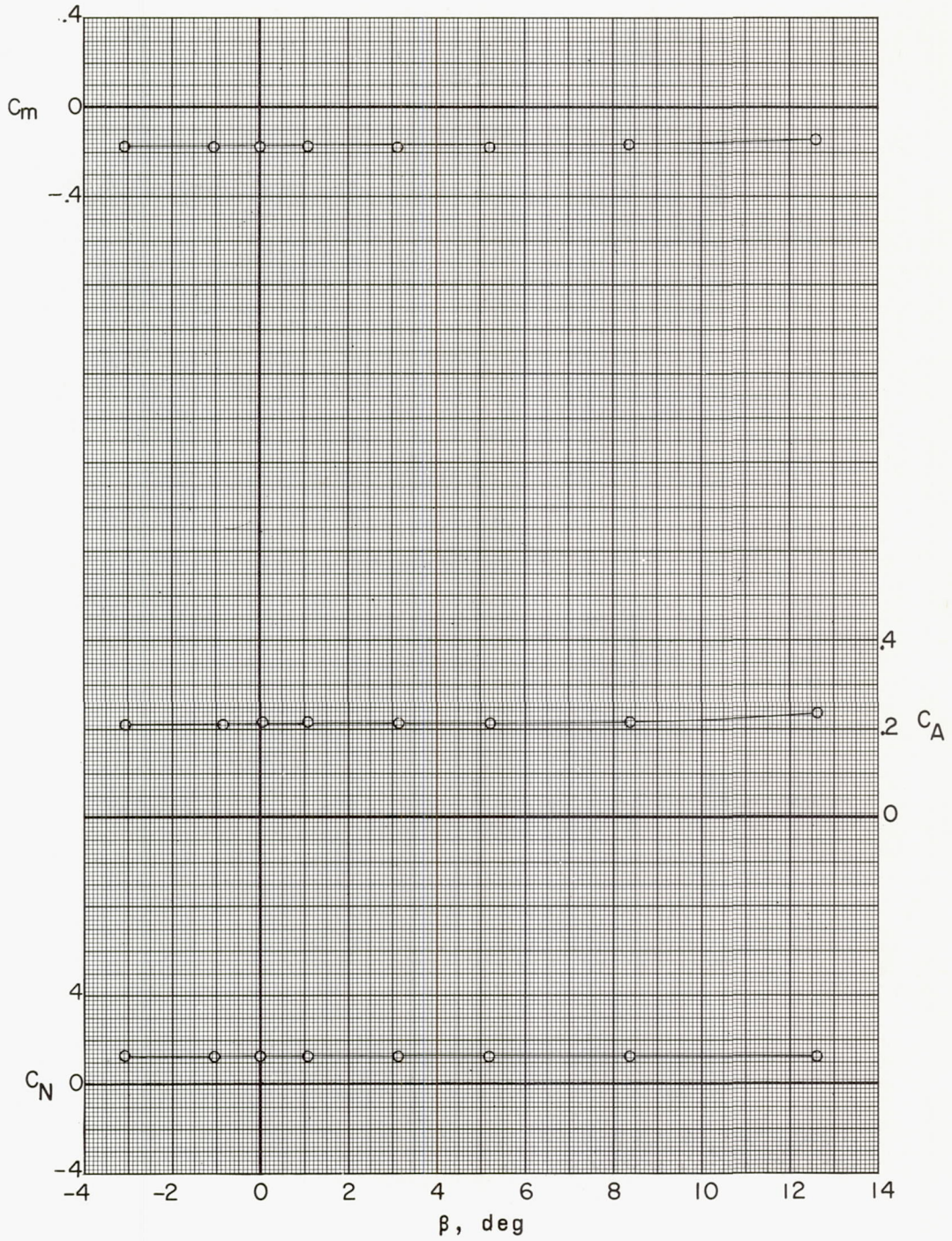

(b) Concluded.

Figure 13.- Continued.

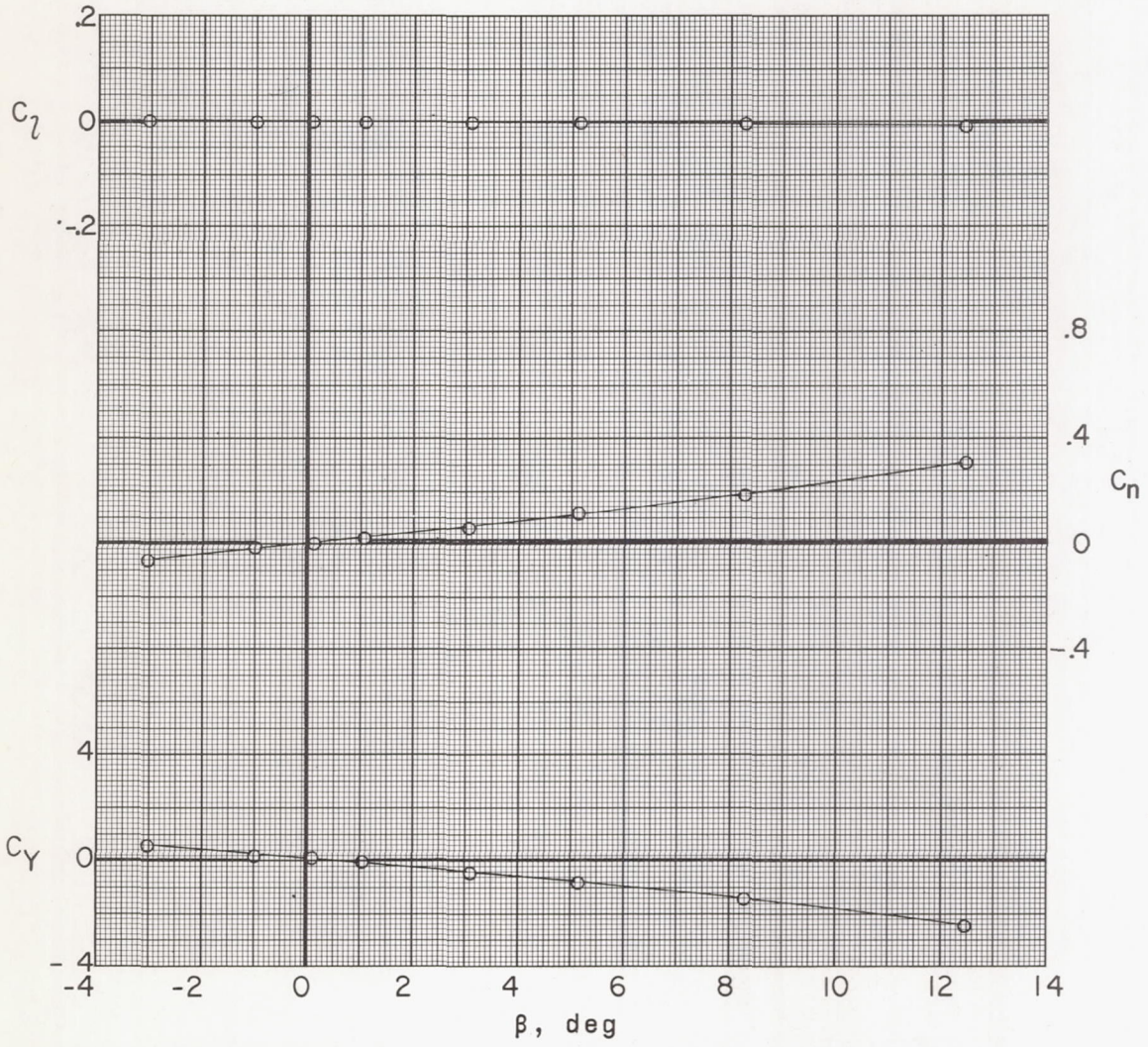

(c) M = 3.22.

Figure 13.- Continued.

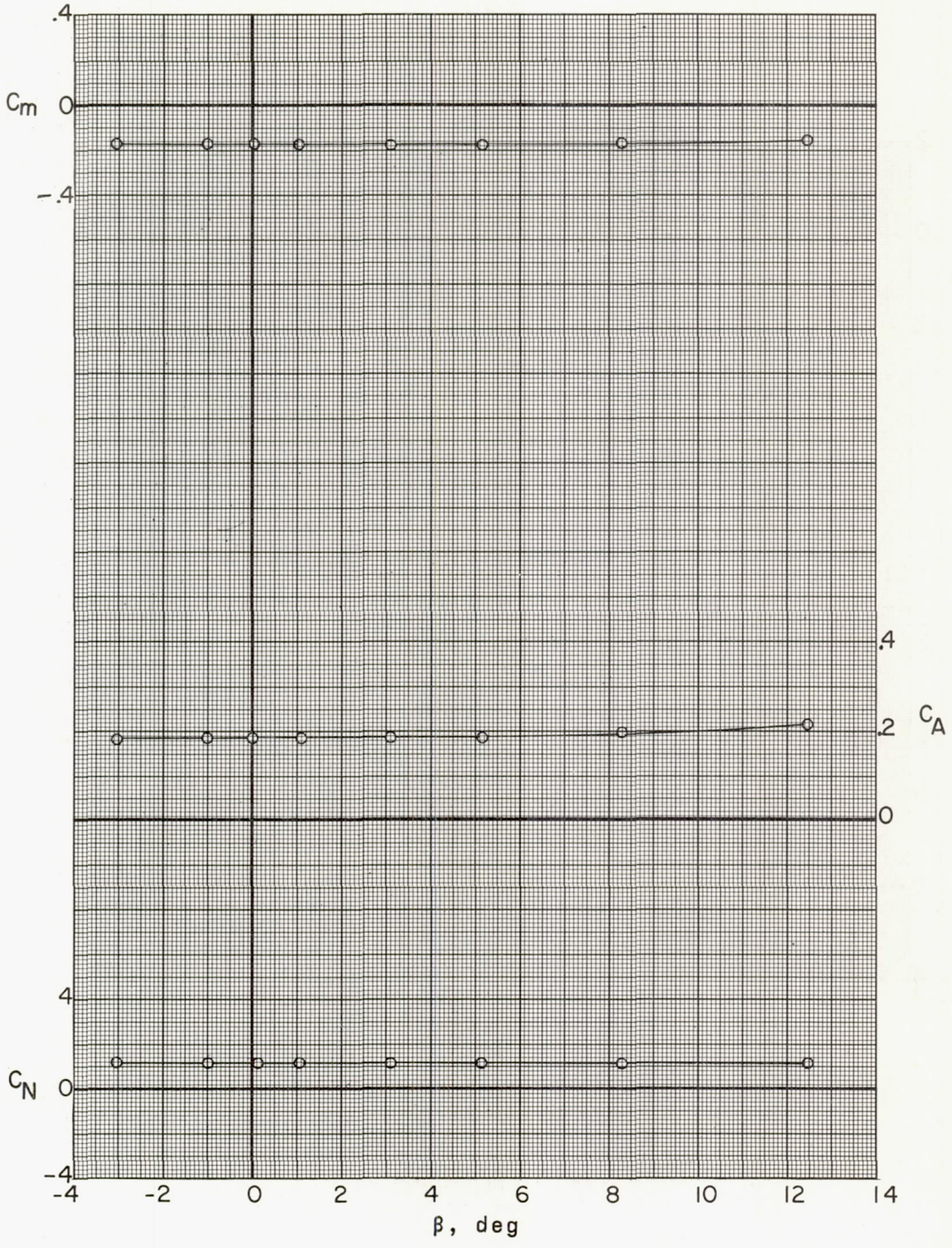

(c) Concluded.

Figure 13.- Continued.

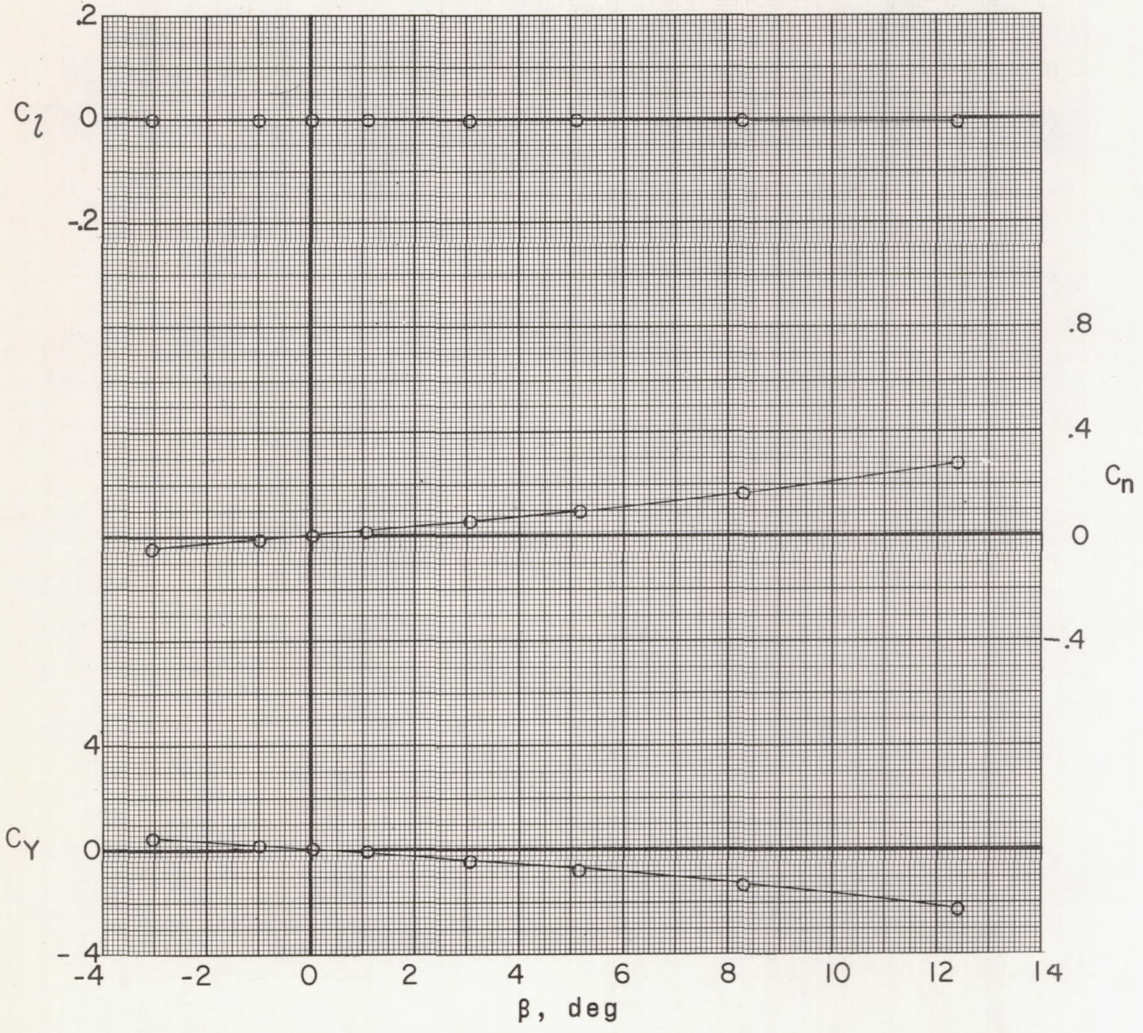

(d) M = 3.71.

Figure 13.- Continued.

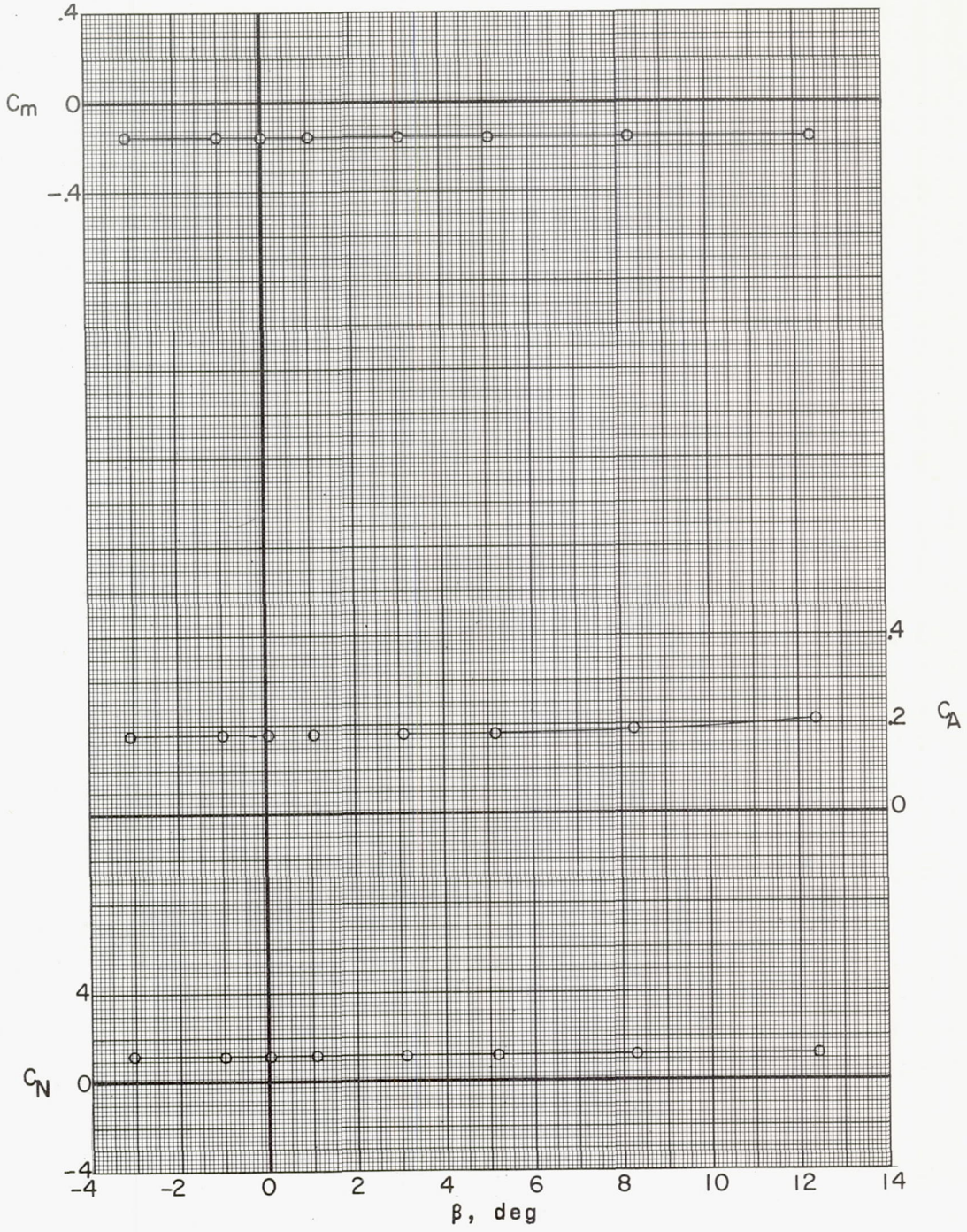

(d) Concluded.

Figure 13.- Continued.

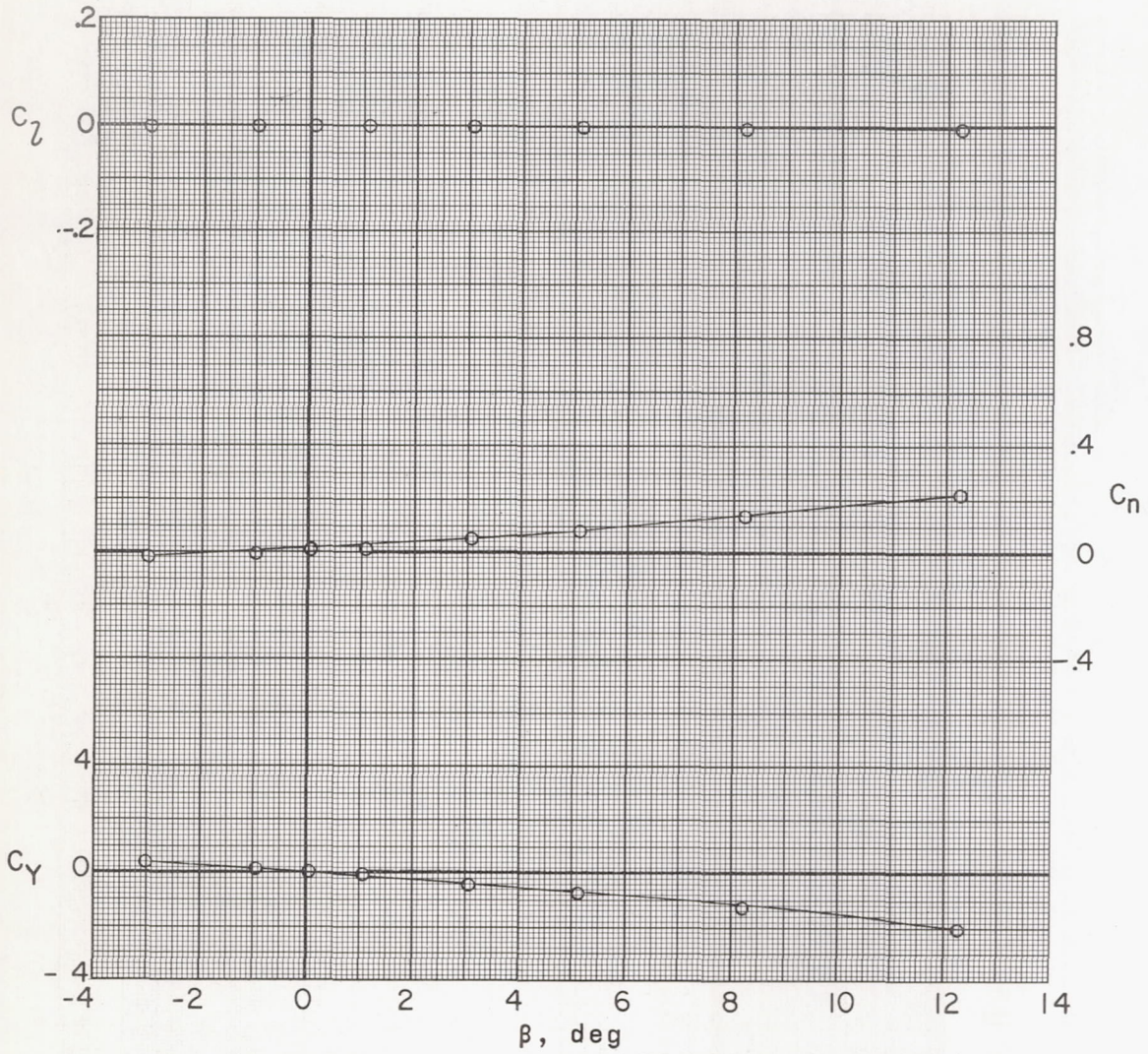

(e) M = 4.65.

Figure 13.- Continued.

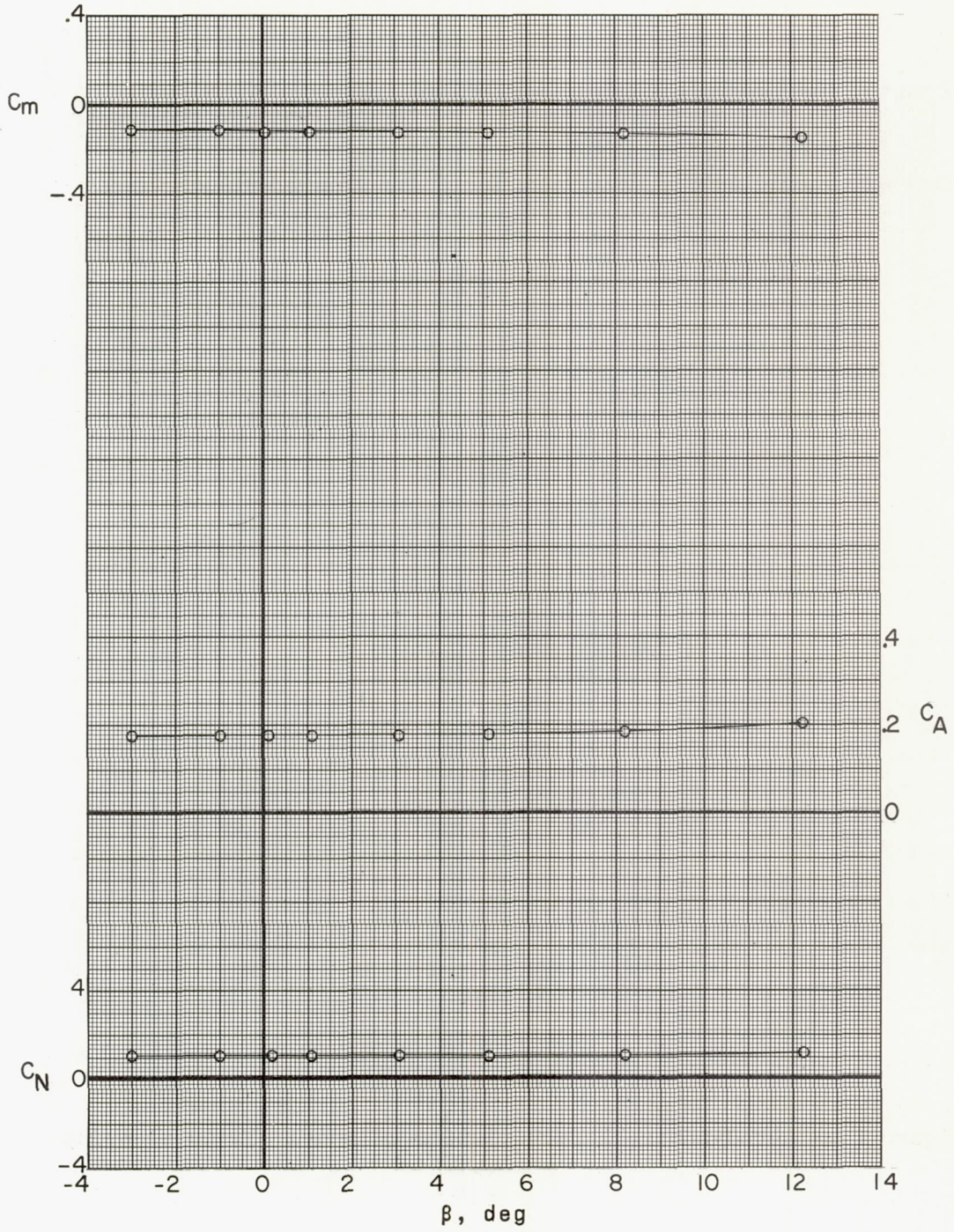

(e) Concluded.

Figure 13.- Concluded.

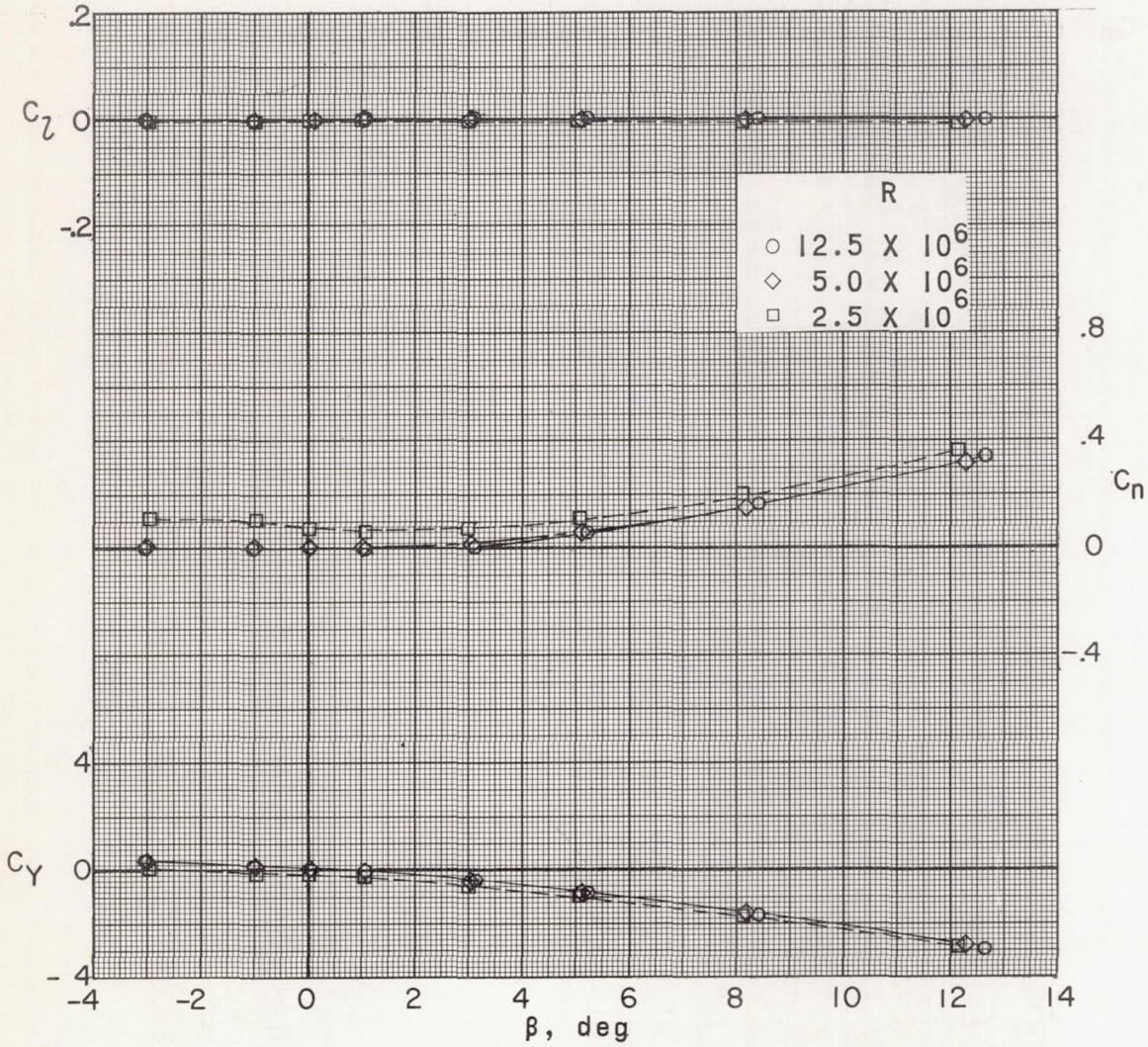

(a) M = 2.29.

Figure 14.- Aerodynamic characteristics of model III in sideslip. $\alpha = 14.6^\circ$.

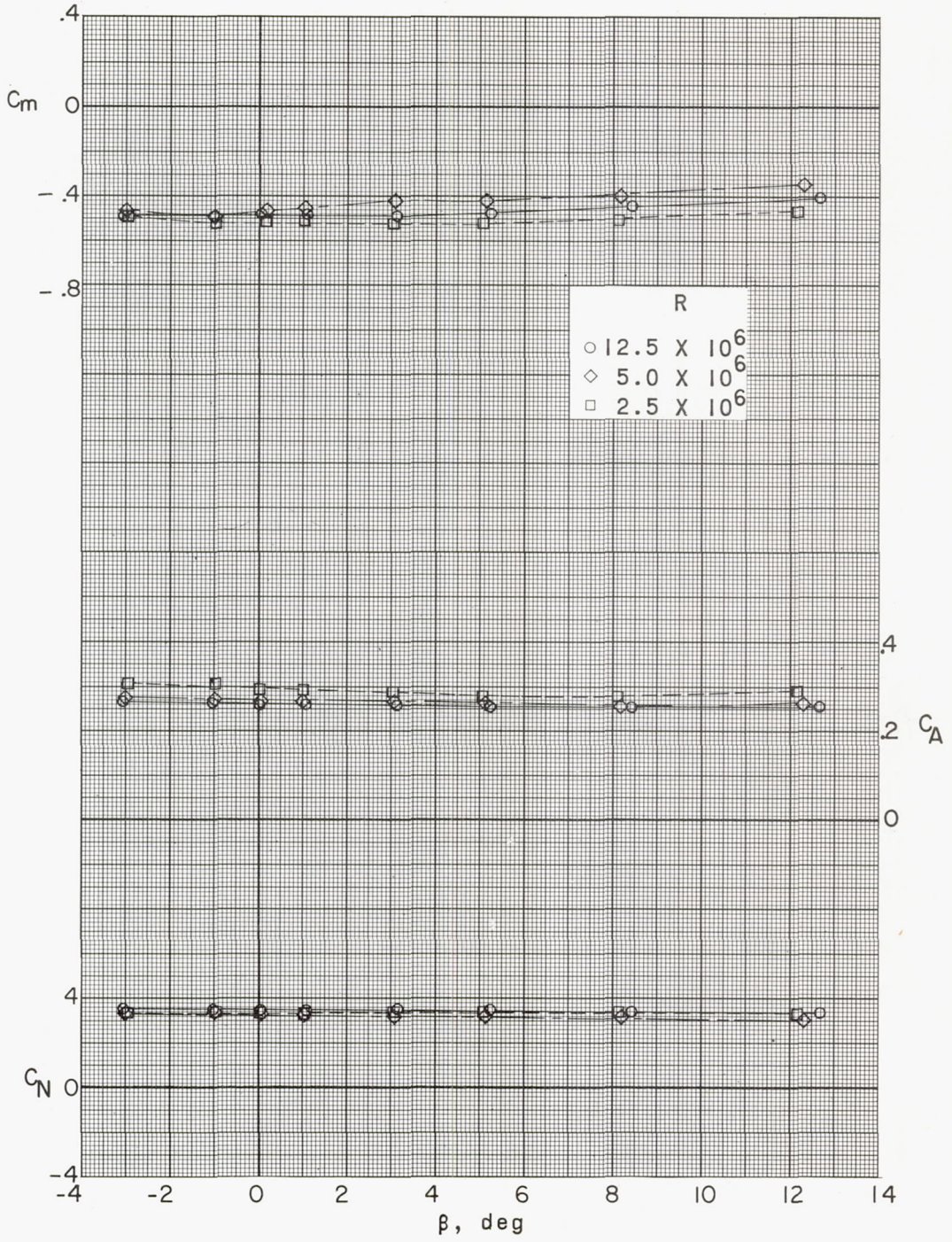

(a) Concluded.

Figure 14.- Continued.

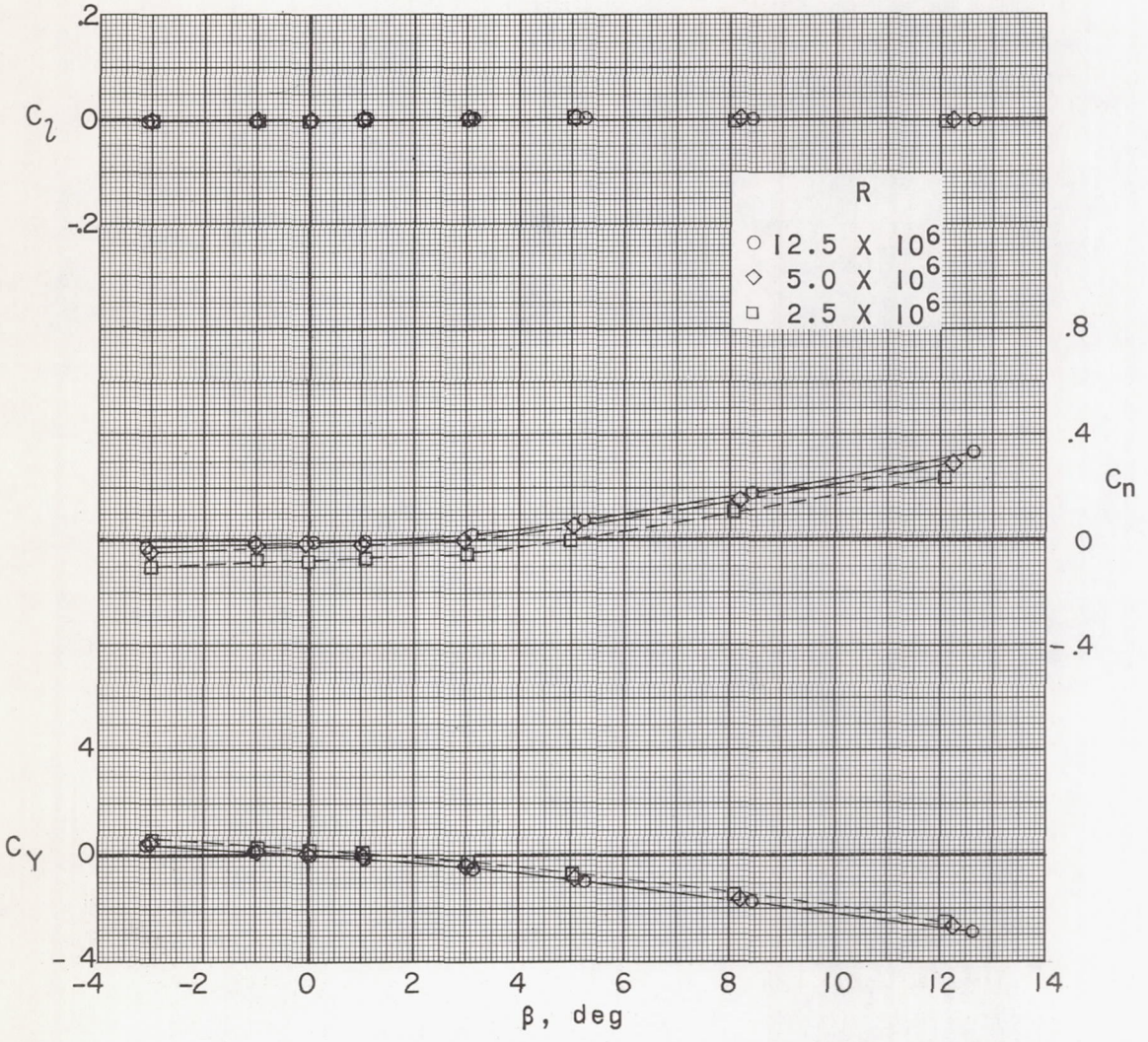

(b) M = 2.75.

Figure 14.- Continued.

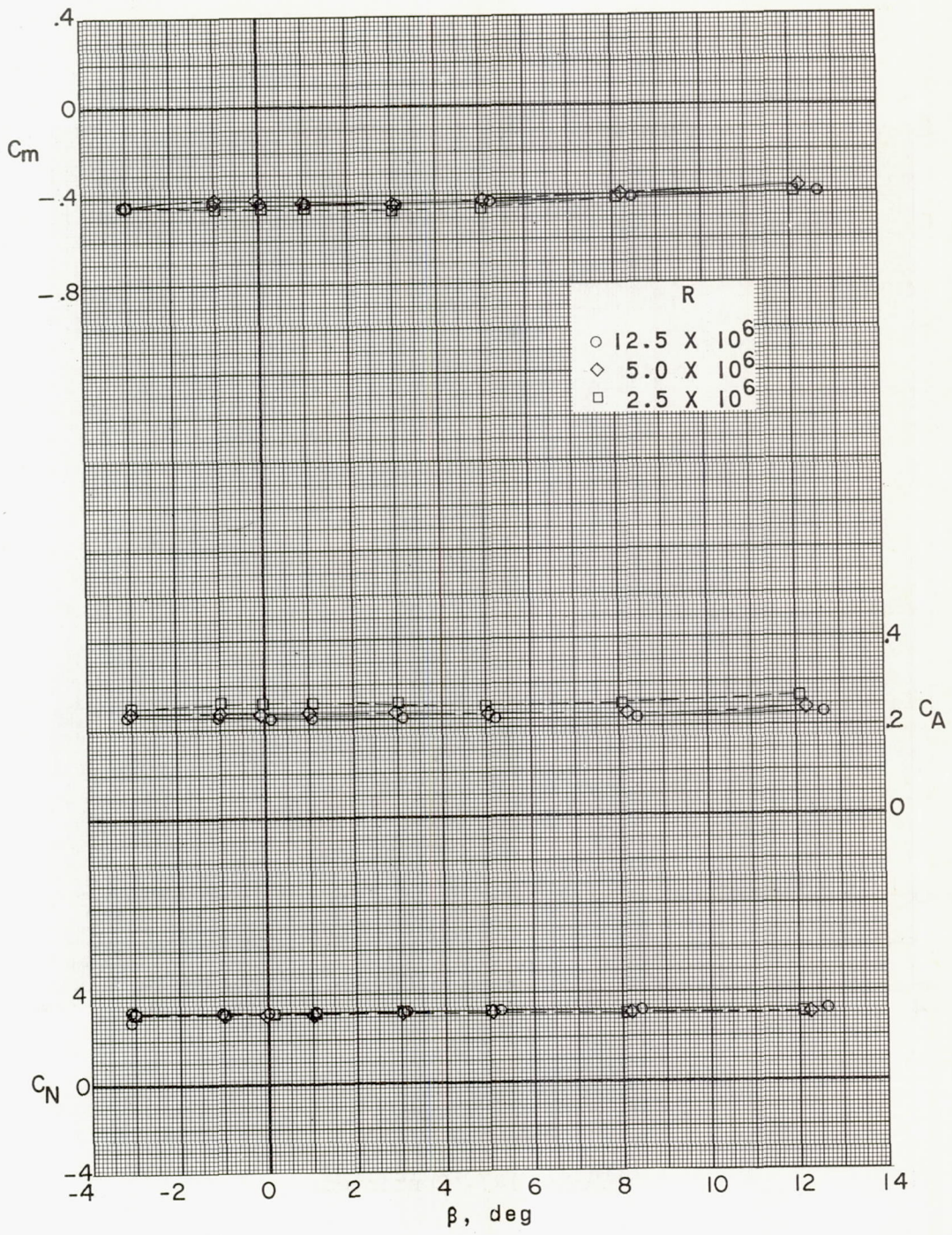

(b) Concluded.

Figure 14.- Continued.

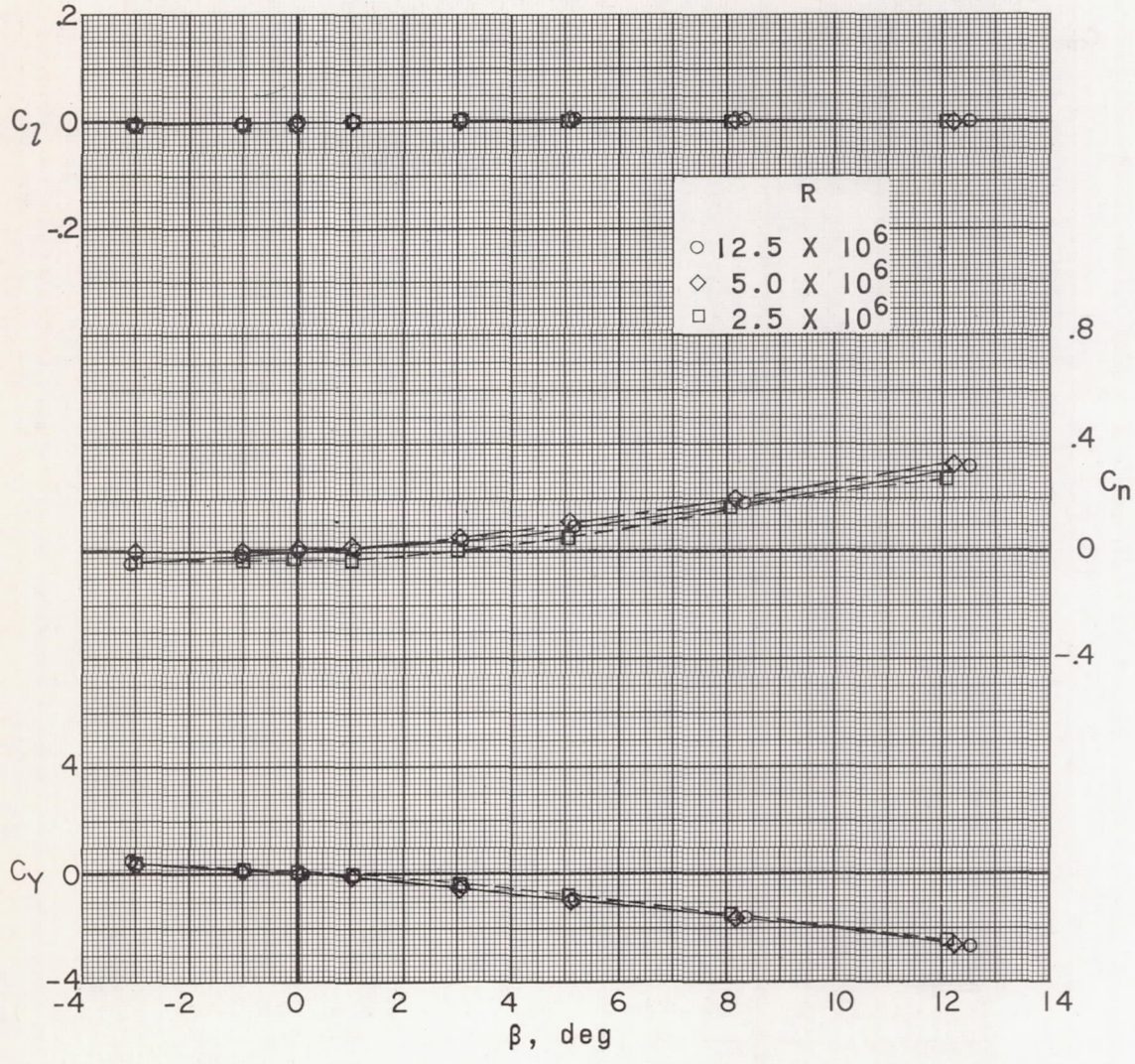

(c) M = 3.22.

Figure 14.- Continued.

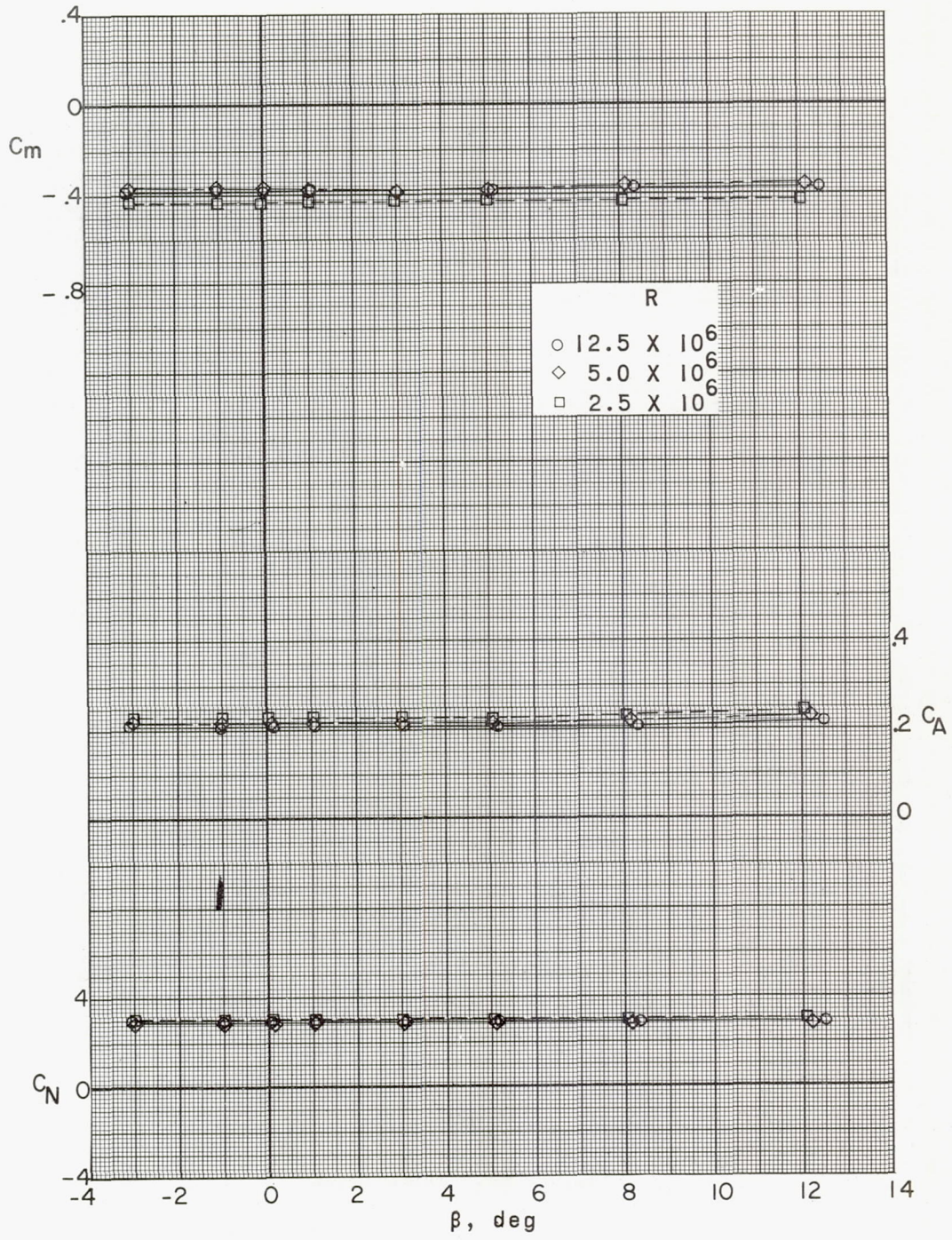

(c) Concluded.

Figure 14.- Continued.

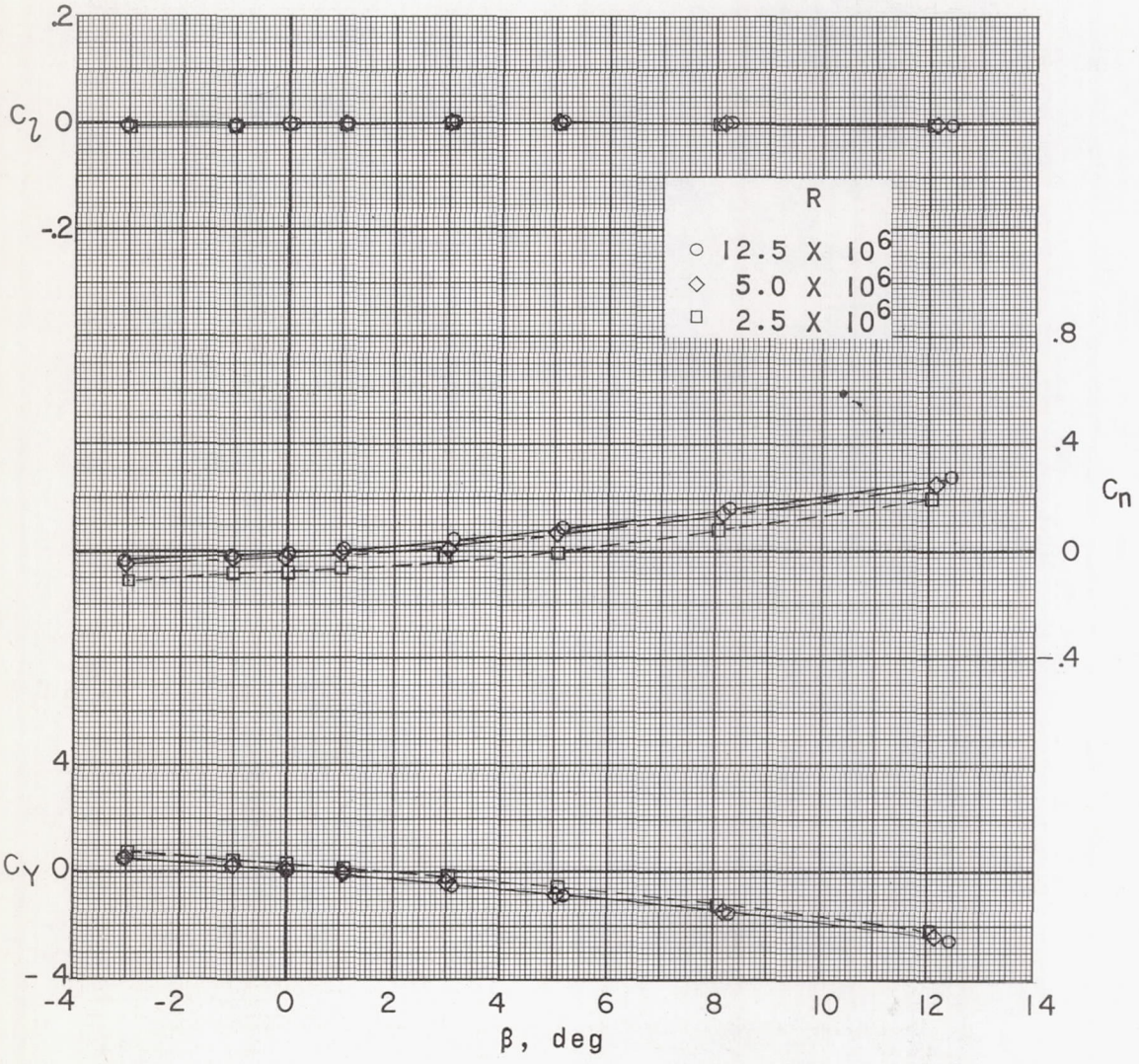

(d) M = 3.71.

Figure 14.- Continued.

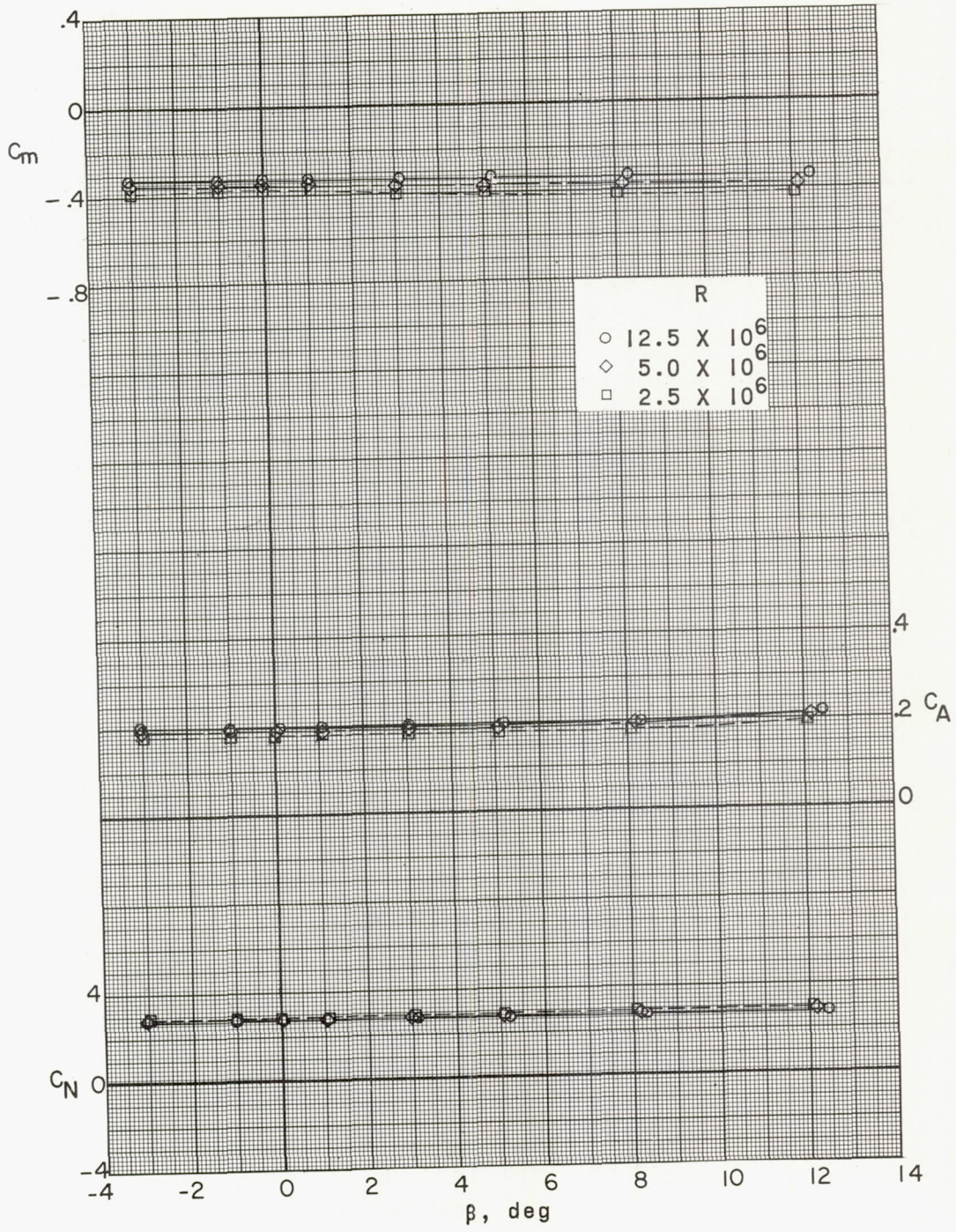

(d) Concluded.

Figure 14.- Continued.

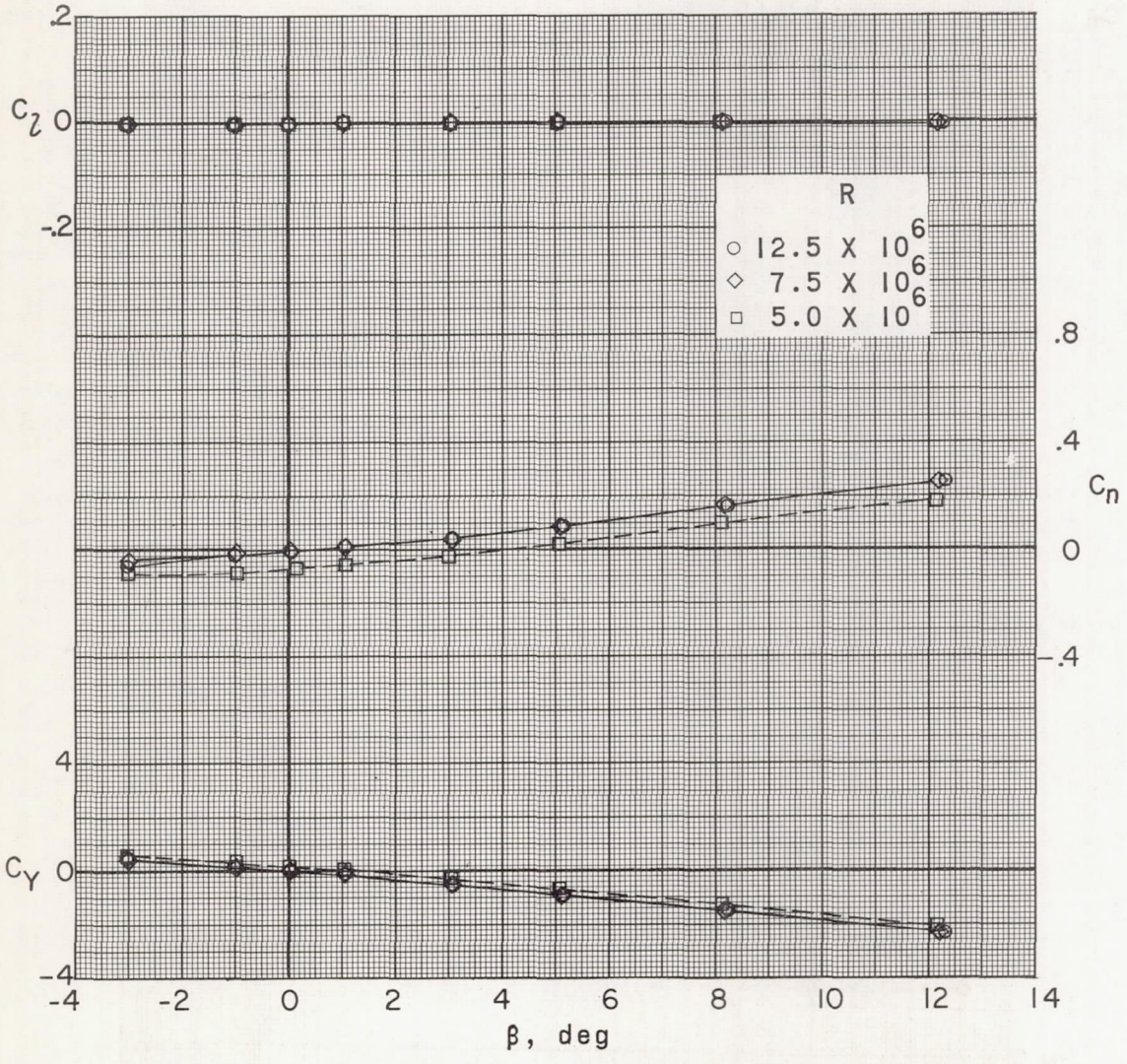

(e) M = 4.65.

Figure 14.- Continued.

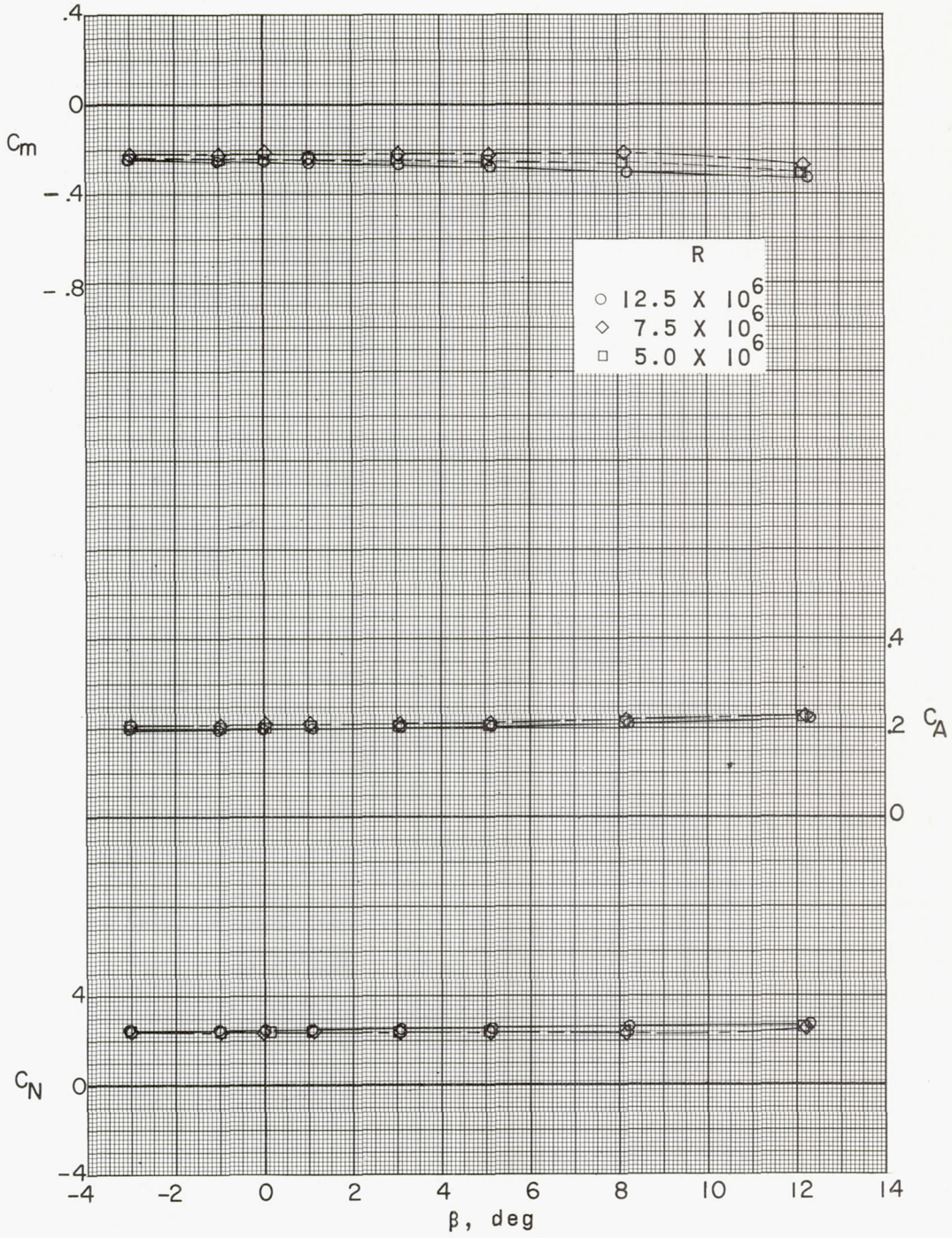

(e) Concluded.

Figure 14.- Concluded.

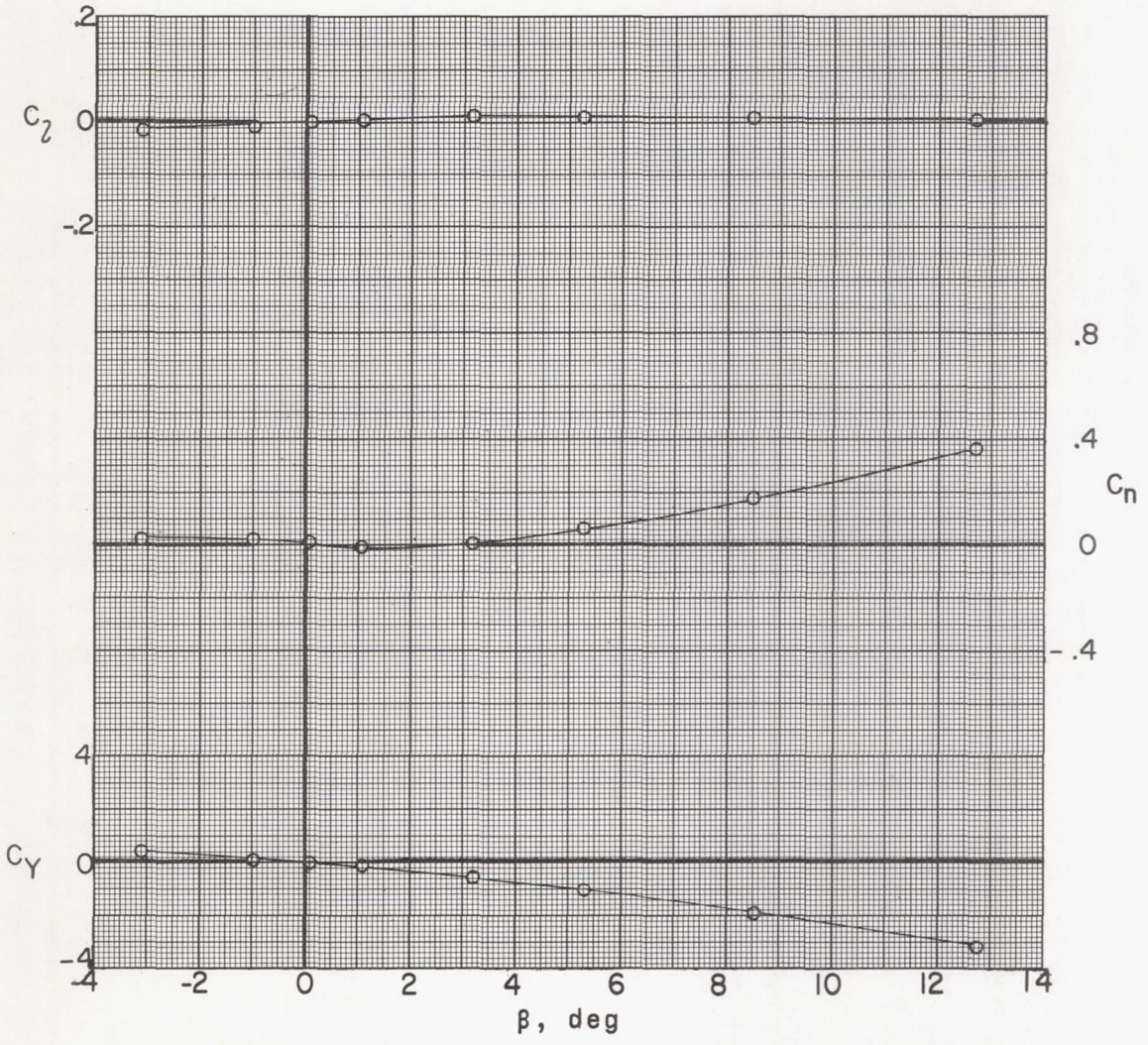

(a) M = 2.29.

Figure 15.- Aerodynamic characteristics of model III in sideslip. $\alpha = 20.9^{\circ}$; $R = 12.5 \times 10^6$.

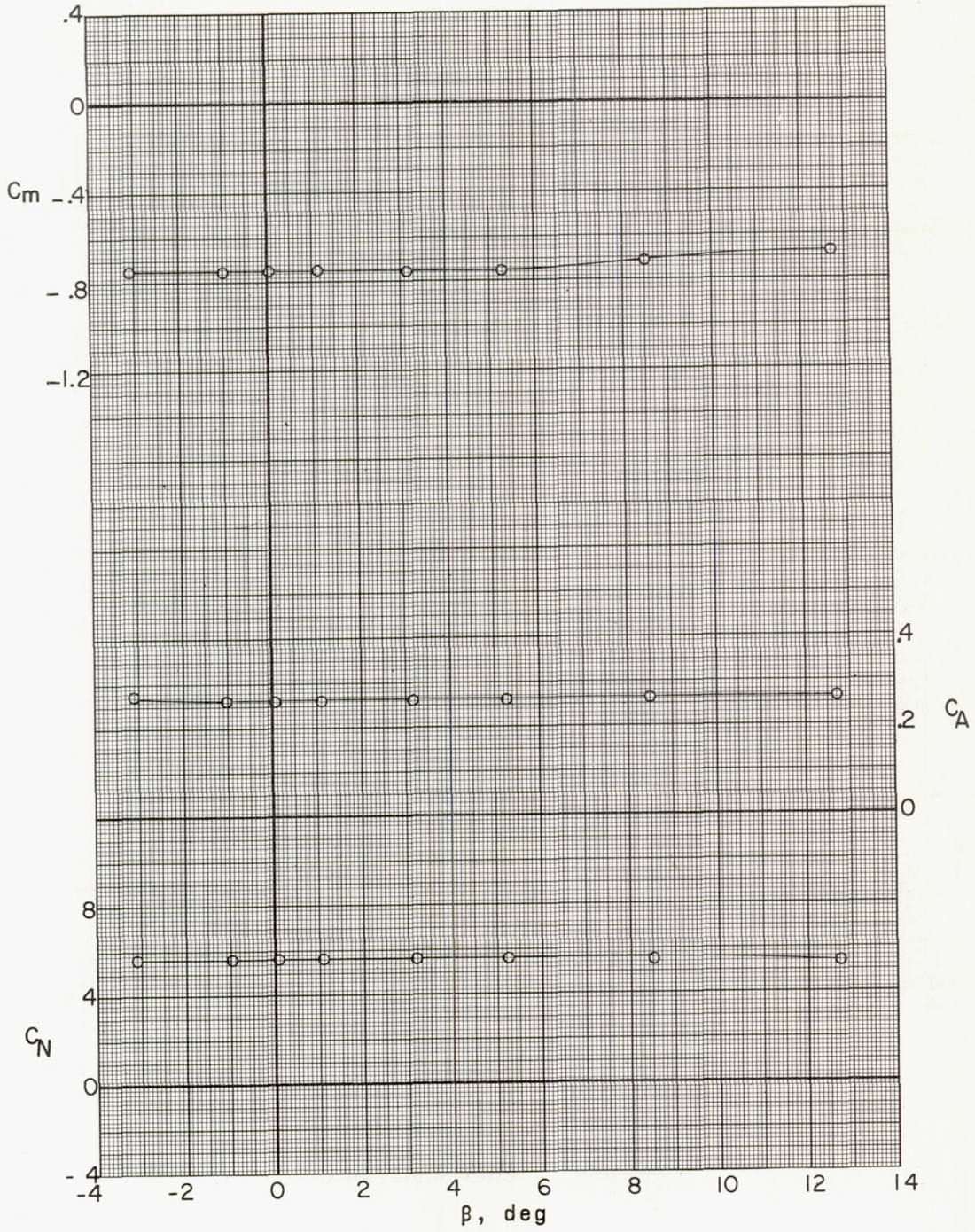

(a) Concluded.

Figure 15.- Continued.

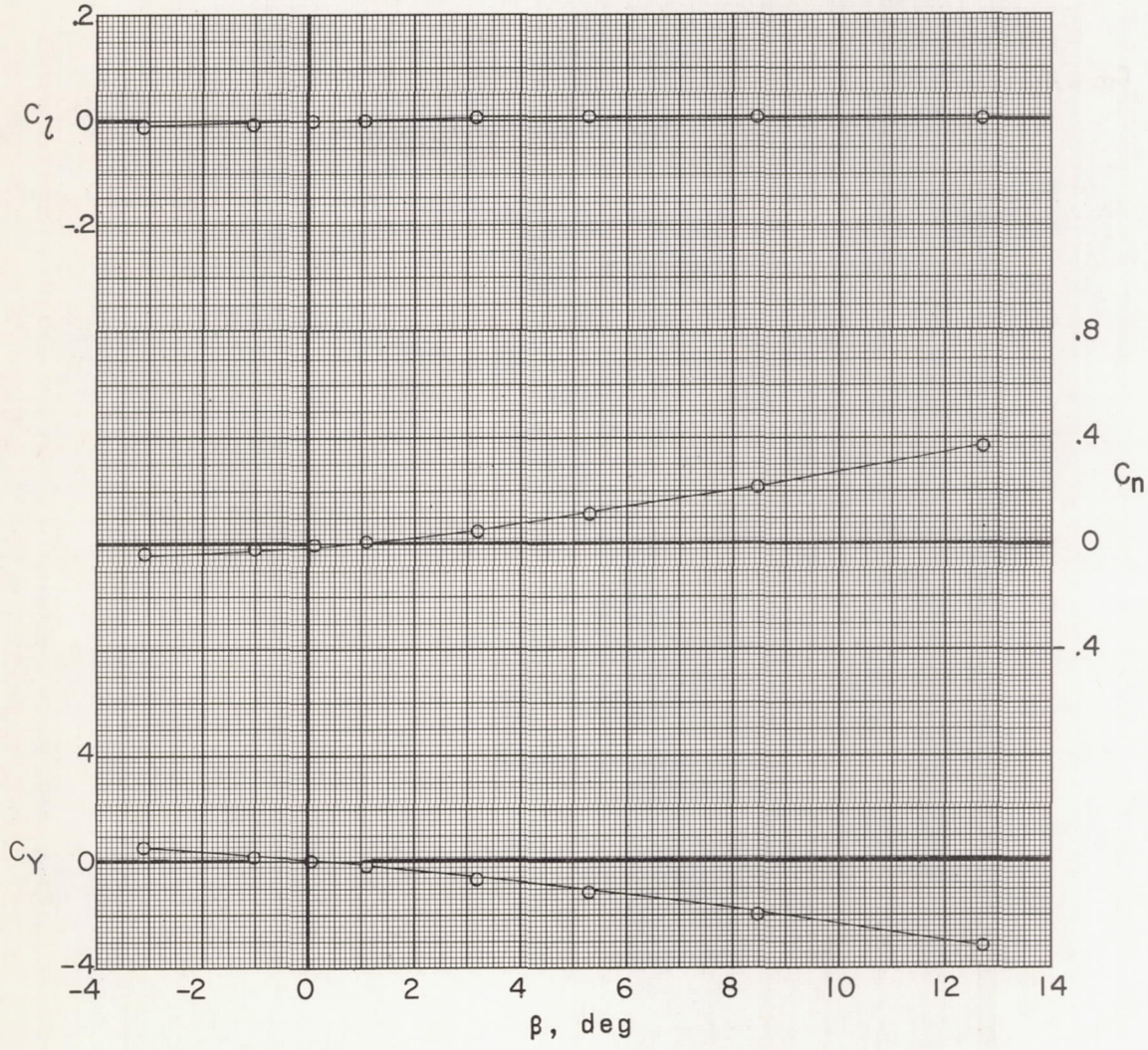

(b) M = 2.75.

Figure 15.- Continued.

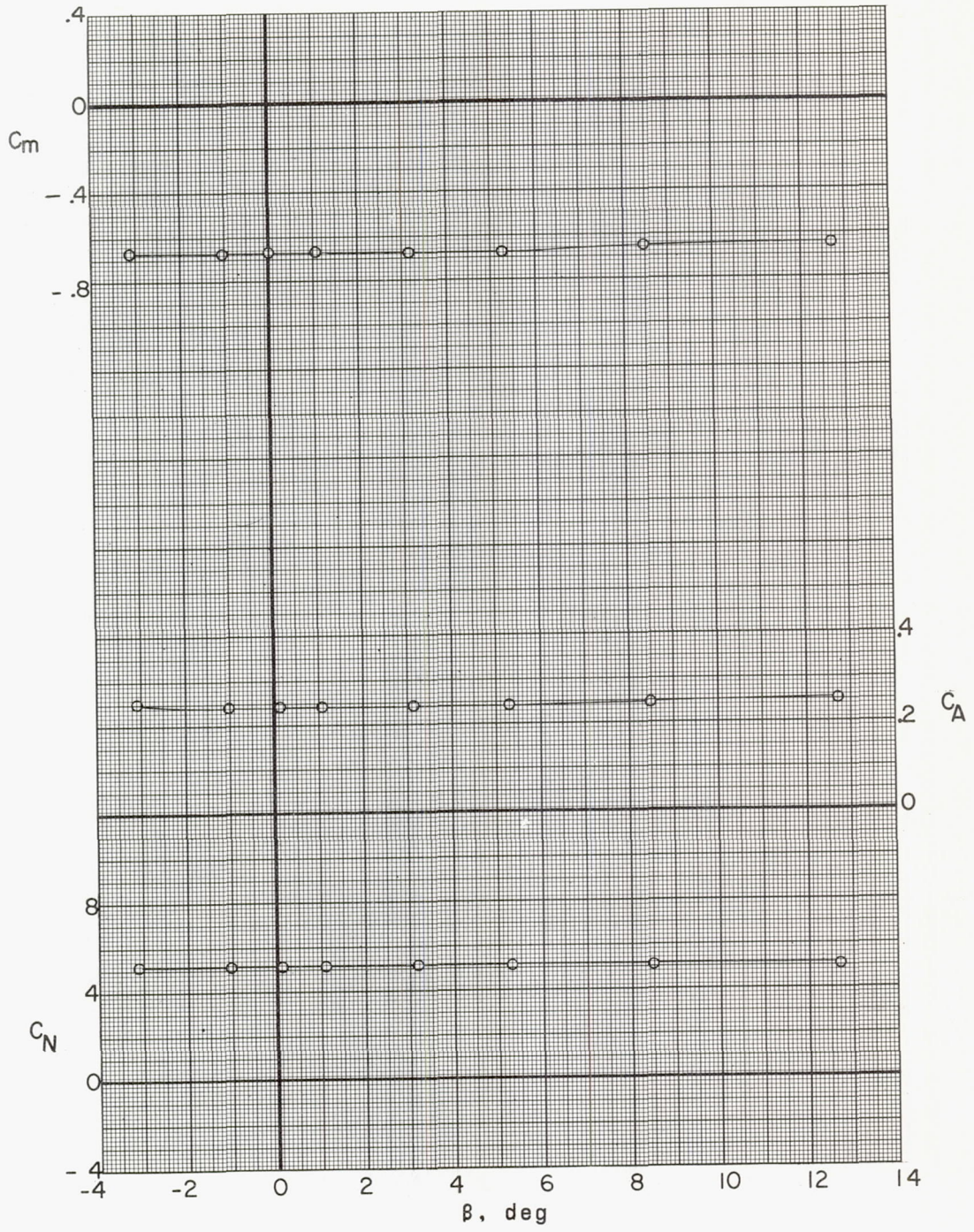

(b) Concluded.

Figure 15.- Continued.

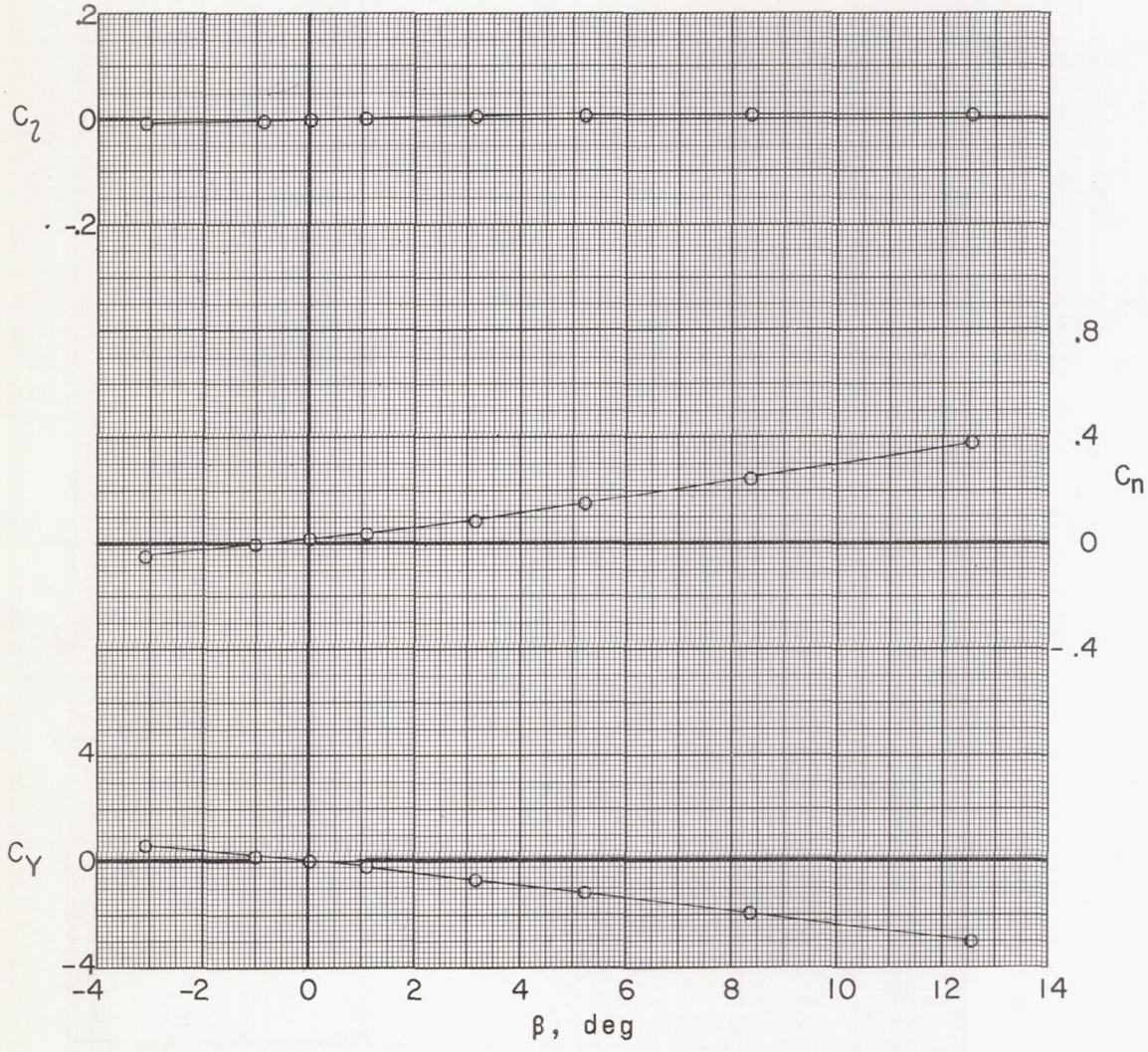

(c) M = 3.22.

Figure 15.- Continued.

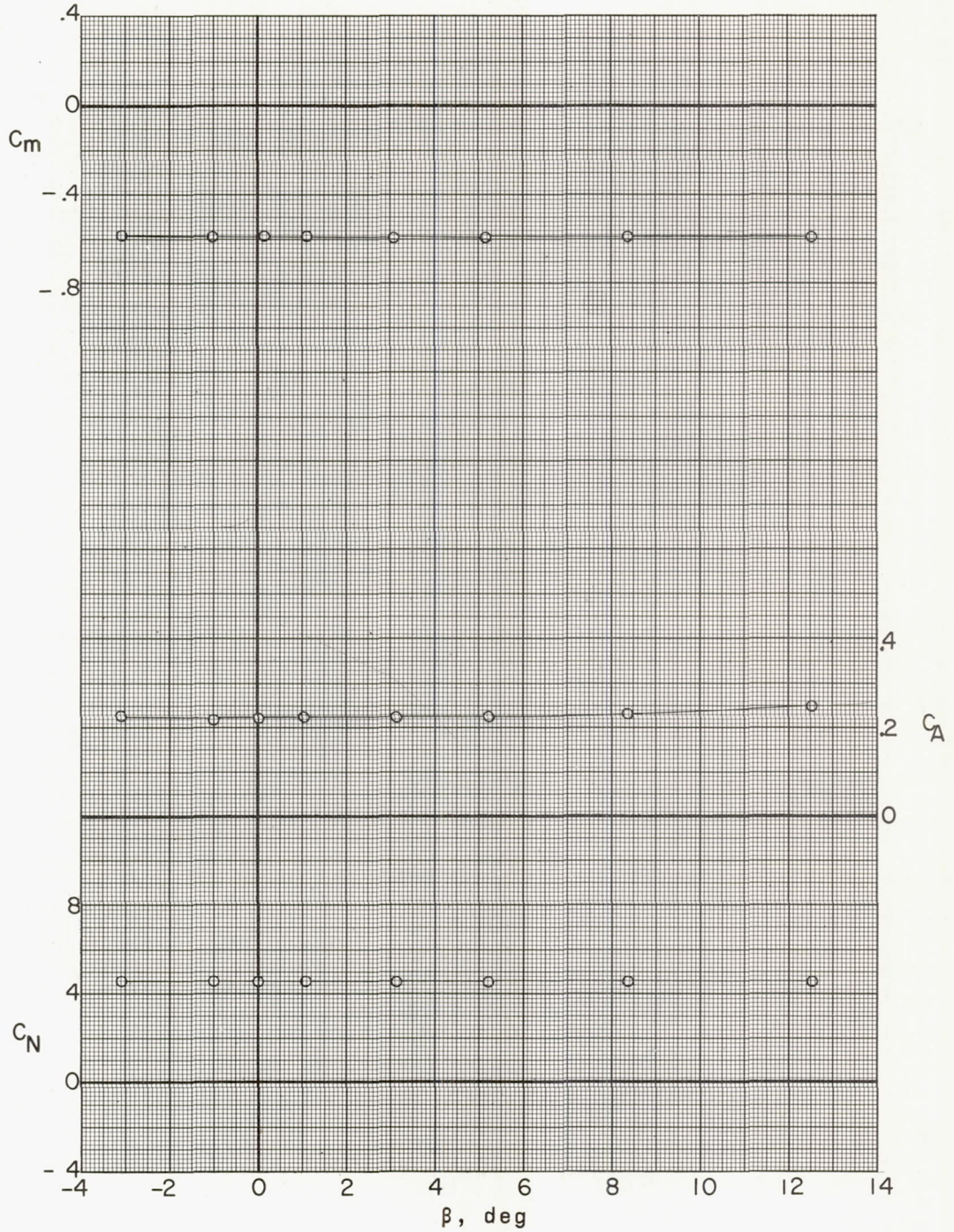

(c) Concluded.

Figure 15.- Continued.

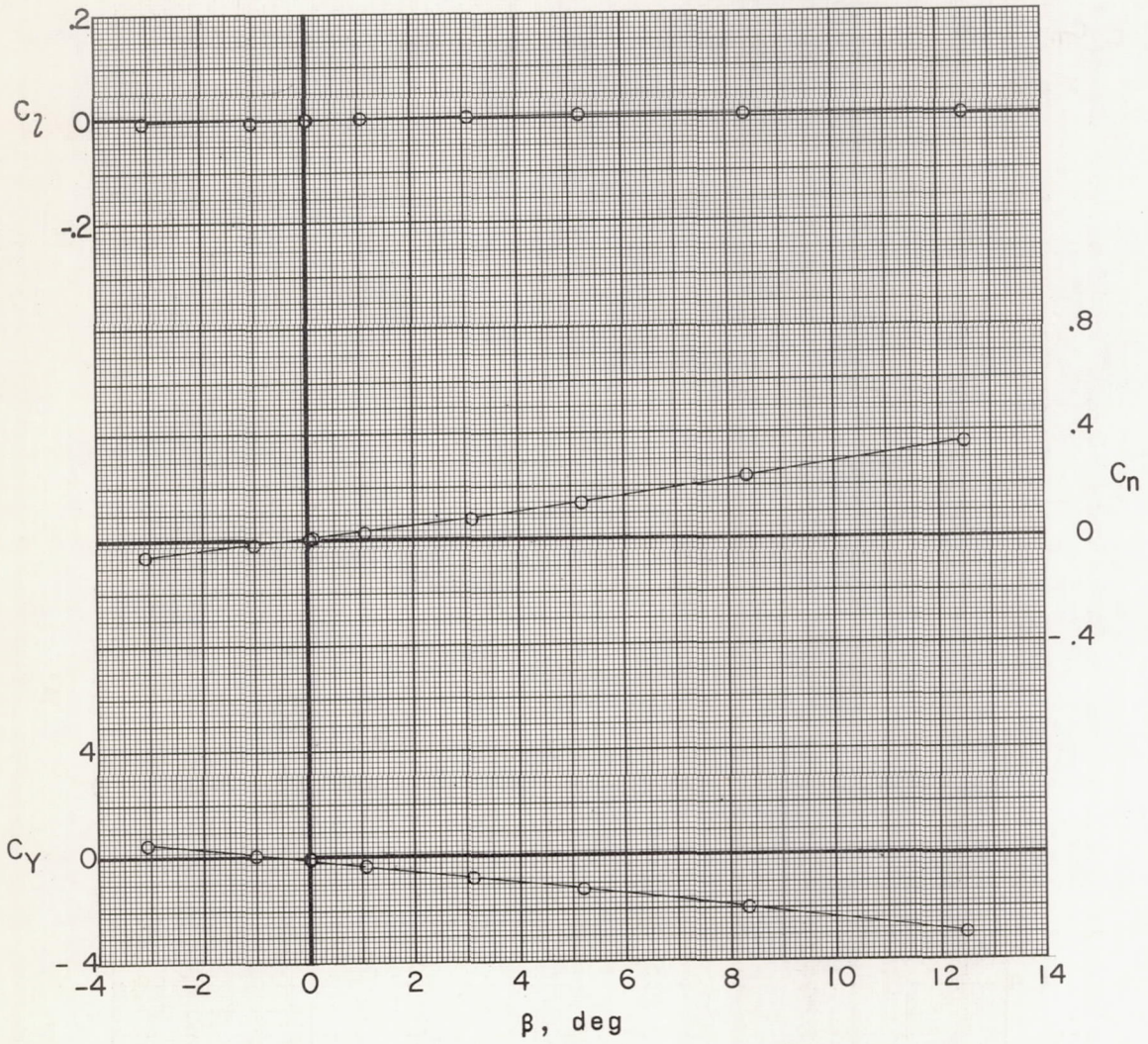

(d) M = 3.71.

Figure 15.- Continued.

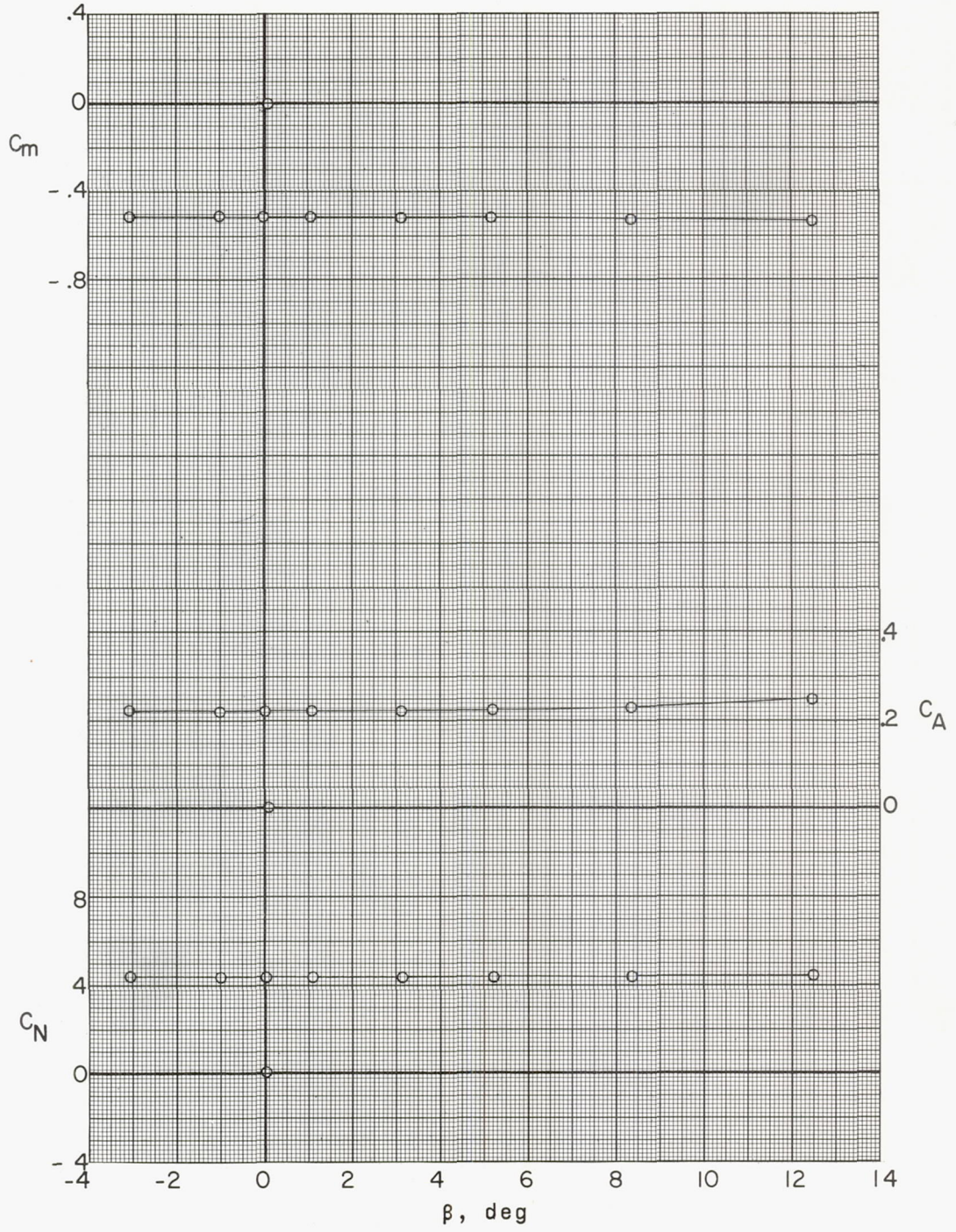

(d) Concluded.

Figure 15.- Continued.

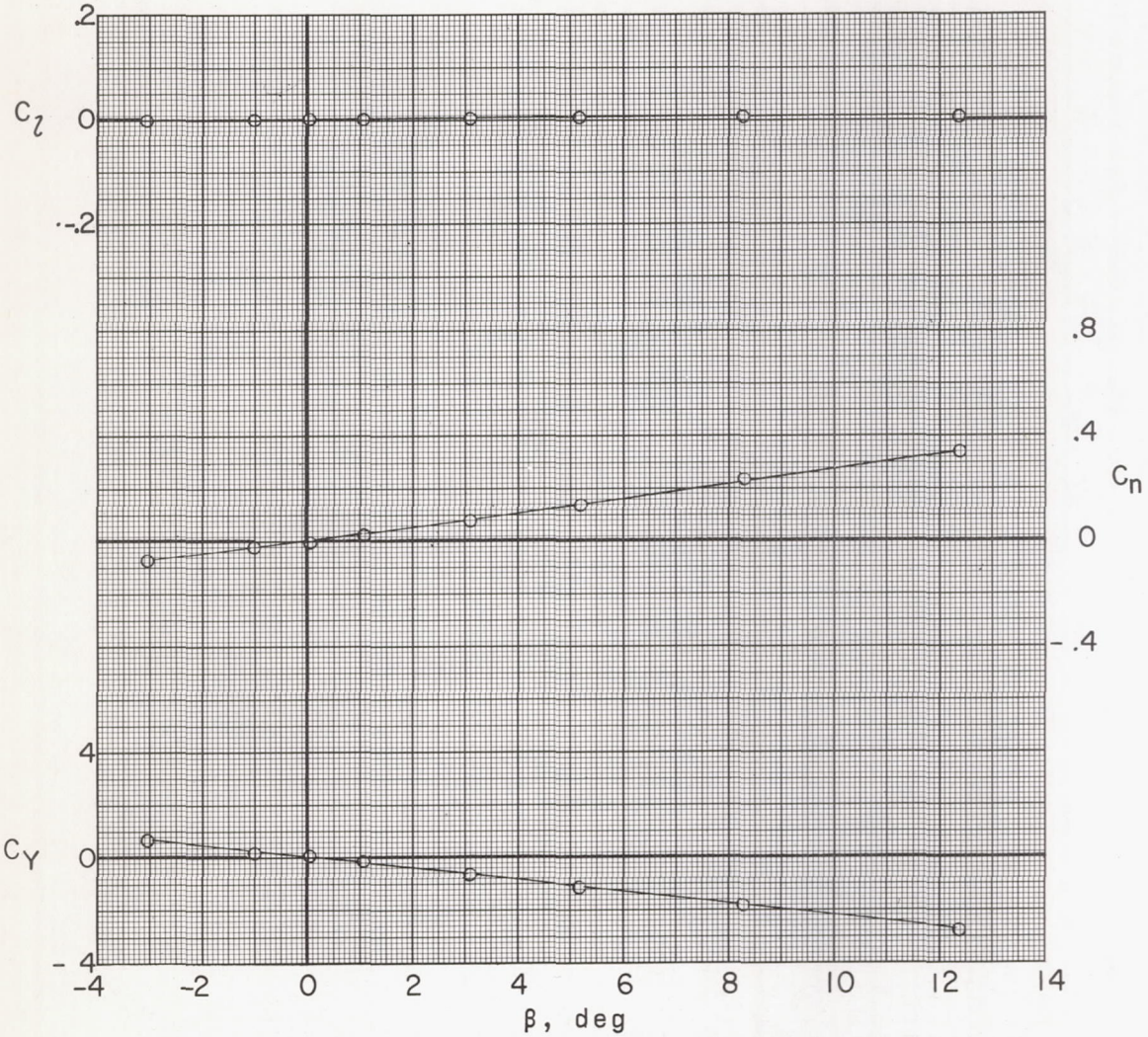

(e) M = 4.65.

Figure 15.- Continued.

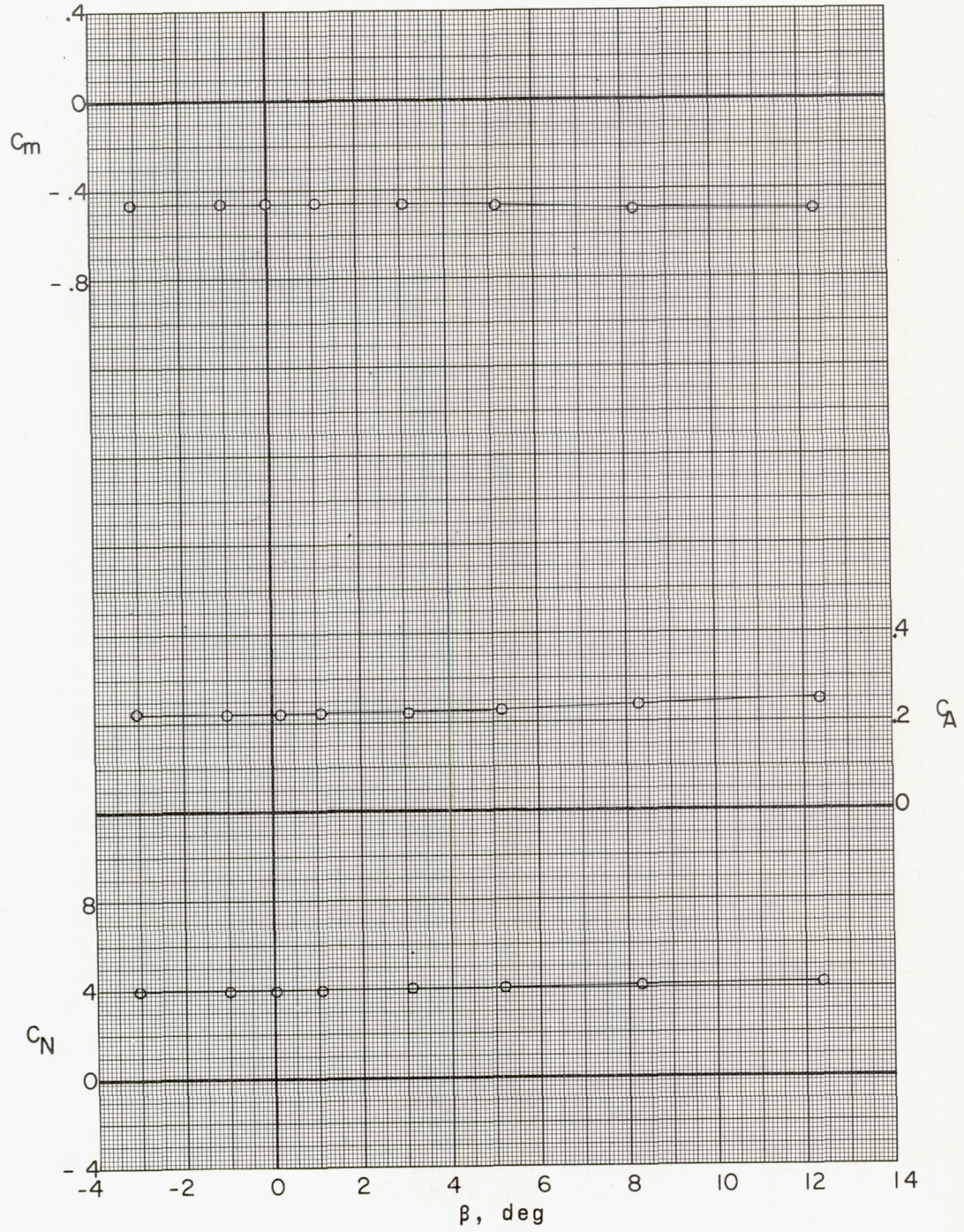

(e) Concluded.

Figure 15.- Concluded.

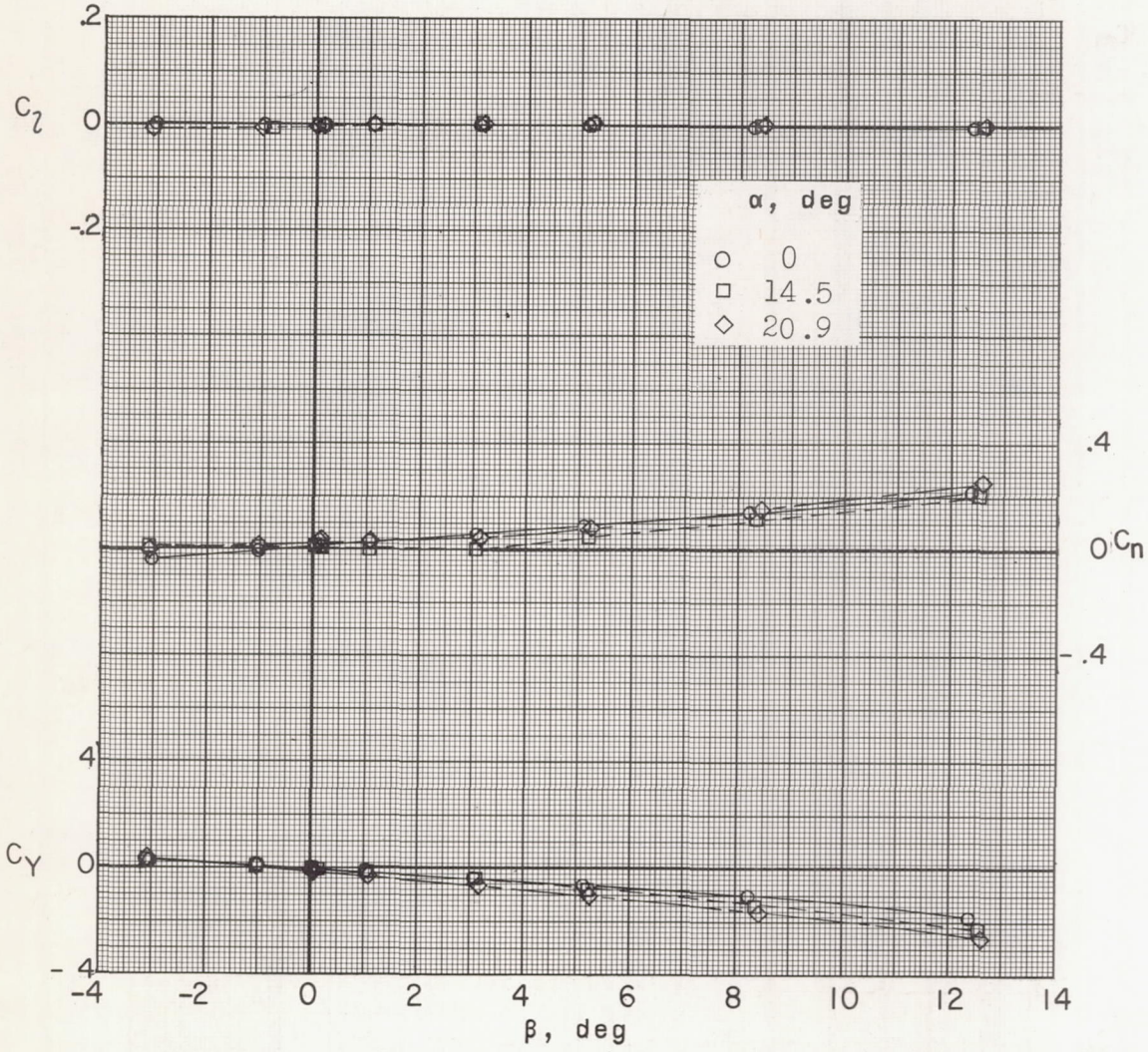

(a) M = 2.29.

Figure 16.- Aerodynamic characteristics of model IV in sideslip. $R = 12.5 \times 10^6$.

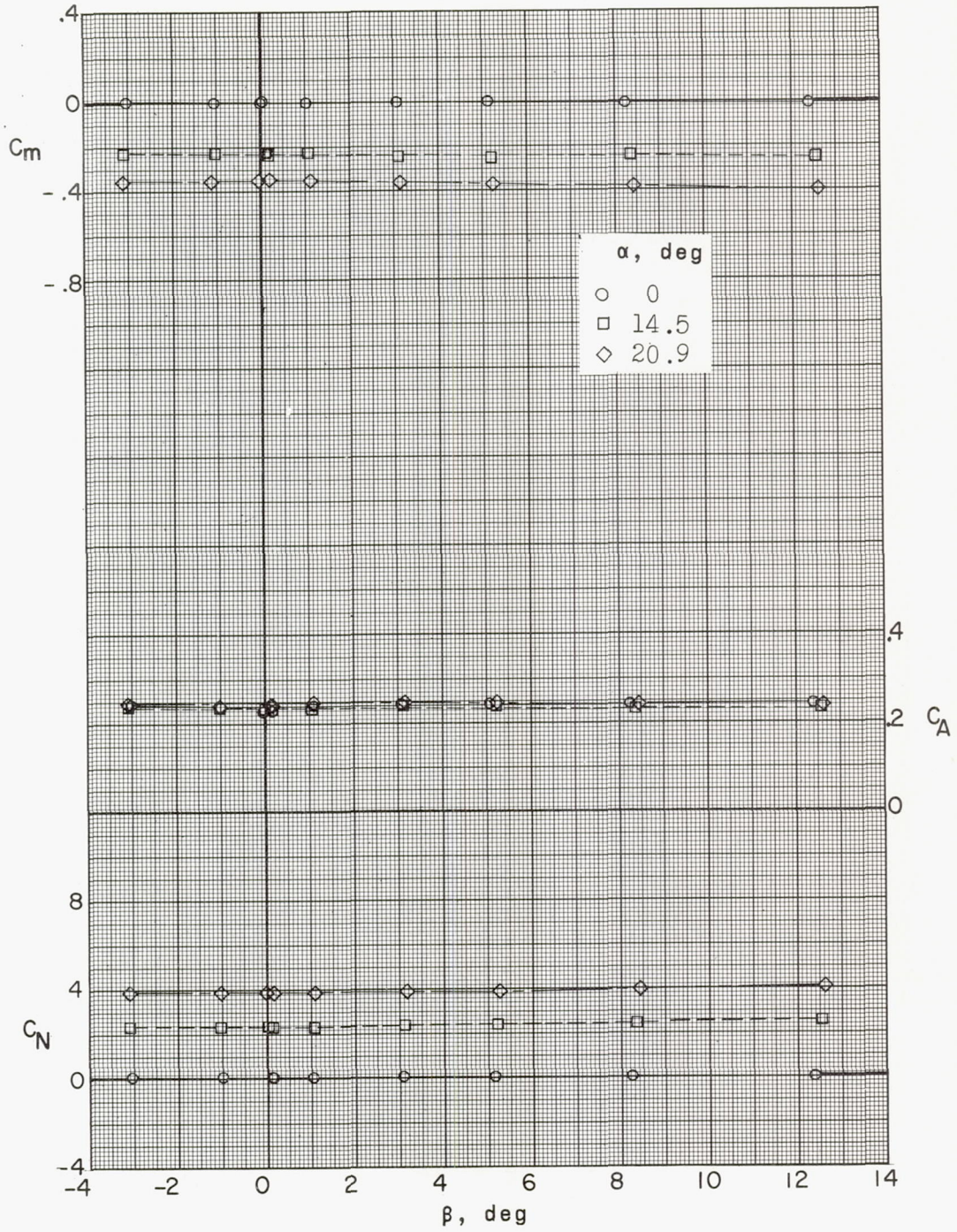

(a) Concluded.

Figure 16.- Continued.

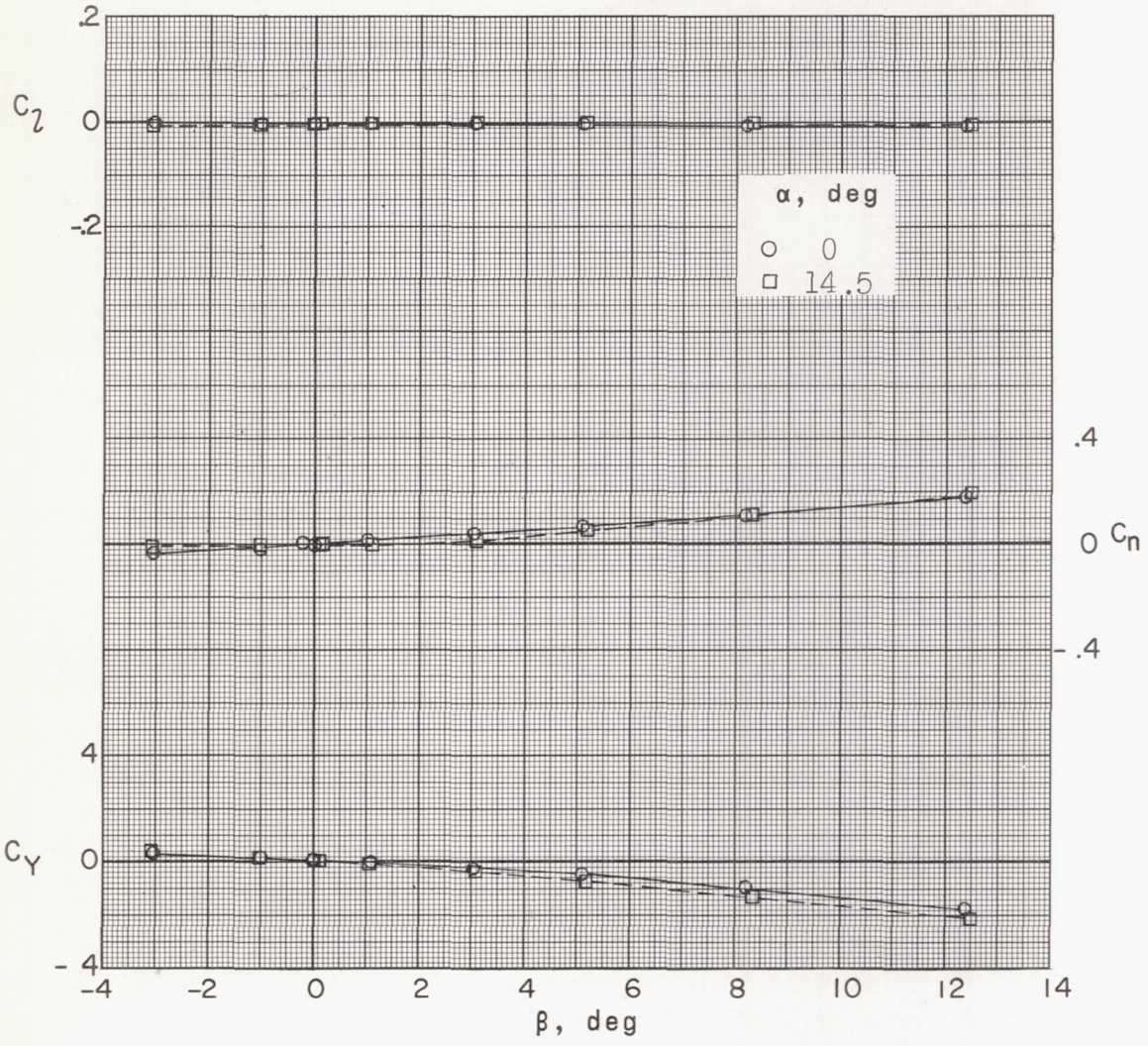

(b) M = 2.75.

Figure 16.- Continued.

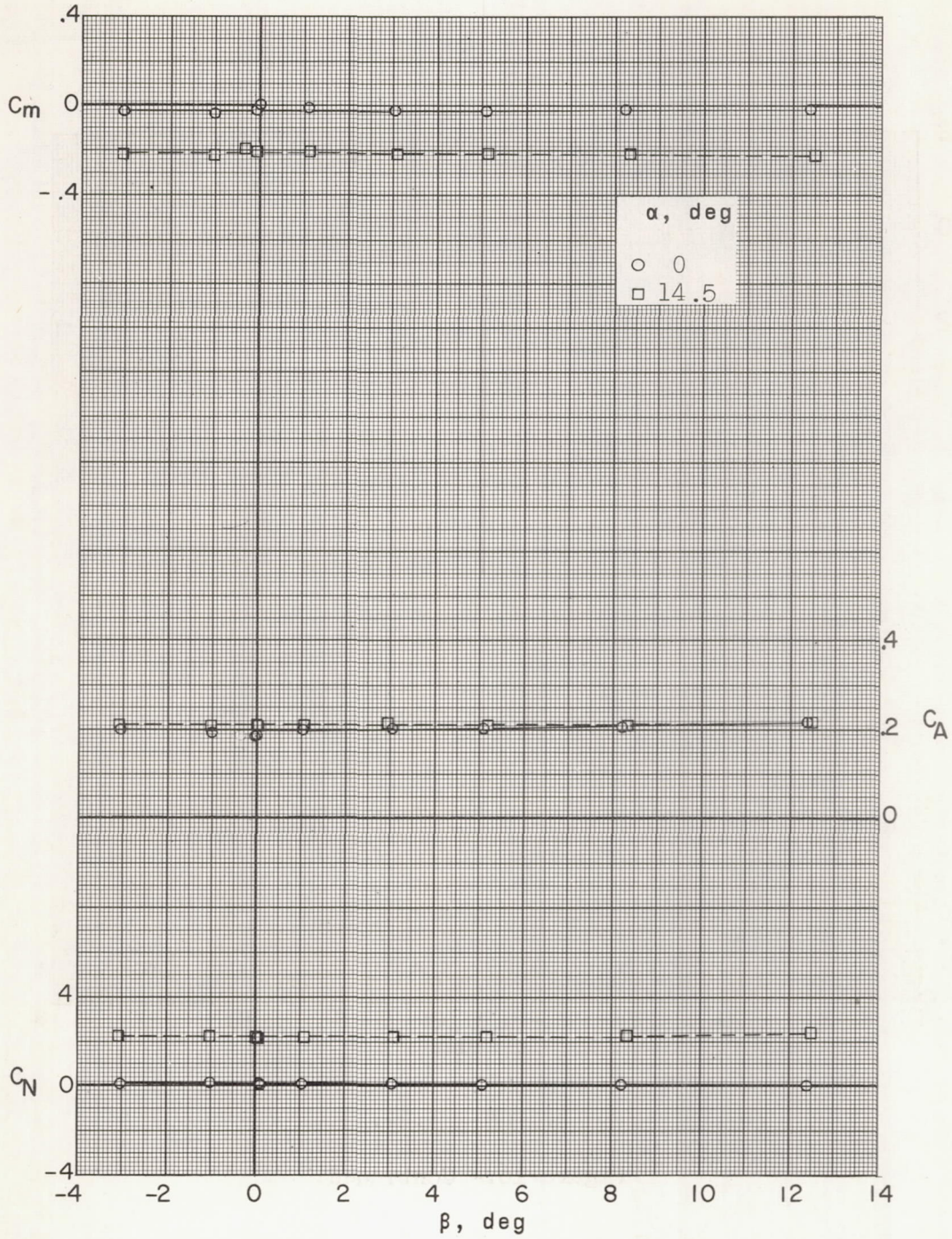

(b) Concluded.

Figure 16.- Continued.

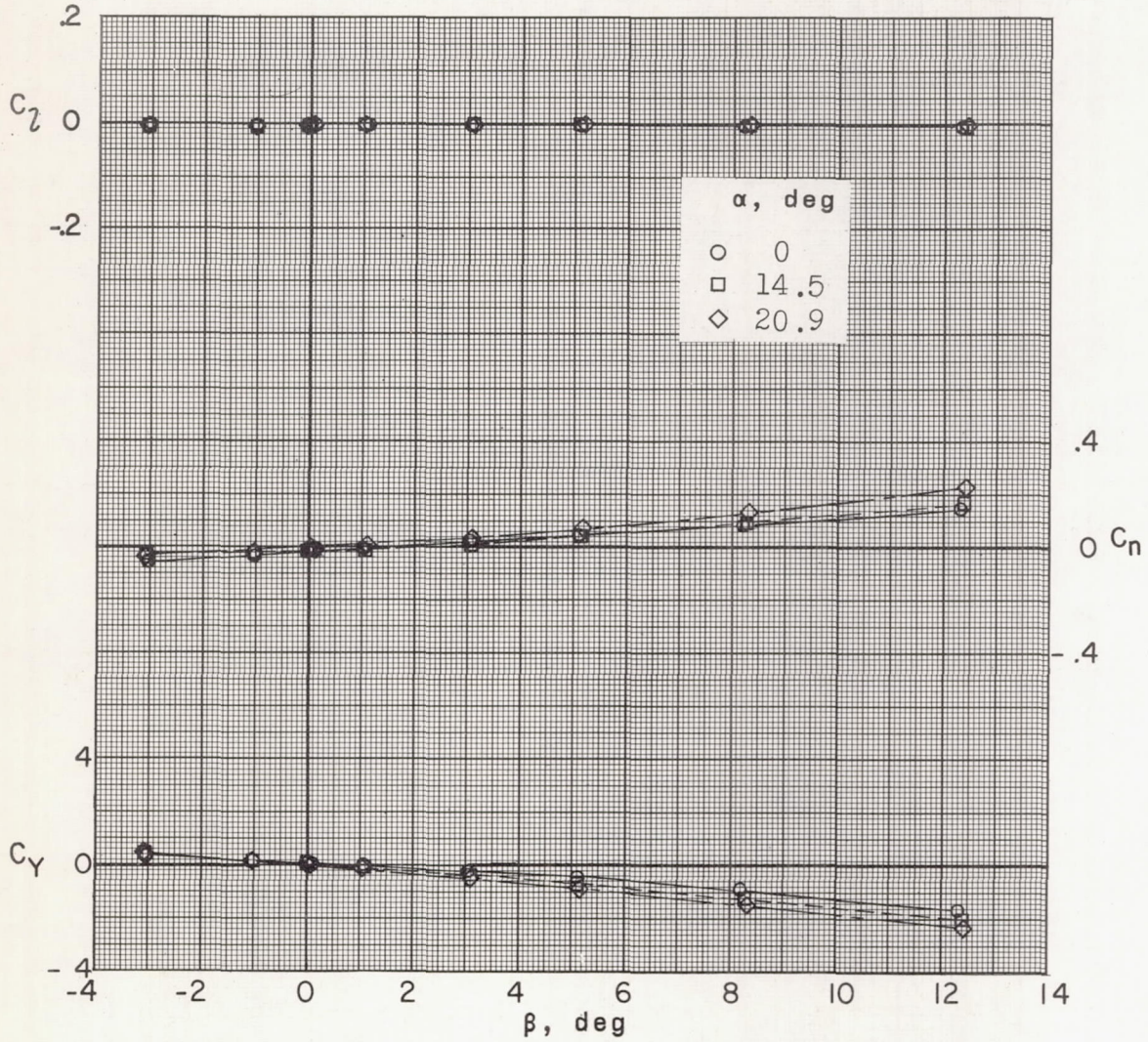

(c) M = 3.22.

Figure 16.- Continued.

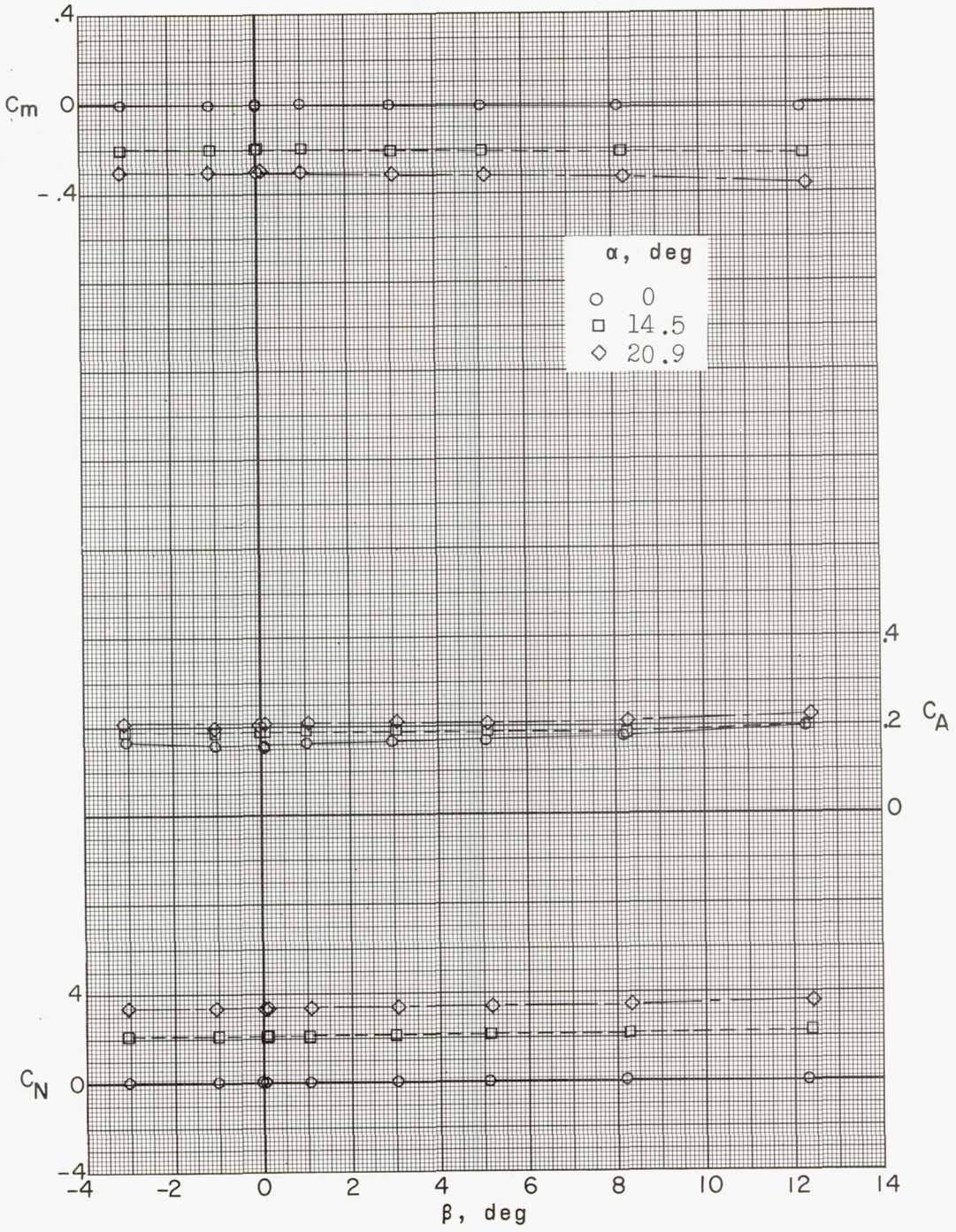

(c) Concluded.

Figure 16.- Continued.

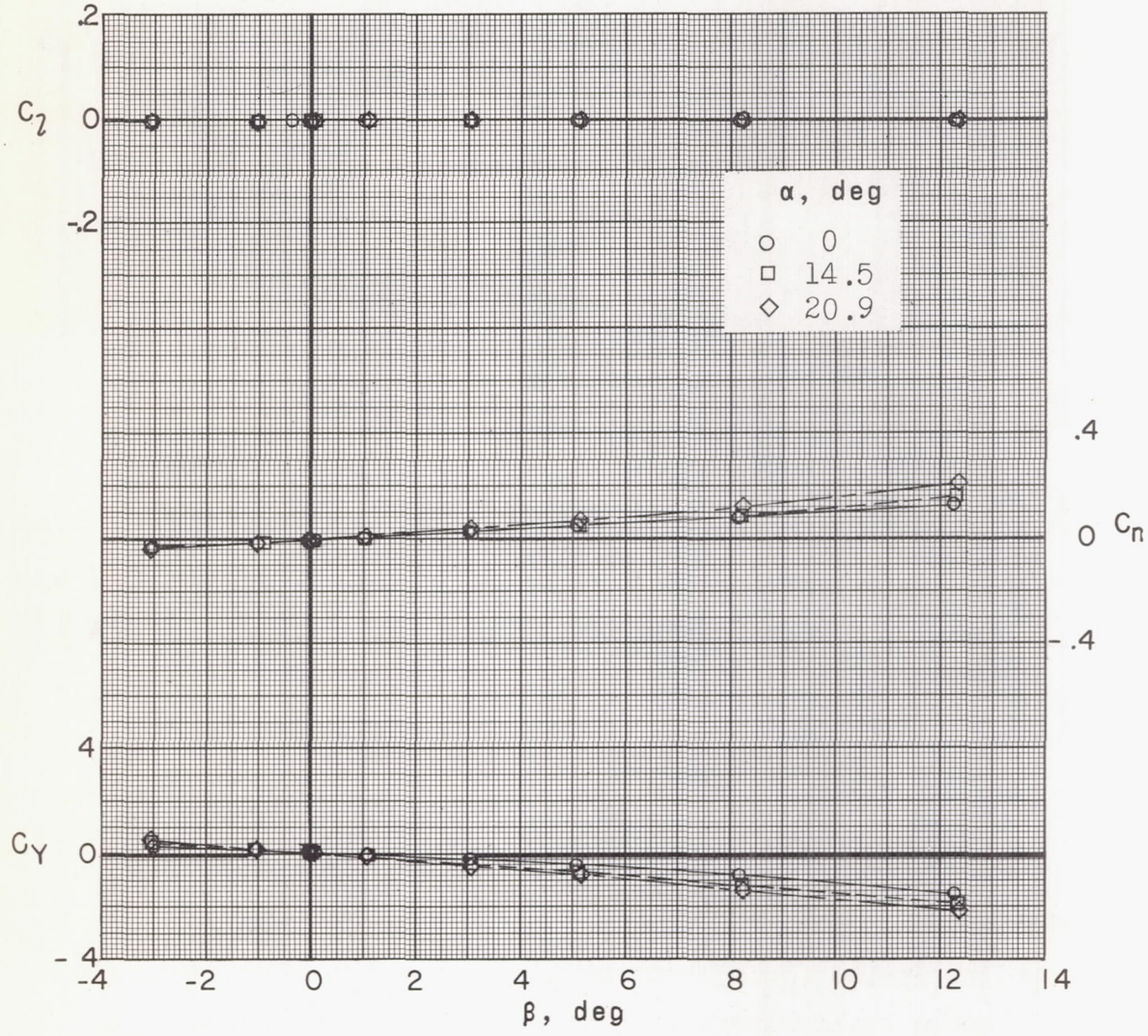

(d) M = 3.71.

Figure 16.- Continued.

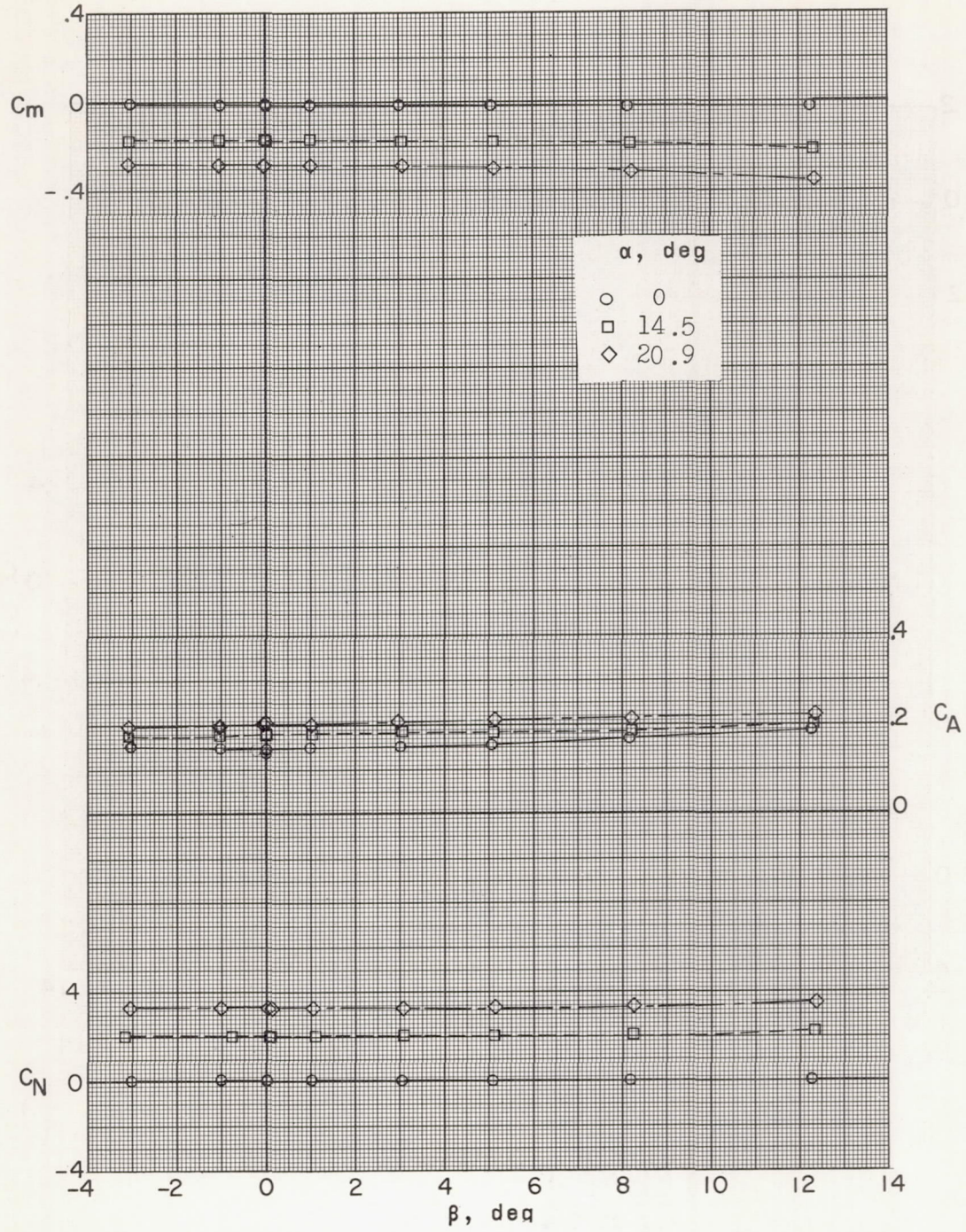

(d) Concluded.

Figure 16.- Continued.

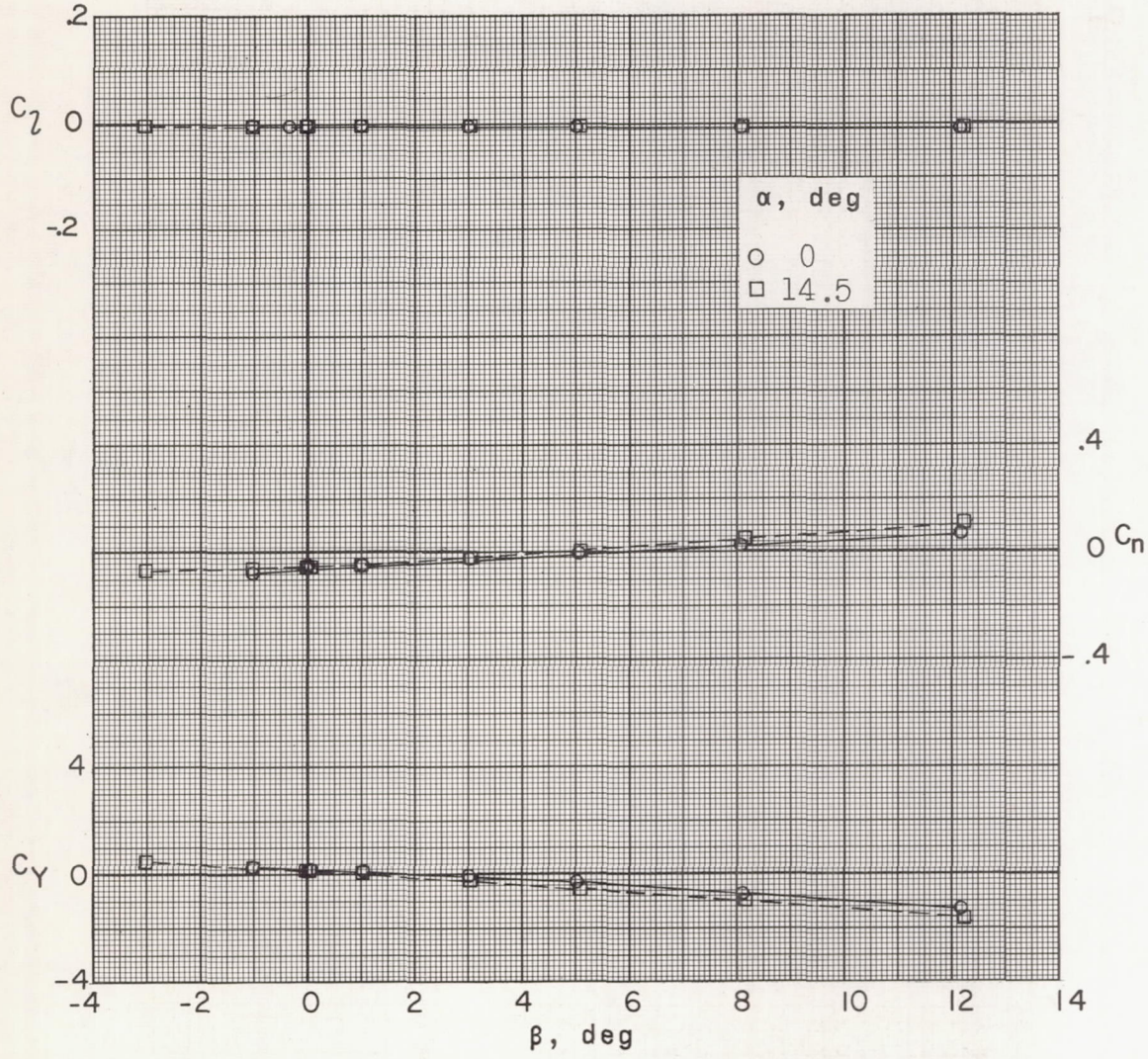

(e) M = 4.65.

Figure 16.- Continued.

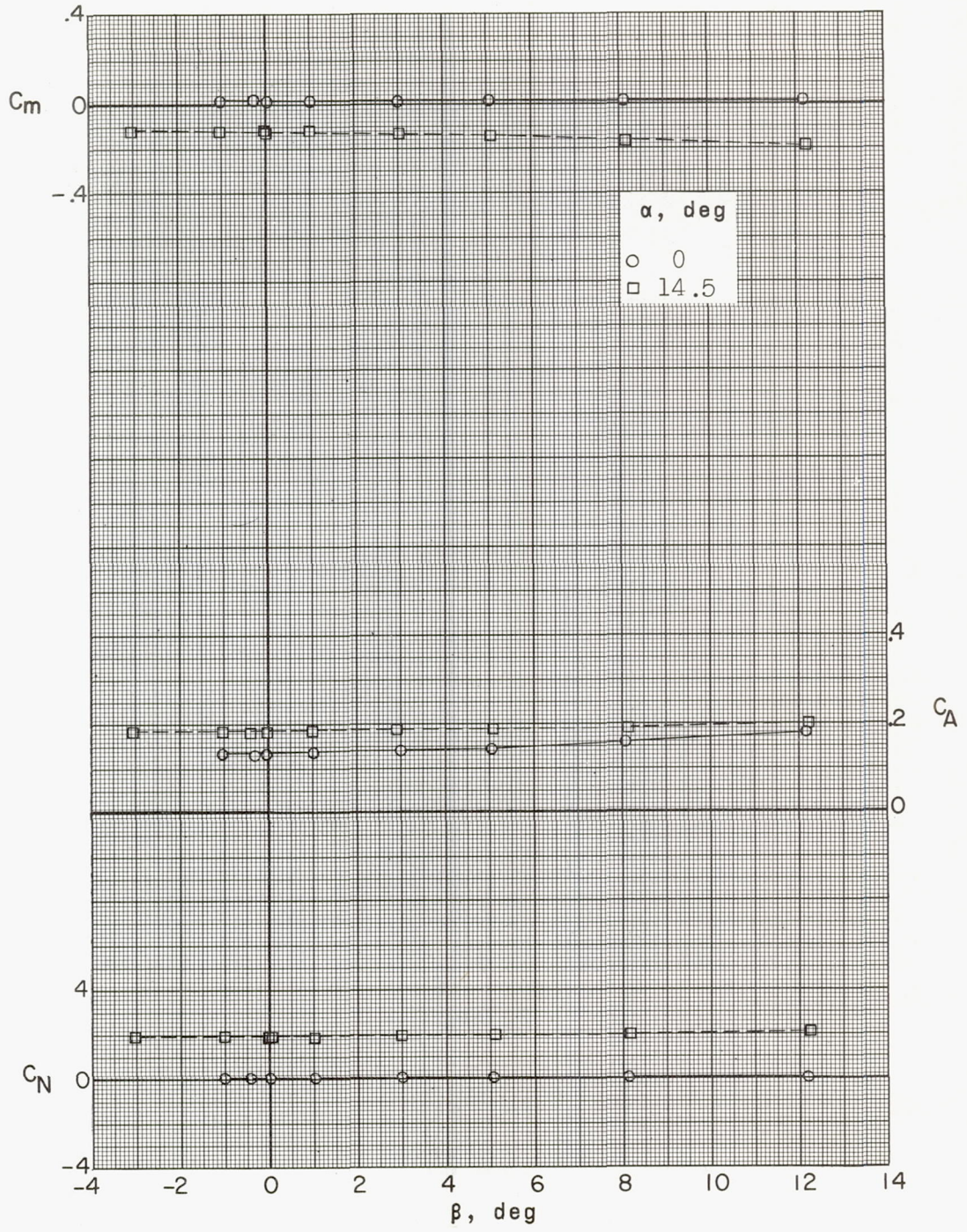

(e) Concluded.

Figure 16.- Concluded.

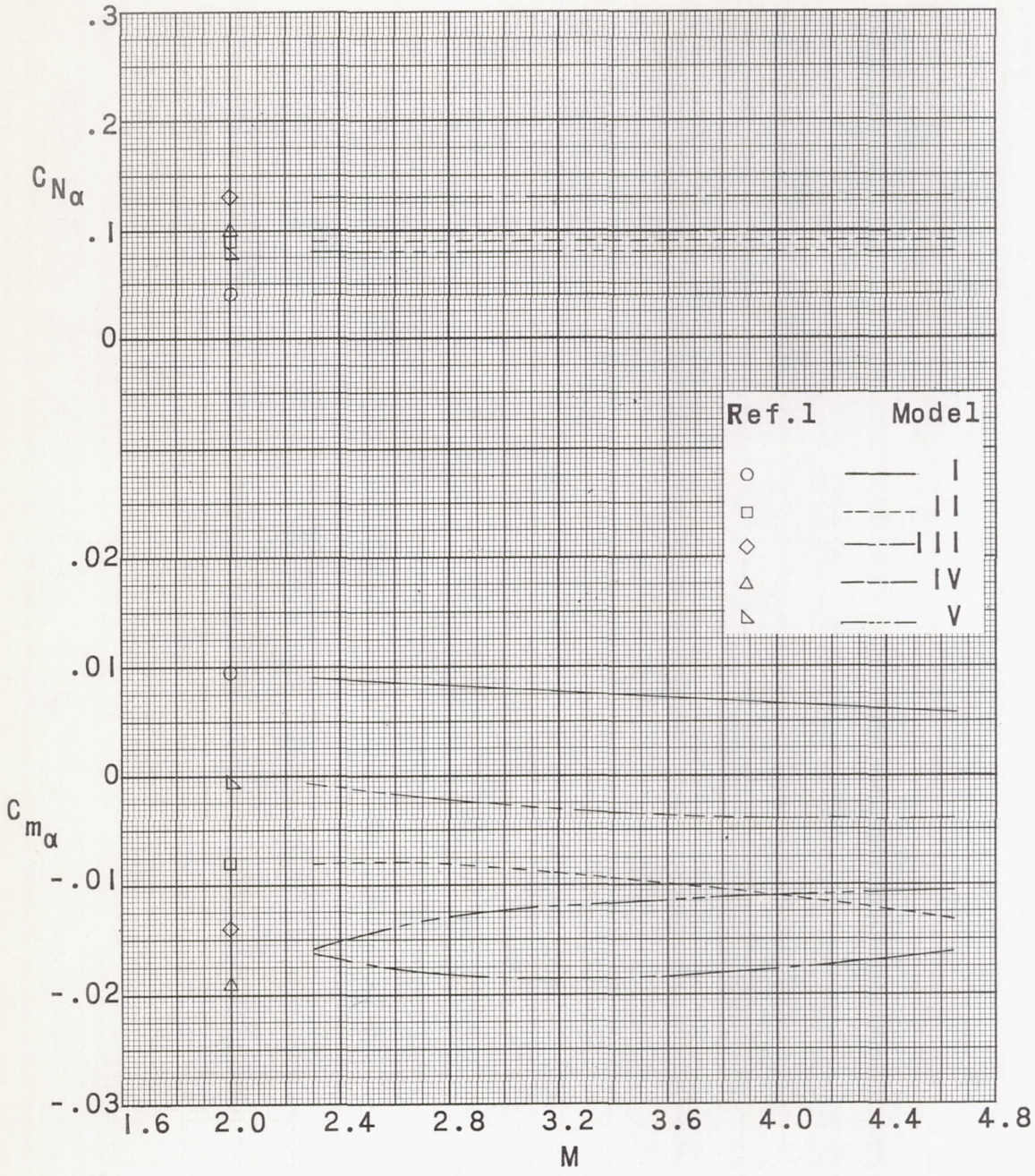

(a) $\alpha \approx 0^\circ$.

Figure 17.- Longitudinal stability characteristics of the five missile configurations.

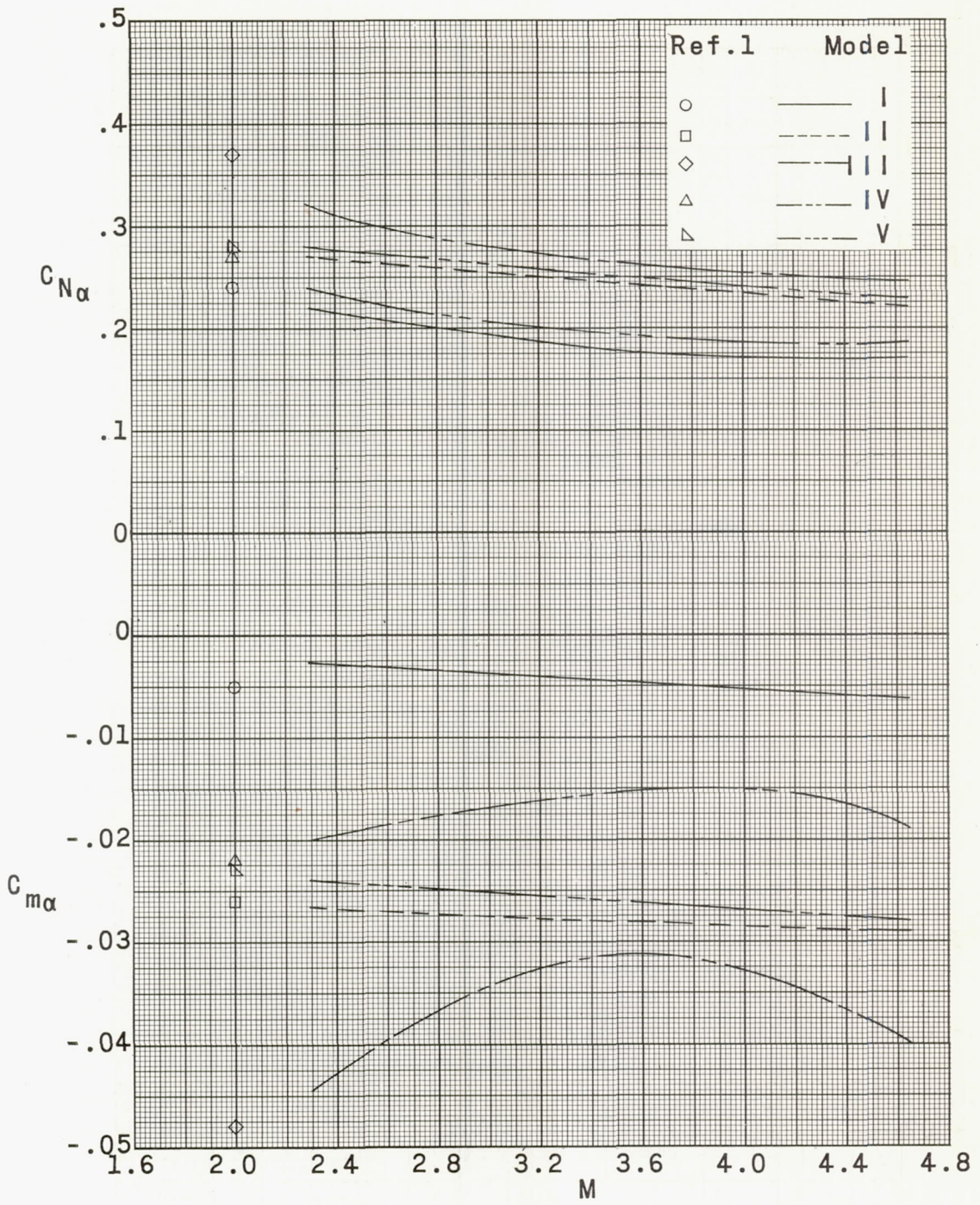

(b) $\alpha = 16^\circ$ to 20°.

Figure 17.- Concluded.

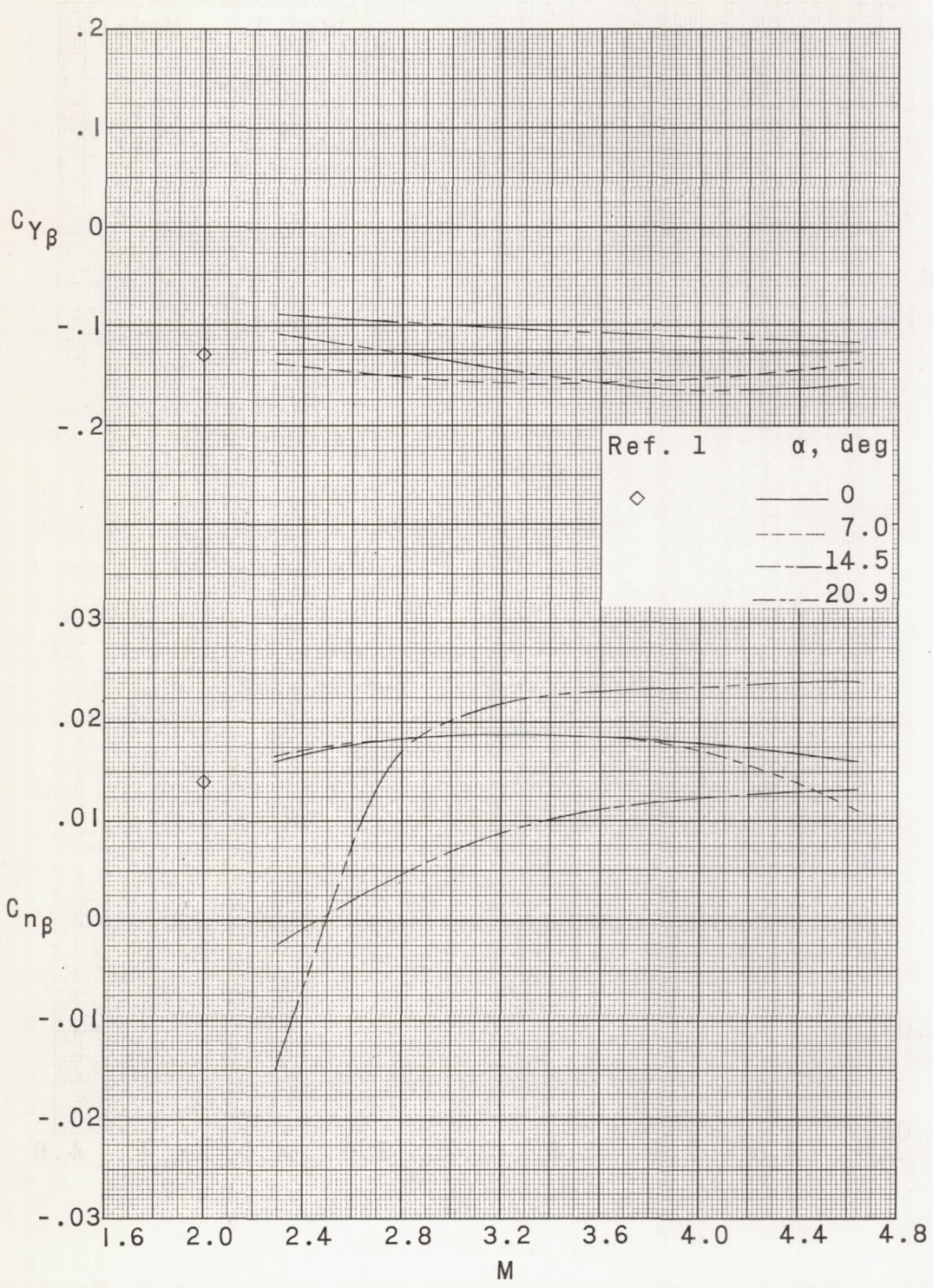

Figure 18.- Lateral stability characteristics of model III.

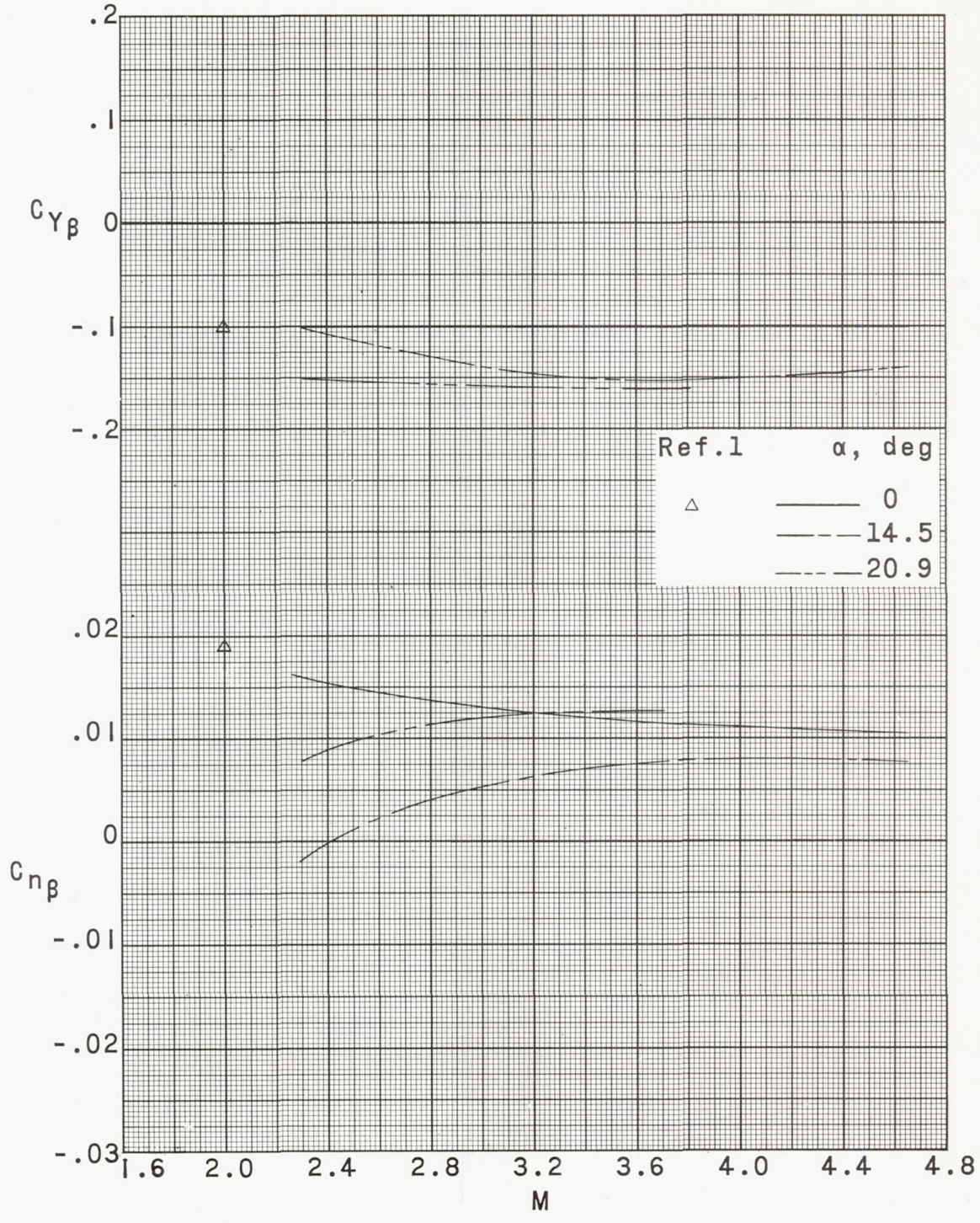

Figure 19.- Lateral stability characteristics of model IV.